*UNIVERSITY OF CALIFORNIA, MERCED*

# Aluminum ion batteries: Electrolytes and Cathodes

by

Luke Reed

A dissertation submitted in partial satisfaction of the requirements for the degree Doctor of Philosophy

in

Chemistry and Chemical Biology

in the

Graduate Division

of the

University of California, Merced

Dissertation Committee:

Professor David F. Kelley, Chair
Professor Erik J. Menke, Advisor
Professor Andy LiWang
Professor Shaowei Chen

2015

This page intentionally left blank

The dissertation of Luke Reed, titled *Aluminum-ion Batteries: Electrolytes and Cathodes*, is hereby approved:

_____ Date: _____
Erik Menke

_____ Date: _____
Andy LiWang

_____ Date: _____
Shaowei Chen

Chair: _____ Date: _____
David Kelley

University of California, Merced

# Table of Contents

*For my family.*

## Acknowledgements

First, I want to thank my PI, **Erik Menke**, for being an incredibly patient advisor and for letting me explore many things in the lab. I've never known anyone so calm and unflappable; thank you for the advice, thoughts, insightful discussions and enduring patience through the years. I wish you the best of luck for the rest of your career.

**Dave Kelley**, my committee chair, you allowed me a great deal of time in your office even though I wasn't one of your students, thank you for all the thoughts and discussions. Nobody asks questions like you do, keep scaring us grad students with questions on napkins, we need it!

**Jason, Blessing, Diana, Ivy, Matt, Celine** and everyone in the Hein crew! You all know who you are! Thank you for everything, you've been great friends and supporters. I have so many good memories of all of you and the time we spent together. Good luck with the future, I know you'll all do great wherever you end up. Just for all of you I'll revive my facebook account and actually check it now and then!

**Dave Russell**, the most recent addition to my list of friends! Thanks for all the help with NMR and all the talks and advice about jobs and the future. It's been great to know you and find out that even us former physics guys can get make it in life!

**Paul Bowyer**, without all your help and instruction I still wouldn't know how to collect DOSY data. Thank you for all the advice and direction. I hope to make some research samples in the future that show more than one peak! My best wishes for you in the future and congratulations on getting a green card!

**My family**: my wonderful wife and son. Thank you both for everything you've done to help me along. It's wonderful to know you'll be with me wherever the next adventure takes us.

**My parents and sisters**: Thank you for helping, supporting, pushing and encouraging me every step of the way. Life is much better with a close family.

I know there are many people I haven't named. Please know that I'm grateful to all of you for the conversations, fun and friendship through the years. *You are not forgotten!*

Portions of this work have been funded by the American Chemical Society through the Petroleum Research Fund (52056-ND10) and NSF (EEC-0832819). Thank you!

## Curriculum Vitae

Education

Ph.D., Chemistry and Chemical Biology 2015
Dissertation: "Aluminum-ion batteries: electrolytes and cathodes"
Research advisor: Professor Erik Menke
*University of California, Merced*

M.S., Environmental Systems 2008
Thesis: "Kohler integrating optics for concentrating photovoltaics"
Research advisor: Professor Roland Winston
*University of California, Merced*

B.S., summa cum laude, Physics 2004
*California state university Stanislaus*

Publications

"Copper Prussian blue analogue as a cathode for a trivalent electrochemical system", Reed, L; Menke, E., submitted

"Aluminum trifluoromethanesulfonate – diglyme a multivalent solvate ionic liquid", Reed, L; Menke, E., submitted

"The roles of V2O5 and stainless steel in rechargeable Al-ion batteries", Reed, L.; Menke, E., Journal of the Electrochemical Society, 2013, Volume 160, Issue 6, A915-A917

"Characterization of single walled carbon nanotubes synthesized using iron and cobalt nanoparticles derived from self-assembled diblock copolymer micelles", Fu, Q; Reed, L.; Liu, J.; Lu, J Applied Organometallic Chemistry, 2010, Volume 24, Issue 8, 569–572

"Test results of a concentrating photovoltaic module using Kohler integration optics for flux homogenization", Reed, L.; Winston, R.; Ritschel, A.; Zang, W.; Baertsch, R., Photovoltaic Specialists Conference, 33rd IEEE ISSN: 0160-8371 (2008)

"Field results of a Kohler integrating photovoltaic system", Reed, L.; Winston, R.; Ritschel, A. Proceedings of the SPIE, Volume 6670, pp. 667006-667006-7 (2007)

"High-Concentration mirror-based Kohler integrating system for tandem solar cells", Benitez, P; Cvetkovic, A; Winston, R.; Diaz, G.; Reed, L.; Cisneros, J.; Tovar, A.; Ritschel, A.; Wright, J., Photovoltaic Energy Conversion, Conference Record, IEEE 4th World Conference 2006, IEEE Cat. No. 06CH37747

Posters and Presentations

"Investigation of Fundamental Thermodynamics of Potential Al-Ion Electrolytes" Poster presented at spring MRS 2014

"The role of V2O5 and stainless steel in Al-ion batteries" Talk presented at MRS, spring 2013

"Aluminum Deposition Utilizing an Ionic Liquid Electrolyte for Novel Battery Applications" Poster presented at spring MRS 2011

"Test results of a concentrating photovoltaic module using Kohler integrations optics for flux homogenization" Talk presented at IEEE Photovoltaic Specialists Conference, 33rd PVSC, San Diego, 2008

"Field results of a Kohler integrating concentrating photovoltaic system" Talk presented at SPIE conference, San Diego, 2007

# List of Figures

# List of Tables

## Abstract

Title: Aluminum-ion batteries: electrolytes and cathodes
Name: Luke Reed
Degree: Doctor of Philosophy
Institution: University of California, Merced, 2015
Committee Chair: David F. Kelley

Great abundance, trivalent oxidation state, high volumetric energy density and inherent safety make aluminum a desirable source of power. Attempts to use aluminum as an electrochemical energy source have been made since the 1800s. To date no great success has been achieved due to difficulties with finding a suitable electrolyte and cathode material. This dissertation explains some of the author's efforts to overcome these difficulties.

Chapter two reports the results of an investigation of an aluminum anode cell utilizing an ionic liquid electrolyte. Vanadium pentoxide was selected as the cathode material for this cell. The initial results appeared to show reversible aluminum ion based electrochemistry. Closer investigation showed that side reactions with the stainless steel current collector were responsible for the observed behavior.

Chapter three discusses the physicochemical properties of a concentrated aluminum triflate based electrolyte. The FTIR and NMR spectroscopic data show evidence of complex ion pairing taking place in the electrolyte. The electrochemical measurements show this electrolyte to have good ionic conductivity and a wide electrochemical window.

Chapter four shows the results of using the new electrolyte with a hexacyanoferrate cathode material. The electrochemical response of the system shows some degree of rechargeable behavior. This presents what may be the first evidence of aluminum ion intercalation / de-intercalation into a host material from an organic electrolyte.

# Chapter 1

# Aluminum based electrochemical systems: a literature review.

# 1.1 Aluminum metal – theory and background relevant to battery systems.

As the third most abundant element in the earth's crust, after oxygen and silicon, aluminum offers an intriguing possibility as a metallic anode for electrochemical systems. Its relatively high density of 2.7g/cm$^3$ coupled with its trivalent ionic state provide it with a theoretical volumetric capacity of 8040mAh/cm$^3$, nearly four times that of lithium and more than twice that of magnesium. While its gravimetric capacity is lower than that of lithium, 2900mAh/g vs 3800mAh/g, the extremely high volumetric capacity makes it remarkably appealing for use in devices or systems where minimal size is the most valuable attribute for the energy source, such as portable electronic devices and electric vehicles. While this theoretical view of aluminum shows its potential for wide applicability as an anode material it is hindered in its development by several thermodynamic and kinetic hurdles which present substantial obstacles to aluminums implementation on a broad scale as an electrochemical power source. One of the thermodynamic difficulties with aluminum is that its redox potential versus the S.H.E. is -1.67V, this is 0.7 volts more positive than magnesium and 1.3 volts more positive than lithium. Thus, as alluded to in a recent review[1], any aluminum ion battery in which the cathodes electrochemical properties, i.e., discharge and charge potentials, were not greatly varied from those seen in magnesium or lithium ion batteries would operate at 0.7 to 1.3 volts lower than the comparable battery making use of the latter two metals. This loss of potential could be further exacerbated by the kinetic hindrance imposed by the almost ubiquitous layer of aluminum oxide formed on the aluminum anode and by any irreversible, thermodynamic "holes", formed on the cathode by reconstitution reactions of the aluminum ions and the cathode host material. Table 1 displays the effects of the oxide layer on the potential of aluminum electrodes in a variety of electrolytes. It can be seen that the effect of the oxide layer is to shift the redox potential of the aluminum to more positive values; in the case of neutral and acid electrolytes the shift is large enough to bring aluminum to a cathodic position relative to zinc in spite of the 0.9V theoretical difference.

**Table 1.1 Potentials of Al, Mg and Zn in several electrolytes vs. the SHE.**

| *Metal* | *1.0M NaCl* | *1.0M $Na_2SO_4$* | *1.0M $Na_2CrO_4$* | *1.0M HCl* | *1.0M $HNO_3$* | *1.0M NaOH* | *1.0M $NH_4OH$* | *Sat. $Ca(OH)_2$* | *Sat. $Ba(OH)_2$* |
|---|---|---|---|---|---|---|---|---|---|
| *Al* | 0.52 | 0.16 | 0.37 | 0.46 | 0.15 | 1.16 | 0.46 | 1.20 | 1.19 |
| *Mg* | 1.38 | 1.41 | 0.62 | 1.34 | 1.15 | 1.13 | 1.09 | 0.62 | 0.54 |
| *Zn* | 0.81 | 0.85 | 0.33 | 0.80 | 0.72 | 1.17 | 1.16 | 1.06 | 1.15 |

The presence of the aluminum oxide passivating layer necessitates an electrolyte capable of its dissolution which inherently implies a corrosive environment. While the chemical nature of aluminum oxide is such that acidic, saline or alkaline media may be utilized to facilitate its removal, these electrolytes are generally corrosive towards any potential cathode materials as well as the casing and current collectors of an actual battery. This greatly limits the potential candidate materials for use as aluminum ion battery cathodes and in certain cases can result in large self-discharge currents, material loss and case corrosion, all of which contribute to limited shelf life as well as capacities far below the theoretical values due to energy loss via side reactions. The possibility of thermodynamically favored reconstitution reactions of the cathode host with the trivalent aluminum ions further restricts cathode selection to materials which exhibit chemical stability in the presence of Lewis acidic aluminum ions and complexes as well as during electrochemical cycling in which the transition metal centers of the cathode material undergoes a redox induced valence change. Furthermore, the electrolyte HOMO/LUMO gap must extend negative of the aluminum anode and positive of the cathode to eliminate spontaneous redox of the solvent molecules. In contrast to lithium ion electrochemical systems no formation of a stable solid electrolyte interphase is known for aluminum surfaces. It is, therefore, a requirement of aluminum based electrolytes that they be electrochemically stable in the desired potential window of the aluminum battery. This places a limitation on the anodic potential of the aluminum cell as few electrolyte systems exist in which reversible aluminum deposition and stripping may occur while simultaneously offering anodic stability beyond 2V vs. $Al/Al3^{+}$.

## 1.2 Electrochemical properties of Al and Al-alloys: corrosion control and electrodeposition.

An alternative to the pure aluminum anode is an alloyed or doped aluminum metal anode. Incorporation of proper alloying elements can reduce or eliminate the formation of a stable aluminum oxide layer, thereby activating the aluminum metal and reducing the polarization losses. Several studies have investigated the effects of alloys in the anode or additives in the electrolyte on the potential of the aluminum anode and its electrochemical behavior in a range of electrolytes[2–13]. The results of one such study have been adapted for table 2, showing the potential change of aluminum with varying amounts of zinc alloy in several electrolytes.

**Table 1.2. Potential of Al and some of its alloys with zinc versus the SHE in various electrolytes.**

| *Metal* | *1.0M NaCl* | *Sat. $Na_2SO_4$* | *1.0M HCl* | *1.0M NaOH* | *1.0M $NaCO_3$* | *1.0M $Na_3PO_4$* | *Sat. $Ca(OH)_2$* | *Sat $CaCO_3$* | *Sat. $CaSO_4$* |
|---|---|---|---|---|---|---|---|---|---|
| *Al* | 0.51 | 0.16 | 0.54 | 1.13 | 1.01 | 0.98 | 1.20 | 0.70 | 0.43 |
| *Al/1%Zn* | 0.62 | 0.42 | 0.68 | 1.22 | 1.20 | 1.19 | 1.23 | 0.65 | 0.36 |
| *Al/5%Zn* | 0.70 | 0.48 | 0.74 | 1.24 | 1.16 | 1.20 | 1.23 | 0.71 | 0.48 |
| *Al/10%Zn* | 0.71 | 0.32 | 0.78 | 1.24 | 1.18 | 1.19 | 1.24 | 0.64 | 0.50 |
| *Al/15%Zn* | 0.68 | 0.28 | 0.78 | 1.21 | 1.19 | 1.15 | 1.20 | 0.53 | 0.46 |

The results of this study on the potential of aluminum and some of its zinc alloys make it clear that the composition of the anode can play an important role in the degree of passivation and hence polarization of the anode. This can have a dramatic effect on the potential of the anode, shifting it as much as 240mV in the case of pure Al vs Al/10%Zn in 1.0M HCl.

## Electrochemistry in aqueous electrolytes

The beneficial effects of additives or alloys are partially negated by a typical corresponding increase in the rate of anode corrosion. This is particularly true in the case of aluminum anodes and results in the need for corrosion inhibitors to attain an acceptable rate of self-discharge[14]. Chromate additives have been shown to be effective corrosion inhibitors for storage of dry cells, causing local polarization which protects the anode[15]. Mercury was also investigated as an inhibitor of self-discharge at both the anode and cathode due to the very high overpotential of hydrogen evolution at a mercury surface. Mercury proved to be beneficial in the case of zinc and magnesium dry cells but resulted in an increase in corrosion rate of aluminum anodes due the destruction of the oxide film[14]. Naturally, the work with mercury was in the early days of battery development and is no longer acceptable, in general, given its environmentally destructive properties.

A 1987 study of the electrochemical properties of aluminum-gallium alloys in alkaline and neutral electrolytes was conducted by Tuck, Hunter and Scamans[7]. This was perhaps the first study to carefully examine the activation mechanism of aluminum by gallium. The results provided insight into the diffusion of $Al^{3+}$ ions through localized deposits of gallium metal and the breakdown of the alumina layer as gallium deposits formed. They also showed that liquid gallium metal was necessary by cooling the alloys to 10C, resulting in temporary loss of activation.

Of particular note in the area of corrosion inhibition of aluminum and its alloys is the work of Macdonald et al, conducted in the late 1980s. In a series of papers on the application of aluminum alloys as anodes in aluminum-air batteries, Macdonald et al conducted an extensive investigation of the corrosion behavior of numerous aluminum alloys in conjunction with a wide range of solution phase and alloy phase corrosion inhibitors. Their work examined the performance of pure aluminum, aluminum alloys such as Alloy BDW (Al-1Mg-0.1In-0.2Mn) and Alloy 21 (Al-0.2Ga-0.1In-0.1Tl), in inhibited and uninhibited 4M KOH over a range of temperatures[3,4,16,17]. The inhibited electrolytes contained inorganic oxyanions such as $SnO_3^{2-}$, $Ga(OH)^{4-}$, $In(OH)_3$, $MnO_4^{2-}$, $BiO_3^{3-}$ and their combinations. The parameters of interest in these studies were the open circuit corrosion rate ($i_{corr,ocp}$), the discharge voltage ($E_D$) and the corrosion rate under a load ($i_{corr,d}$).

Their analysis showed $K_2MnO_4$ to be the most effective single component inhibitor at a concentration of $10^{-3}$, providing high coulombic efficiencies of 90% and better for high current discharges. However, the inhibition of standby corrosion was not substantially changed.

Of the two component inhibitors studied the stannate + indium hydroxide inhibitors showed a reduction in open circuit corrosion currents by a factor of 4 to 5 and showed coulombic efficiencies of up to 96% at discharge currents of 400 mA $cm^{-2}$.

By way of comparison, the commercial aluminum alloys of the time, Alloy BDW and Alloy 21 showed open circuit corrosion rates of 1 to 2 orders of magnitude lower than pure aluminum in solutions containing inhibitors. The drawback of these alloys was their lower coulombic efficiencies in the case of Alloy BDW and their more positive open circuit potential as well as toxic components (thallium) in the case of Alloy 21.

MacDonald's further work consisted of studies on several other aluminum alloys, again in 4M KOH utilizing polarization curves and Tafel plot analysis, as well as an electrochemical impedance study to elucidate the mechanism of aluminum corrosion in alkaline media[3,4].

## Electrochemistry in organic electrolytes

In contrast to the limited thermodynamic stability of aqueous electrolytes organic electrolytes offer enhanced stability while maintaining, to a great extent, the simple preparation of aqueous systems. Because of the enhanced stability the reduction potential of these electrolytes can be low enough to allow the electrodeposition of aluminum metal. Additionally, in certain cases the

deposition is reversible and high coulombic efficiencies can be obtained for the plating/stripping of aluminum metal. This, in principle, offers the opportunity to use aluminum metal as a reversible anode in a secondary battery however there are challenges associated with organic electrolytes which limit their practical utility in a commercial battery.

The difficulties with organic electrolytes are a generally low solubility of aluminum compounds, low conductivity and high flammability. Because of these limitations organic electrolytes for aluminum electrochemistry are used almost exclusively at the industrial scale for the electrodeposition of aluminum metal. The flammable nature of the electrolytes is particularly limiting for commercial applications.

Some of the first investigations of aluminum electrodeposition from organic solvents investigated aprotic, polar solvents such as acetonitrile, DMF, pyridine, propylene carbonate and others[18]. It is postulated that these efforts failed due to the highly charged nature of the $Al^{3+}$ ion. Its high coulombic charge density results in a tightly solvated ion for which the decomposition of solvent molecules is more energetically favorable than the desolvation energy. This is supported by the work done in chapter three of the dissertation in which the electrochemical properties of aluminum ions chelated by diglyme are measured as well as calculated.

Early work on aluminum electrodeposition from organic electrolytes was done by Brenner et al. They were able to successfully electrodeposit aluminum metal from a bath of aluminum chloride and lithium aluminum hydride dissolved in diethyl ether[19]. They also investigate the effects of several additives on the quality of the electrodeposited aluminum. While successful, the composition of the bath is sufficiently hazardous as to be undesirable for large scale use. Other work investigated LiAlH4 and AlCl3 in tetrahydrofuran and molten alkyl aluminum compounds[18,20]. These were sufficiently promising to be investigated at pilot plant scale but obviously still possess hazardous properties. In 1976 electrodeposition of aluminum from aromatic hydrocarbons was investigated by Peled and Gileadi[18]. They found poor quality electrodeposition from a simple $AlBr_3$ in toluene or benzene but addition of a Lewis basic molecule such as an aromatic hydrocarbon or an amine improved the quality of the deposit. Further addition of a bromide or iodide salt resulted in higher current efficiencies, a reduced tendency for dendrite formation and aluminum purity of 99.5%, equal to the source aluminum.

Further examples of aluminum electrodeposition from organic solvents can be found in the review by Zhao and VanderNoot[21].

## Electrochemistry in molten salts

Another type of electrolyte capable of reversible aluminum electrochemistry is molten salt eutectics. These are typically composed of aluminum chloride, sodium chloride, potassium chloride and lithium chloride in some molar ratio.

One of the first investigations of aluminum electrodeposition kinetics in molten salt electrolytes was undertaken by Del Duca in 1971. Her work on $AlCl_3$-NaCl and $AlCl_3$-(LiCl-KCl) mixes elucidated the kinetics of aluminum electrodeposition in these molten salts. Her results showed exchange current densities of 1 to 56 mA/cm$^2$ dependent upon the temperature and nature of the electrolyte in use. She was also able to show that the rate determining step at low overpotentials was caused by diffusion limitations and by charge transfer at high overpotentials. Interestingly, her results lend evidence for the creation of low valent aluminum ions being the rate limiting step during anodic dissolution[22].

In 1972 another investigation of the electrochemistry of aluminum in molten salts was undertaken by Holleck and Giner[23]. They examined aluminum electrodes in $AlCl_3$ – KCl – NaCl between 100 and 160C and found the aluminum electrochemistry to be reversible and capable of high current densities, up to 100 mA cm$^{-2}$ at 156C. The melts exhibited passivation of the aluminum electrode after sufficient current had passed due to local changes in concentration and the precipitation of salts on the electrode surface.

Three years after Del Ducas' investigation Gale and Osteryoung examined the subvalent ion effect during aluminum anodization in molten NaCl-$AlCl_3$[24]. By careful experimentation they determined that low level impurities in the melts limited the precision of the measurements by causing corrosion losses. These losses prevented the positive establishment of subvalent aluminum ions but the study did show the use of anodic stripping in determination of corrosion losses.

Another class of molten salt, room temperature molten salts, or ionic liquids introduced an entirely new way of electrochemically manipulating aluminum. Chapter 2 of the dissertation deals with the investigation of an ionic liquid as a secondary aluminum ion battery electrolyte. A short review of ionic liquids for aluminum electrochemistry will be given there.

## 1.3 Aluminum battery history; reports in the literature – early attempts

The history of efforts to incorporate aluminum into batteries can be traced to as early as 1855[25]. This first report, by Hulot, made use of aluminum as a cathode rather than anode, coupled with a zinc-mercury amalgam anode and dilute sulfuric acid as the electrolyte. The first report of a cell utilizing an aluminum anode appears to be the Buff cell, reported in 1857[26]. Three decades later a patent filing reported an amalgamated aluminum zinc alloy as an anode with a carbon cathode[27]. In 1907 H. T. Barnes and G. W. Shearer showed that a Mg – Al cell with $Al_2(SO4)_3$ electrolyte could attain an unexpectedly high voltage of 2.1 volts. They concluded that this high potential difference was due to the spontaneous generation of hydrogen peroxide at the aluminum surface, resulting in an in-situ generated $H_2O_2$ electrode[28]. In 1948 a series of chlorine depolarized primary cells were reported by Heise et al[29] with aluminum and aluminum amalgam yielding voltages of 2.05 and 2.45 volts respectively. These cells were designed as reserve batteries for heavy duty applications with the chlorine to be stored separately and added when the battery was needed. Clearly the use of chlorine gas limited the widespread applicability of these systems and prevented them from being highly developed.

The first attempts to utilize aluminum as an anode in Leclanche type cells took place in the 1950s when Sargent reported an Al || NaOH + ZnO || $MnO_2$ system[30]. This was followed by Ruben with development of an Al || MnO2 cell with a manganese chloride tetrahydrate electrolyte[31,32] and Cahoon who found a method to improve the shelf life of aluminum Lelanche type cells by utilization of an alternative separator[33]. While these efforts showed some measureable progress in making an aluminum dry cell no commercialization ever took place, most likely due to the more developed state of zinc dry cells and the remaining difficulties associated with aluminum.

In the 1960s to the 1970s a trend away from dry cells began and work was conducted on metal air batteries. The theoretical values for cost, energy density and power delivery make aluminum, in particular, appealing as a metal air battery. Some of the first aluminum air batteries were reported by Zaromb[34] and Bockstie[35]. During the course of their work they found that addition of zinc oxide, certain ammonium salts, or mercury to the electrolyte greatly reduced the rate of aluminum anode corrosion in the strongly basic, 10M hydroxide, electrolytes. While the reduction in the rate of corrosion was, in certain cases, sufficient to stabilize the aluminum anode to a rate of corrosion low enough for use in a battery the nature of the stabilization was such that at random times the corrosion rate would experience a sudden

increase, followed by a return to the original, lower rate[35]. This unpredictable behavior would be generally unacceptable in a commercial device.

As discussed above Holleck and Giner studied the electrochemistry of aluminum metal in the $AlCl_3$-KCl-NaCl eutectic melt as a possible electrolyte for high energy density aluminum batteries. They found the aluminum electrochemistry to be reversible and showed that the operating temperature of the battery could be reduced from over 100C to 61C by the addition of LiCl. In conjunction with the aluminum anode they revisited chlorine in the form of a carbon/chlorine cathode and elucidated the kinetics of the chlorine electrochemistry[23,36]. However, they also found that the aluminum anode was passivated in these melts under certain conditions by formation of a solid salt layer due to local concentration changes at the metal surface during current flow. Additionally, the cathodic deposition of aluminum resulted in highly dendritic surfaces and the use of chlorine gas is generally not desirable in a power source.

The major failing of these early efforts was their inability to simultaneously remove the ubiquitous oxide layer while also inhibiting the corrosion of the anode and cathode. The oxide layer of an aluminum anode causes a range of problems for researchers attempting to develop aluminum electrochemical cells. Its presence causes polarization losses of electrode potential, resulting in the actual potential of a cell being considerably lower than the theoretical value. This potential loss is the reason aluminum is cathodic of zinc in certain electrolytes, explaining the use of Hulot of aluminum as a cathode. The oxide layer further inhibits cell performance by causing what is known as “delayed action” which is a time delay during which the cell reaches its operating potential during discharge. This delay is due to the gradual breakdown and removal of the oxide layer from the aluminum anode surface.

## 1.4 Aluminum batteries – more recent efforts

Despite the extended period of research conducted on aluminum ion batteries no electrochemically rechargeable aluminum ion battery has been commercialized to date and very few primary aluminum cells are utilized in any application; a notable example being the aluminum – silver oxide reserve battery used for powering underwater vehicles and torpedoes, shown below.

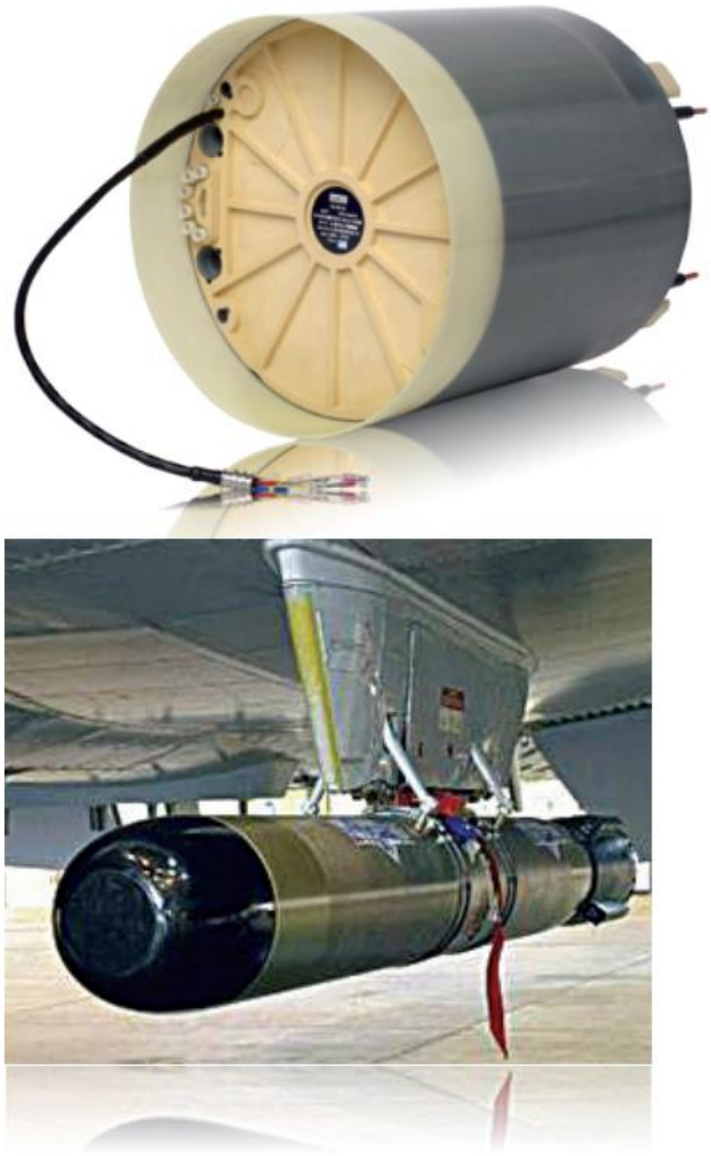

Figure 1.1. A commercial aluminum – silver oxide battery used to power a torpedo. Image is from an advertisement by Saft Batteries.

More recent efforts to develop aluminum ion batteries have focused on attempting to advance aluminum air technology or on finding a suitable combination of cathode and electrolyte to allow reversible intercalation. There are several recently reported secondary aluminum cells which at first glance appear to demonstrate reasonable electrochemical properties and cyclability using an aluminum metal anode in conjunction with various oxides such as

$V_2O_5$ nanowires[37], amorphous $VO_2$[38] and $TiO_2$[39] nanotubes. These systems have yet to be fully investigated, leaving good alternative explanations to the demonstrated behavior, and both reports utilizing vanadium oxides have been shown to be incorrect interpretations of the data[40]. The following sections of the dissertation report on specific examples of the research done in the field of aluminum ion batteries since the 1980s. There are surprisingly few reports in the scientific literature on aluminum batteries of any kind. Many of those that are published portray rather glaring errors which will be pointed out without apology. Primary cells will be discussed first in simple, roughly, chronological order. Secondary cells will be discussed as well however, this section will of necessity, be brief as there are very few reports which make any claim to represent a rechargeable aluminum ion battery.

## Primary Aluminum Batteries

As with past research most of the recent research and development in aluminum primary batteries has utilized alkaline aqueous electrolytes. Aqueous systems are simple to handle, inexpensive and exhibit better conductivity, lower viscosity and non-flammability in comparison to organic electrolytes. They offer the added advantage of removing the aluminum oxide layer by simple addition of a hydroxide salt. Additionally, there is little reason to explore organic or ionic liquid electrolyte based aluminum ion primary batteries unless a cathode material is identified which offers significant increase in the attainable potential and capacity beyond that offered by aqueous systems. Because of this there are few reports on organic electrolyte aluminum ion batteries but those which exist are included below. Ionic liquids are also gaining attention as possible electrolytes and a few reports can be found which make use of them for both primary and secondary batteries.

Research in the aluminum field during the 1980s was primarily focused on aluminum air systems for applications ranging from electric vehicles to space propulsion. Few publications exist from this decade and only those focusing on the electrochemical properties of aluminum and its alloys gained attention and provided lasting impact. These studies were conducted by Macdonald etal and were discussed in the section above, covering the electrochemistry of aluminum metal. The remaining investigations are included as references for completeness but are not reviewed as no measurable impact was produced by their results[2,41–62].

During the 1990s Licht became the standout researcher in the field of aluminum ion batteries. He developed several aqueous based aluminum batteries capable of producing high power at high efficiencies[63–68]. In 1993

Licht undertook the study of one of the most theoretically promising systems: the aluminum/sulfur redox couple. This couple offers a theoretical capacity of 1672mAh/g based on full utilization of the sulfur cathode during the reaction:

$$2Al + 3S \rightarrow Al_2S_3$$

With a theoretical voltage of 1.106V and an energy density of 1184Wh/kg or 2676Wh/L the aluminum/sulfur cell would be a lost cost, high energy density cell could the theoretical values be approached[69]. Remarkably, Licht etal discovered that bulk sulfur could be utilized as a cathode by making use of a polysulfide electrolyte and a CoS coated electrode. This system enabled the reduction of polysulfides which in turn resulted in the bulk sulfur being chemically drawn into solution to maintain the polysulfide concentration.

Licht studied this system in alkaline aqueous electrolytes. The relevant half reactions for this system are:

$$Al + 3OH^- \rightarrow Al(OH)_3 + 3e^- \qquad E = 2.30V \text{ vs. SHE}$$

$$S_4^{2-} + 4H2O + 6e^- \rightarrow 4HS^- + 4OH^- \qquad E = -0.51V \text{ vs. SHE}$$

For an overall cell reaction and potential of:

$$2Al + S_4^{2-} + 2OH^- + 4H2O \rightarrow 2Al(OH)_3 + 4HS^- \quad E = 1.79V$$

Based on the potassium salts used to make the polysulfide electrolyte the theoretical energy density of this cell would be 647 Wh/kg.[68] The actual values obtained were a voltage of 1.3V and an energy density of 170Wh/kg based on the dry materials mass. These values were obtained after extensive testing of multiple combinations of aluminum alloy types, additives to the electrolyte and temperature variation. The large deviation of actual values to theoretical can be attributed to polarization losses at the aluminum anode and parasitic side reactions such as:

$$Al + OH^- + 3H_2O \rightarrow Al(OH)_4^- + 3/2H_2$$

Any side reaction results in sub-optimal utilization of the anode and reduction in the measured energy density.

Interestingly, Licht et al, revisited the aluminum/sulfur system four years later and found that the coulombic efficiency for the electrochemical oxidation of the aluminum anode unexpectedly increased to almost 100% by utilizing high current discharge, greater than 100mA/cm$^2$, and high polysulfide concentrations, 3 *m* and higher.[70] This dramatic increase from the 82% efficiency of a polysulfide free electrolyte and the minimum of 41% in 1.0 *m* $K_2S_3$ was attributed to the passivation of the aluminum surface in the presence of a high concentration of dissolved polysulfides. Unfortunately, this

passivation resulted in a cathodic shift of several hundred millivolts of aluminum the anode, thereby decreasing the cells open circuit voltage to 1.2V and the discharge voltage to 0.9V.

In 1999 Licht again demonstrated the high power capabilities of aluminum by investigating the discharge of an aluminum anode, permanganate aqueous cell.[65] This cell showed a high initial open circuit voltage of 2.3V and exhibited high rate capabilities of $3W/cm^2$ at 100C and $1W/cm^2$ at 75C with low polarization losses of 0.1-1.0mV$cm^2$/mA. The high rate discharge prevented the direct chemical attack of permanganate on aluminum, thereby increasing the coulombic efficiency of the anode to 90%. While this cell demonstrated excellent power delivery the requirement for high temperature operation and the necessity for rapid stirring place severe restrictions on its practical capabilities. Additionally, the current density was limited to $2A/cm^2$ or less due to the formation of a passivating layer of $MnO_2$ at higher current densities.

One of the few reports aside from Lichts' work was by Zoski and Medeiros on the use of sodium hypochlorite for high power aluminum batteries using seawater as the solvent[71]. They were able to obtain current densities of up to 1200 mA $cm^{-2}$ at a potential of about 1.2V. The applicability of the battery to practical applications was limited by the requirement for a palladium coated nickel current collector as a reducing surface for the catholyte as well as the relatively low voltage.

As the general interest in multivalent batteries grows more research groups have begun investigating aluminum batteries. Some with promising initial results although numerous problems remain.

One of the first papers from the early 2000s was again from Lichts' group[72]. They investigated fluorinated graphite cathodes with an acetonitrile based electrolyte. They obtained capacities of up to 450 mAh g-1 at a discharge potential of approximately 1.1V. They found the percent fluorine and the composition of the electrolyte to be critical in the performance of the batteries. Cells with higher fluorine content and 15-20% hydroxide additive gave the most satisfactory performance. Based on spectroscopic evidence they hypothesize the mechanism of discharge to be faradaic in nature.

Two of the most interesting papers are investigations of primary cells. One, by Xue et al, describes the discharge of a simple, separator free, battery. The cells were made by mixing graphite and iodine in a 2:8 weight ratio and pressing it into a pellet to form a cathode. The anode was simply aluminum metal, the cell was assembled by placing the aluminum metal in direct contact with the cathode pellet. This very unique electrochemical system could be discharged at rates up to 0.5C or 5 mA $cm^{-2}$ for a capacity of about 120 mAh g-

[1], albeit at low voltages. The discharge mechanism was shown to be diffusion of iodide ions through the $AlI_3$[73].

Another interesting paper by Li et al, investigated aluminum nanorods synthesized by vapor deposition as the anode for an aluminum air battery[74]. Using an $La_{0.6}C_{0.4}CoO_3$ catalyst cathode and a 4M KOH/ethanol electrolyte they obtained excellent capacities of 450 mAh $g^{-1}$ over voltages of 1.4 to 0.8 volts compared to 220 mAh $g^{-1}$ for a similar cell made with commercial aluminum powders.

Several papers reporting investigations of aluminum air systems have recently been published. Nestoridi et al, studied aluminum anodes with brine electrolytes. Their work examined pure aluminum and aluminum alloys containing tin and gallium in sodium chloride. They confirmed tin and gallium to be activating agents, observing an increasing in potential of 600mV from pure aluminum to alloy aluminum[75]. A. A. Mohamad utilized a gelling agent with potassium hydroxide electrolytes to make a liquid free aluminum air cell[76]. The tortuous path of the gelled electrolyte limited the discharge to low current densities of 0.8 mA $cm^{-2}$ and capacities of 105 mAh $g^{-1}$ were measured. Corrosion of the aluminum anode was also observed.

Two unusual systems, one making use of an aluminum anode with a surface layer of $Al_2(WO_4)_3$ and a KOH electrolyte and another using $Al_2O_3$ as the surface layer with a NaCl electrolyte were published by Mori[77,78]. The claims of the first report are that the aluminum tungstate acts as an aluminum ion conductor and that the cell is rechargeable. As electrochemical recharging of an aqueous based aluminum air battery is thermodynamically improbable it is highly likely that the cycling behavior observed is simply a concentration polarization/depolarization effect due to the tortuous path of the $Al_2(WO_4)$ layer and not any form of electrochemical recharging. The second report falls into the same thermodynamically forbidden claim. Another, similar and equally amazing claim has been made by Hibino et al who report a rechargeable aluminum air cell using a Sb doped $SnP_2O_7$ as an anhydrous hydroxide conducting electrolyte[79]. The same basic principles governing Mori's work are assumed to exist for Hibino et al.

A more credible effort is reported by Pino et al in their investigation of commercial aluminum alloys for aluminum air batteries[80]. They investigated 3 alloys with air cathodes and NiOOH cathodes. The results showed that commercial alloy Al2000 was the most promising alloy based on its lower corrosion rate of 0.1 to 0.3 mg $cm^{-2}$/min vs 0.3-0.6 mg $cm^{-2}$/min for other alloys as well as its lower polarization potentials for aluminum air cells. They found capacities of 120 Ah $kg^{-1}$ for the aluminum air and 161 Ah $kg^{-1}$ for the Al/NiOOH cell.

Cho et al also investigate the effects of aluminum purity on aluminum air battery performance, comparing 2N5 and 4N purity aluminum in NaOH electrolytes[81]. They found that the impurities in 2N5 inhibited its use in standby and low power discharge compared to the 4N with efficiencies of 51% for 4N and 19% for 2N5 at low power discharge. However, at high power the effects of the impurities are minimized and the efficiency of discharge for 2N5 reaches 76% versus 72% for 4N high purity aluminum.

Another gel electrolyte based aluminum air cell was investigated by Zhang et al using PAA gel with potassium hydroxide electrolyte[82]. At low current density discharges their cells exhibit relatively high potentials of 1.2 to 1.3 volts and allow capacities of up to 1166 mAh $g^{-1}$ Al.

Three non-aqueous aluminum air cells have recently been reported. Revel et al used the ionic liquid aluminum chloride: ethyl methyl imidazolium chloride, an aluminum anode and an air cathode, obtaining discharges of up to 0.6 mA $cm^{-2}$ and low self-corrosion rates of 3.60 nm $h^{-1}$ in the acidic melt[83]. While this is a novel application of a long known ionic liquid the voltages obtained were below 1 volt at all current densities and the ionic liquid used is known to highly moisture sensitive.

Another aluminum – air battery with an ionic liquid electrolyte was explored by Gelman et al using 1-ethyl-3-methylimidazolium oligo-fluoro-hydrogenate ionic liquid[84]. This ionic liquid has been shown to be air and water stable and allowed sustained discharged above 1.5 volts for low current densities. The measured capacities were up to 70% of the theoretical value of 200 mAh $cm^{-2}$ for aluminum. This system shows initial promise for an aluminum – air battery although the cost of using any ionic liquid is prohibitive in comparison to aqueous electrolytes.

An interesting split-cell dual-electrolyte approach was adopted by Wang et al, using a 3M KOH in anhydrous methanol organic electrolyte at the aluminum anode and a 3M KOH aqueous phase at the air cathode[85]. They were able to obtain impressive capacities of ~1500 to 2500 mAh $g^{-1}$ Al using inexpensive household aluminum foil at potentials of 0.95 to 1.2 volts.

One of the few aluminum dry cell batteries reported in the recent literature was investigated by Sivashanmugam et al in their work on Al/$MnO_2$ cells[86]. Using a "D" cell configuration and an aluminum chloride/ammonium chloride/chromium chloride aqueous gel electrolyte they showed the performance of the Al/$MnO_2$ cell to be equal to or slightly better than current Zn/$MnO_2$ cells with two types of commercial aluminum alloys, obtaining 4.2Ah at 100 mA current drain with a coulombic efficiency of 85%.

In spite of the many efforts to find an optimized electrolyte and an aluminum alloy which minimizes corrosion while improving discharge potentials no published aluminum primary battery has approached the thermodynamically predicted 2.34 volts in alkaline electrolytes. A very intriguing ab initio investigation of the aluminum air battery was recently published and provides insight into the generally wide gap between theoretical and practical voltages seen in aluminum air systems[87]. Using a stepwise hydroxide-assisted mechanism for anodic aluminum dissolution in alkaline media Chen et al predict the OCP of an aluminum electrode be -1.87 volts versus the SHE at pH 14.6, rather than the generally used -2.34. They attribute this difference to "an electronic factor, the asymmetry between the individual electrochemical steps as the bonds to the surface increase in strength with the number of adsorbates" and to the interactions of $Al(OH)_3$ in the bulk. Their results have important implications for aluminum air batteries, implying that the maximum OCP achievable for this electrochemical system will be around 1.87 volts, thereby greatly reducing the quality of the energy produced by an aluminum air cell.

Several ionic liquids offer appealing electrochemical and physical properties for the electrochemistry of aluminum. These include members of the pyridinium and imidazolium families. With proper purification and controlled ratio of aluminum source to organic counter-ions the electrochemistry of an aluminum anode can be controlled with 100% coulombic efficiency. The physical properties of the deposited aluminum can be controllably adjusted from dendrites to nanocrystalline deposits by adjusting the current density of deposition and organic additives, which can play a crucial role in modifying several properties of the ionic liquid electrolyte. The electrochemical window of ionic liquids is one of the most appealing features in their use as aluminum ion electrolytes. In contrast to water and organic electrolytes, both of which suffer from relatively low electrochemical stability in either the anodic or cathodic direction, ionic liquids can have stable electrochemical windows of several volts. In many cases this window can be adjusted by controlling the Lewis acidity or basicity of the melt by changing the ratio of aluminum salt to organic salt. The table below shows the electrochemical window for several ionic liquids as a function of aluminum to organic ratio.

**Table 1.3. Electrochemical windows of several binary and ternary ionic liquids at room temperature.**

| Ionic Liquid Studied (Numeric ratios are mol%) | Working Electrode | Potential Window (V) |
|---|---|---|
| 55-45 $AlCl_3$/EMIMCl | Tungsten | 2.9 |
| 50-50 $AlCl_3$/EMIMCl | Tungsten | 4.4 |
| 40-60 $AlCl_3$/EMIMCl | Tungsten | 2.8 |
| 60-40 $AlCl_3$/PMMIMCl | Glassy Carbon | 2.9 |
| 50-50 $AlCl_3$/PMMIMCl | Glassy Carbon | 4.6 |
| 40-60 $AlCl_3$/PMMIMCl | Glassy Carbon | 3.1 |
| 50-45.5-4.5 $AlCl_3$/EMIMCl/LiCl | Tungsten | 4.3 |
| 50-47.6-2.4 $AlCl_3$/EMIMCl/NaCl | Tungsten | 4.5 |

One recent example of attempts to employ ionic liquids as aluminum ion battery electrolytes was published by Rani, et al. The reported battery made use of electrochemically fluorinated graphite as a cathode and $AlCl_3$ with 1,3-di-n-butylimidazolium bromide (bim) ionic liquid electrolyte in a 0.5:1 molar ratio of $AlCl_3$ to bim. This battery reportedly provides a discharge capacity of 225mAh/g which was stable over 40 cycles. While these numbers are reasonably high for an Al-ion battery there are several details missing from this report which make it impossible to state that they have obtained a successful intercalation/deintercalation of aluminum ions. Primarily the authors fail to state the details of the test cell and it is therefore not possible to rule out redox chemistry originating from the current collectors. They also fail to mention any purification procedures relating to the ionic liquid, this is a necessary step for most ionic liquids as a variety of impurities are known to exist in as-synthesized ionic liquids. Finally, the authors utilize a molar ratio of 0.5:1 aluminum salt to bim which places the electrolyte in the Lewis basic regime. It is known that Lewis basic $AlCl_3$-ethylmethylimidazolium chloride ionic liquids do not allow aluminum redox to occur at an aluminum metal surface. It is highly unlikely that the $AlCl_3$-bim ionic liquid would provide

aluminum redox chemistry at the aluminum anode and it is suggested that electrolyte breakdown is occurring rather than reversible electrochemistry of aluminum.

## Secondary Aluminum Batteries

*Aqueous electrolytes*

To the best of the authors' knowledge only 5 credible reports of aqueous based, secondary, aluminum ion battery systems exist. Of these, 3 present plausible data but are open to alternative explanations due to the nature of the $TiO_2$ nanotube systems investigated. The final 2 report on the same copper hexacyanoferrate material used in chapter four of the dissertation and will be discussed in the introduction to that chapter. The first report examined the aluminum ion storage behavior of $TiO_2$ nanotube arrays in aqueous $AlCl_3$ solutions[39]. Cyclic voltammetry of the aluminum chloride electrolytes shows widely separated peaks in the presence of $Al^{3+}$ ions while no peaks are visible in magnesium chloride and lithium chloride. The charge – discharge curves show reversible capacities of about 75 mAh $g^{-1}$. Although the electrochemical data appear to display reversible aluminum ion insertion and removal it is not clear that the mechanism is in fact intercalation of the ions into the $TiO_2$ as claimed, or if the activity is due to surface reactions and pseudo capacitance. A second report using black mesoporous anatase $TiO_2$ nanoleaves shows capacities of 278 mAh $g^{-1}$ in aqueous $Al(NO_3)_3$ electrolytes[88]. This results of this report are even more likely to be due to surface area pseudo capacitance as the nanoleaves had a high surface area of 314 $m^2$ $g^{-1}$. Additionally, only the first discharge curve is shown, making assessment of the behavior of the battery difficult. A third paper investigating $TiO_2$ nanotube arrays showed that the presence of the chloride anion was necessary for electrochemical activity in aqueous electrolytes[89]. Little activity was observed in the presence of aluminum sulfate while the addition of sodium chloride resulted in clear peaks in the cyclic voltammograms. Although the presence of both aluminum ions and chloride anions are clearly needed for electrochemical activity to occur it is still not clear that the mechanism of activity is aluminum ion insertion into the $TiO_2$ crystal structure.

*Organic and ionic liquid electrolytes*

To the best of the author's knowledge there are no credible reports of a rechargeable aluminum ion battery using an organic electrolyte. There are very few reports using ionic liquids, these will be discussed in chapter 2.

*Other electrolytes*

While the bulk of research done on aluminum based batteries has made use of aqueous, organic or ionic liquid based electrolytes there are a few reports of investigations using combinations of these conventional electrolytes with an ion-permeable separator or a solid electrolyte at elevated temperatures. The most recent report of this type employs a dual electrolyte approach with a 3M KOH in methanol anolyte in contact with an aluminum anode, an anion exchange membrane of 450um thickness and 3M KOH in water on the cathode side utilizing a cathode of platinum loaded carbon for oxygen reduction.[85] This configuration resulted in a battery capable of gravimetric capacities of 1810mAh/g at current densities of 20mA/cm2 and plateau voltage of 1.15V. Additionally, the self-corrosion rate of the aluminum is reduced in the organic electrolyte to approximately 5% of that in the analogous aqueous electrolyte. While these numbers and performance characteristics are promising for an aluminum / air primary battery the authors point out that they used an excess of electrolyte to prevent precipitation of $Al(OH)_3$ and that only the weight of aluminum is considered in the calculations. Thus, a more practical analysis of the system would result in greatly reduced values compared to those reported.

Another recent report of an aluminum – air battery makes use of a tungstate membrane which has previously been reported to be an aluminum ion solid state conductor[90,91], and purports to display reversible electrochemistry with an alkaline electrolyte[77]. Several issues are immediately apparent with the claims made in this paper, chief among them being the fact that the conduction mechanism present in the tungstate solid ion conductor was thoroughly investigated and determined to be due to a polyatomic anionic complex, not to the reported $Al^{3+}$ ion.[92] Additionally it is highly unlikely that the recharge mechanism observed would be due to room temperature, aqueous phase reduction of aluminum hydroxide species to aluminum metal as apparently claimed by the author. The thermodynamics of this reaction are such that the reduction potential of the electrolyte would be achieved long before the reduction potential of hydrated aluminum hydroxide.

# Conclusions and outlook

At present, the outlook for aluminum ion batteries is hopeful but clearly many challenges remain. Major obsticles which must be overcome are: 1) finding an inexpensive, air and water stable electrolyte which is capable of reversible aluminum electrodeposition and stripping at the anode and of enabling some type of reversible reaction at the cathode, 2) finding a cathode material which allows some type of reversible reaction with aluminum ions to occur. These

are serious obsticles; any researcher pursuing this study is taking on a challenge which has defeated many scientists over the years; proceed with caution!

# Chapter 2

# An aluminum anode / ionic liquid electrolyte / $V_2O_5$ cathode battery.

# 2.1 Introduction

This chapter discusses an investigation of an electrochemical system composed of an aluminum anode, an ionic liquid electrolyte and a $V_2O_5$ aerogel cathode. There are few reports in the literature of rechargeable aluminum ion batteries. Recent attempts include a $VO_2$ cathode[38] and a $V_2O_5$ thin film[93], both reports fail to show clear control data and the claims are questionable.

The most recent paper to appear in the literature shows chloroaluminate ion intercalation in a graphtic cathode with aluminum metal electrodeposition and stripping at the anode[94]. This is one of the most promising reports of a rechargeble aluminum ion battery, showing ultrafast charge times of 1 minute and extremely long cycle life of 7500 cycles with capacities of about 60 mAh/g. However it is not without problems, the chief issue being that the charging potential of this system is beyond the oxidation edge of the ionic liquid electrolyte. The ionic liquid used generates $Cl_2$ upon oxidation, approximately half the reported capacity can be attributed to this side reaction. Therefore, much work still remains in the fielf of aluminum rechargeable batteries.

For this chapter electrochemical cells based on a $V_2O_5$ composite cathode, aluminum anode, and $AlCl_3$ + 1-ethyl-3-methylimidazolium chloride ionic liquid electrolyte were prepared and characterized to ascertain the role of $V_2O_5$. The $V_2O_5$ was found to be electrochemically inactive in a potential window of 5 mV to 1.5 V vs. $Al/Al^{3+}$. The electrochemical behavior of the cells was found to be independent of the $V_2O_5$ and depend entirely on the stainless steel used as a current collector, thus showing stainless steel and $V_2O_5$ to be of limited use in this electrolyte.

Secondary batteries are an integral part of modern society, enabling technology ranging from fuel-efficient cars to portable electronics. Since its commercial introduction in the early 1990's the lithium ion battery, operating on the 'rocking chair' principle with a graphite anode and lithium metal oxide cathode, has dominated the rechargeable battery market. Continuing, dedicated research has allowed gradual but steady improvements to operating characteristics of the Li-ion battery such as the working voltage, power and energy density, life cycle, safety and cost, thereby supporting parallel advances in mobile technology and transportation. Unfortunately, even with the recent advances in Li-ion batteries, they still fall far short of the energy density, power delivery and cost needed to effectively compete with other forms of energy storage.

In light of this, there has been a recent renewal in interest for other battery chemistry platforms, focusing primarily on magnesium and aluminum redox chemistry[95,96]. Aluminum, in particular, is promising as it is the most

abundant metal in the Earth's crust and offers theoretical energy density and power competitive with or superior to lithium[69,97]. The idea of an aluminum anode battery has appealed to researchers for decades but its development has been hindered by lack of suitable electrolytes, insulating surface oxides, dendrite formations and low energy density[11,65,98–100]. However, a recent paper by Jayaprakash et al. appeared to successfully demonstrate a rechargeable aluminum battery prepared by combining a room temperature ionic liquid electrolyte with a vanadium pentoxide ($V_2O_5$) nanowire composite cathode[37]. The battery suffered from an unexpectedly low voltage and energy density, but seemed to demonstrate that rechargeable aluminum batteries are possible with the proper choice of electrolyte. In order to better understand the underlying chemistry and the poor properties of the battery, in particular the lower than expected voltage, we have carried out a series of experiments studying the role of the $V_2O_5$ in the composite cathode of this electrochemical system.

## 2.2 Materials and Methods

Two types of electrochemical cells were prepared, jar cells and Swagelok cells. All assembly and electrochemical testing was carried out in a glovebox with $O_2$ and $H_2O$ maintained below 0.5ppm. Experiments in jar cells were conducted in a three electrode configuration with a composite working electrode and aluminum wire (ESPI Metals, 4N purity) serving as the counter and pseudo reference electrode. Electrochemical experiments in Swagelok cells were conducted in a two electrode configuration with an aluminum foil disk as the counter/pseudo reference electrode and a composite working electrode. The composite electrodes for both types of cell consisted of a $V_2O_5$ aerogel, carbon black (Strem Chemicals, acetylene carbon black 99.99%) and polyvinylidene fluoride (pVDF) (Sigma-Aldrich, average molecular weight 180,000) mixture on either a stainless steel mesh (McMaster Carr, type 430) or platinum current collector.

### Aerogel preparation

$V_2O_5$ aerogel was prepared as using the procedure described by Chaput, et al[101]. In brief, vanadium isopropoxide was added to water and acetone at 0°C in a small cylindrical cuvette and mixed by inverting several times. The cuvette was then sealed and the gel allowed to age for several days. After aging the gel was placed in acetone to remove water by solvent exchange. The acetone was

changed once per day for 3 days to ensure complete water removal. The gel was then placed in cyclohexane for further solvent exchange. The cyclohexane was exchanged once per day for 3 days to remove all acetone. The gel was then poured into liquid nitrogen and placed under vacuum to sublimate the frozen cyclohexane. Finally the aerogel was calcined at 350°C for 2 hours to convert the amorphous, mixed valence aerogel to $V_2O_5$.

## Composite coating

After completing the aerogel synthesis a small amount of aerogel was weighed and placed in a mortar. Appropriate amounts of carbon black and pVDF were added to the mortar to achieve the desired weight ratio (e.g. 90:5:5, $V_2O_5$: carbon black: pVDF). Several drops of 1-Methyl-2-pyrrolidone (NMP) (Sigma-Aldrich) were added to obtain the proper consistency and the mixture was then ground with a pestle. The grinding process was continued for some time to ensure complete mixing of the materials. Upon completing the grinding process approximately 15mg of the slurry was applied to a current collector to form the cathode. The cathode was placed in a furnace and the temperature was ramped at 1°C per minute to a final temperature of 120°C. The temperature was held at 120°C for a minimum of 2 hours to remove excess NMP. The furnace was then turned off and allowed to cool until the temperature dropped to approximately 40°C whereupon the cathode was removed and transferred to a glove box.

## Electrolyte preparation

The ionic liquid aluminum chloride:1-ethyl-3-methylimidazolium chloride ($AlCl_3$:EMIC) was used as the electrolyte for all cells. 1-ethyl-3-methylimidazolium chloride (95%) was purchased from Sigma-Aldrich and purified by recrystallization from ethyl acetate and acetonitrile. Aluminum chloride (puriss, anhydrous, crystallized, 99%) was purchased from Sigma-Aldrich and further purified by triple sublimation. The ionic liquid was prepared by slowly mixing molar equivalent amounts of both salts. Further $AlCl_3$ was then added to the equimolar mix until a concentration of 1M $AlCl_3$ was obtained. This concentration corresponds to a molar ratio of 1.2:1, $AlCl_3$: EMIC.

## Swagelok cell assembly

All electrodes used in the Swagelok cell configuration were ½ inch in diameter. Assembly of the Swagelok cells was begun by placing the aluminum anode and separator disks (Whatman glass microfiber GF/C, 5 disks) in the housing with one current collector rod as support. Because of the air and water sensitive nature of the electrolyte, the assembly of the Swagelok cells was completed in a glove box with < 0.5ppm oxygen and water. After the cathode was placed,

several drops of ionic liquid electrolyte were applied and allowed to soak through the cathode and into the separator. The electrolyte was added after the cathode to help ensure good contact between the cathode and the electrolyte. A backing spring was then placed to make electrical contact with the cathode while applying pressure to ensure close proximity of all the components. The assembly was completed with a second current collecting rod.

### Electrochemical tests

All electrochemical tests were carried out using a Gamry series G 750 potentiostat. The scan rate for all cyclic voltammograms was 1mV/s. All chronopotentiometry was run at a constant current of +/- 100μA for two hour charge / discharge cycles between 1 V and 0.05 V.

## 2.3 Results and discussion

Figure 2.1 shows cyclic voltammograms of several electrochemical cells in the jar cell configuration. Figure 2.1 a, b and c show CVs from jar cells using stainless steel current collectors with varying ratios of $V_2O_5$ to carbon black to pVDF (90:5:5 in 'a', 50:25:25 in 'b' and 25:37.5:37.5 in 'c' all ratios by weight $V_2O_5$:carbon black:pVDF) coating while d shows the CV of a jar cell using platinum with a 90:5:5 $V_2O_5$:CB:pVDF composite coating as the working electrode. The current collectors were coated with the $V_2O_5$: carbon black: pVDF composite coating described above. As seen in the figure the electrochemical behavior of the system depends on two variables. First, there is a small dependence on the $V_2O_5$ content of the coating applied to the current collector. Second, there is a large dependence on the material used for the current collector. As the coating ratios are varied on stainless steel there is a small shift in the peak potentials and a small change in the magnitude of the current, which we attribute to differences in the conductivity of the coating as the amount of $V_2O_5$ is varied. Of greater interest is the absence of peaks seen in Fig. 2.1 d in which the composite was applied to platinum. This lack of peaks indicates that all electrochemical activity taking place in the first three images of figure 2.1 can be attributed to the stainless steel with no apparent contribution from the $V_2O_5$.

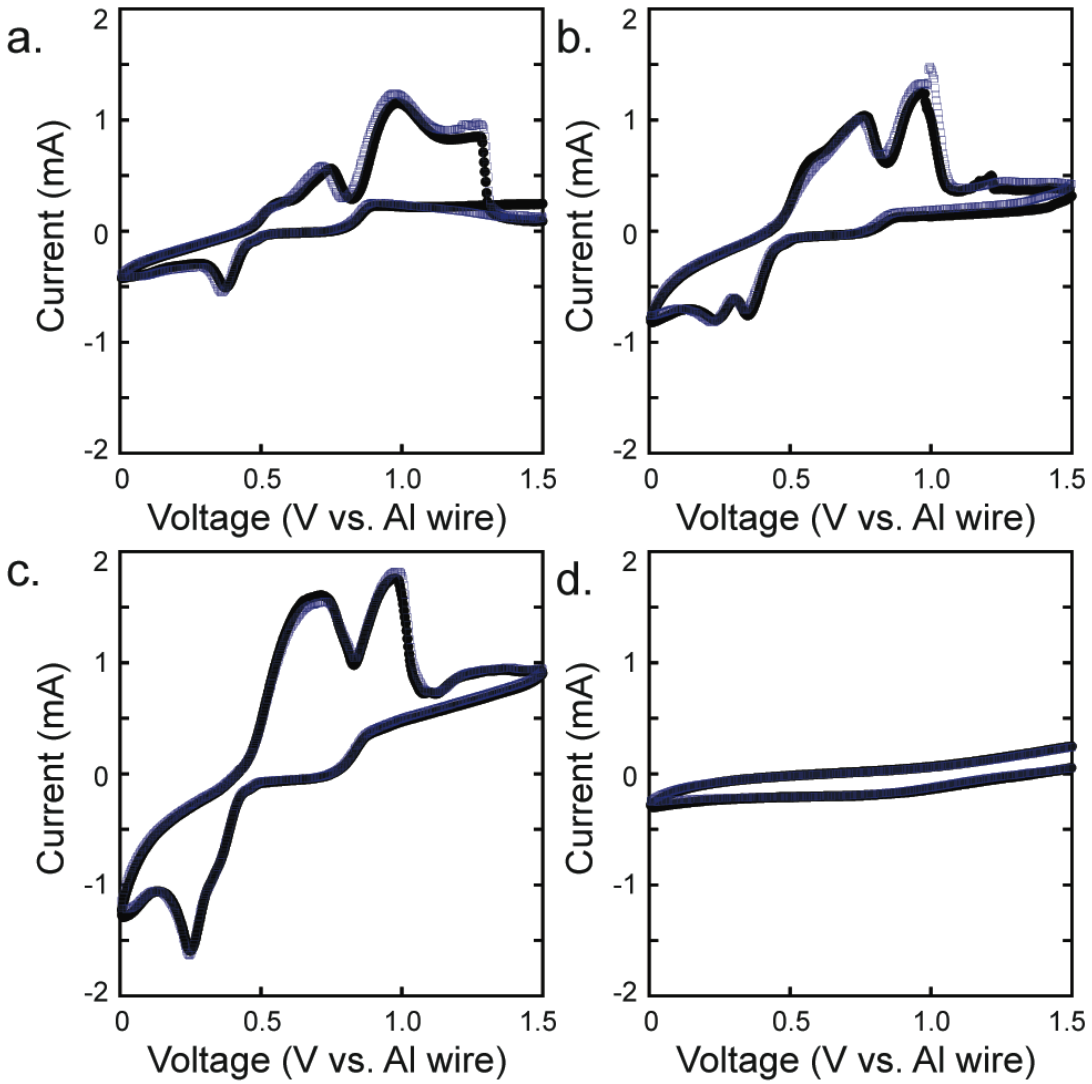


Figure 2.1. Typical jar cell cyclic voltammograms in a 1.2:1 mol/mol $AlCl_3$:EMIC electrolyte showing the second (solid black) and fifth (hollow blue) scans on a) a 90:5:5 by weight $V_2O_5$:carbon black:pVDF on stainless steel cathode; b) a 50:25:25 by weight $V_2O_5$:carbon black:pVDF on stainless steel cathode; c) a 25:37.5:37.5 by weight $V_2O_5$:carbon black:pVDF on stainless steel cathode; and d) a 90:5:5 by weight $V_2O_5$:carbon black:pVDF on platinum cathode, all at 1mV/s scan rate.

Figures 2.2a and 2.2c show cyclic voltammograms and 2.2b and 2.2d chronopotentiograms from Swagelok cells containing 90 wt% and 0 wt% $V_2O_5$, respectively. In 2.2a and 2.2c the potential shift of the reduction and oxidation peaks and the small variation in current magnitude can again be seen as the $V_2O_5$ content is reduced from 90 wt% in 'a' to 0 wt% in 'c'. Notably, the peaks are present in 'c' in spite of the cathode having no $V_2O_5$. The chronopotentiometry data in 2.2b and 2.2d also show the lack of dependence on $V_2O_5$ content with the charge and discharge potentials for both cells being similar. It can also be observed that the potentials of the Swagelok cell containing no $V_2O_5$ show better stability over 20 cycles, indicating that $V_2O_5$ is detrimental to the overall performance of the cell.

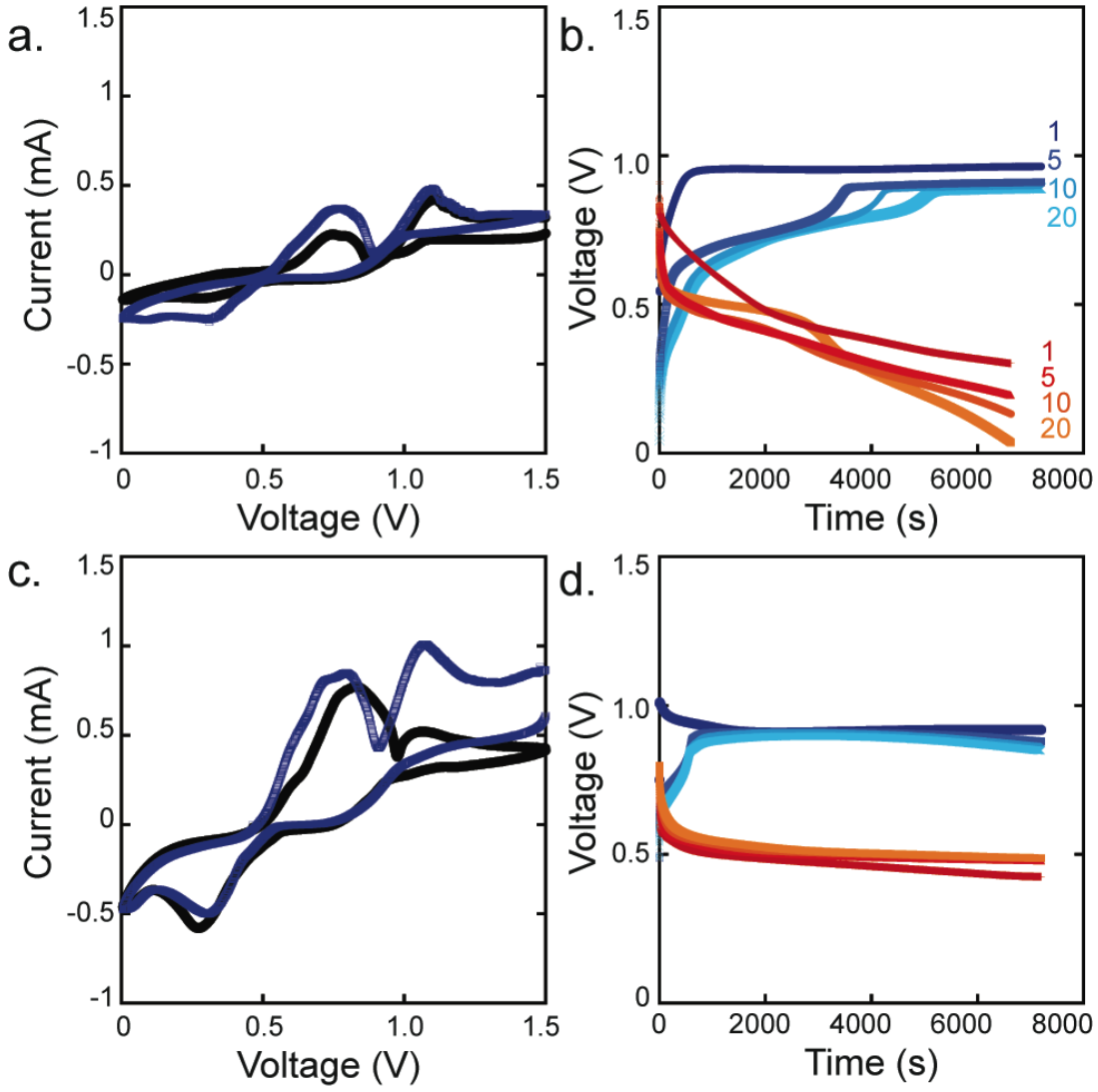

Figure 2.2. a) and c) Typical Swagelok cell CVs in 1.2:1 mol/mol $AlCl_3$:EMIC showing the second (solid black) and fifth (hollow blue) scans on a) a 90:5:5 by weight $V_2O_5$:carbon black:pVDF on stainless steel cathode and c) a 50:50 by weight carbon black:pVDF on stainless steel cathode, both at 0.1mV/s. b) and d) Typical Swagelok cell charge-discharge curves at 100 μA showing the first, fifth, tenth and twentieth charge (blue) and discharge (red) voltages on b) a 90:5:5 by weight $V_2O_5$:carbon black:pVDF on stainless steel cathode and d) a 50:50 by weight carbon black:pVDF on stainless steel cathode.

After cycling the Swagelok cells to failure (approximately 20 cycles), the Swagelok cells were disassembled, the electrodes and separator were rinsed with acetonitrile to remove the electrolyte, and were then examined by SEM. While the anode and cathode had changed very little after cycling, the separator was no longer porous glass fiber, but instead had a dense mat of metal dendrites embedded in it. This can be seen in figure 2.3a, where the piece of the filter paper that was in contact with the aluminum electrode has large amounts of metal on its surface. A higher magnification view of this surface, shown in figure 2.3b, shows a metal dendrite growing into the separator, while energy dispersive X-ray fluorescence, shown in figure 2.3c, reveals the dendrite is composed of aluminum, iron, and chromium.

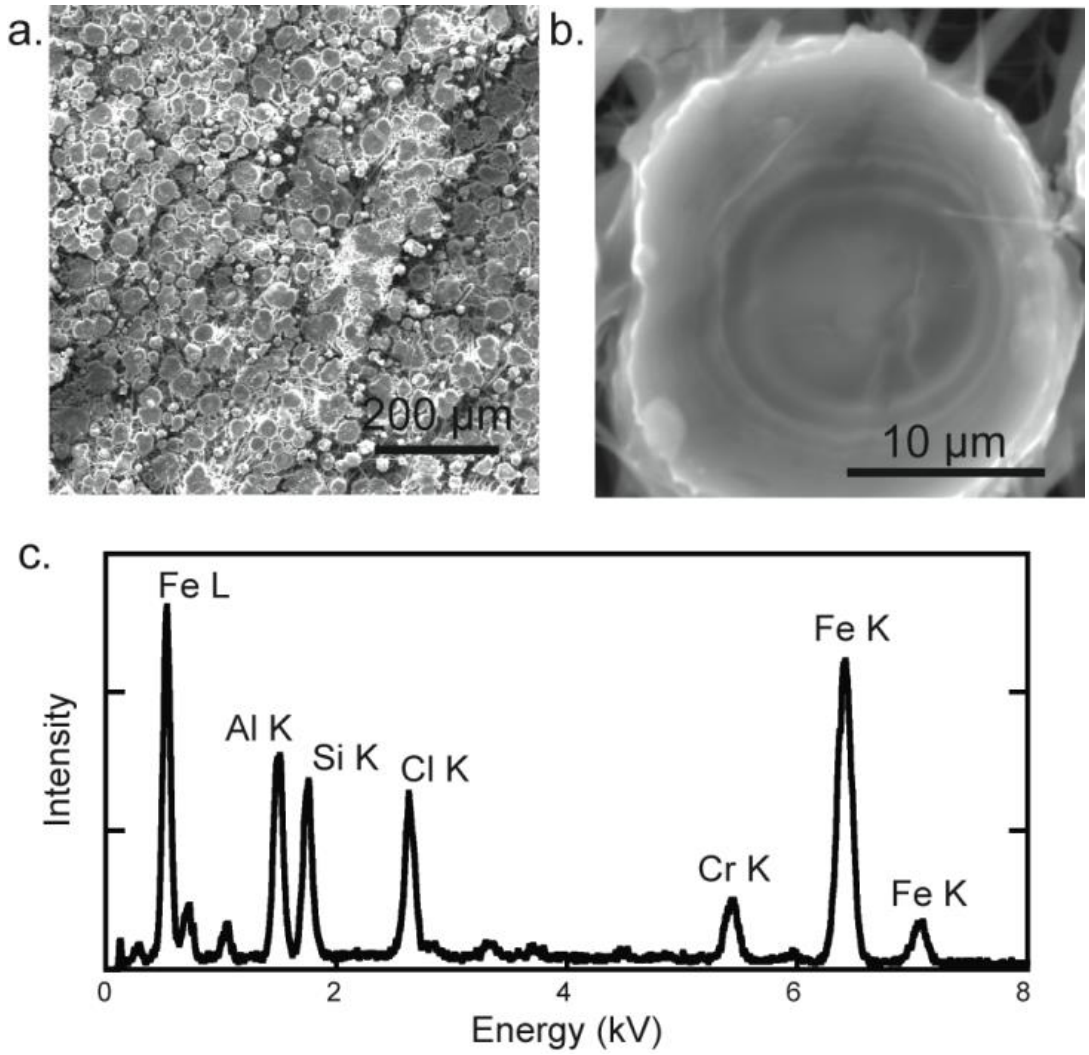


Figure 2.3. a) Low-magnification SEM image of the separator that was in contact with the Al-anode. b) High-magnification SEM image of the separator showing the bottom of a metal dendrite embedded in the separator. c) EDX spectra from image b showing the presence of iron, chromium, aluminium, silicon and chlorine.

The electrochemical behavior of the jar and Swagelok cells, coupled with the presence of iron and chromium on the aluminum electrode, suggest that the following two reactions taking place in these cells:

$$Al + 3/2\ FeCl_2 + AlCl_4^- \leftrightarrow Al_2Cl_7^- + 3/2\ Fe \quad (1)$$

$$Al + 3/2\ CrCl_2 + AlCl_4^- \leftrightarrow Al_2Cl_7^- + 3/2\ Cr \quad (2)$$

Where the forward reactions occur during the discharge step and the reverse reactions occur during charge step. Reaction 1, which has a standard potential of ~0.75 V,[98] dominates the electrochemical behavior of cells due to the high amount of iron in type 430 stainless steel. Reaction 2 is a minor, but still important reaction, as it has a standard potential of ~1.0 V and type 430 stainless steel contains reasonably large amounts of chromium (16-18%). It is also important to note that it was necessary to run a charge cycle before a successful discharge cycle could be obtained in the Swagelok cells, regardless of $V_2O_5$ loading, further suggesting that the $V_2O_5$ is not affecting the electrochemical behavior of the cells.

## 2.4 Conclusions and future work

Investigations into an aluminum-ion battery system composed of an aluminum anode, $V_2O_5$ composite cathode and aluminum chloride 1-ethyl-3-methylimidazolium chloride room temperature ionic liquid electrolyte have been undertaken. Based upon the results of the experiments performed we conclude that the $V_2O_5$ composite cathode shows no electrochemical activity towards aluminum and the battery-like performance can be attributed to reactions with the iron and chromium in the stainless steel current collector. In addition, the transport of iron and chromium to the aluminum electrode, followed by the deposition of iron, and chromium, leads to a gradual decline in cell potential and dendrite formation, causing the cells to fail after approximately 20 cycles. Finally, the stainless steel reactivity in this electrolyte limits the usefulness of either stainless steel current collectors or $AlCl_3$/1-ethyl-3-methylimidazolium chloride ionic liquid electrolytes for secondary Al-ion batteries.

Future studies with the ionic liquid used in the previous chapter could take several approaches. The first approach could be to investigate the electrochemical properties of various graphitic carbons in this ionic liquid. A very recent paper shows that at least some degree of intercalation into graphitic carbons is possible. However, the intercalation takes place at the anodic limit of the electrolyte and it is apparent in the data of this recent work that some amount of electrolyte oxidation is occuring. It may be possible to prevent this by careful control over the nature of the carbon used as the cathode. Elimination of chemically active sites on the carbon by chemical reduction or heat treatment may increase the overpotential of oxidation of the ionic liquid. Another approach would be to investigate the electrochemical response of hexacyanoferrate materials in this ionic liquid. These materials are discussed in chapter four of the dissertation. They offer a highly open crystal structure which may allow intercalation of the $AlCl_4^-$ present in the ionic liquid. To facilitate the movement of ions in the electrolyte it may also be feasible to add small amounts of organic solvents. This would allow tuning of the viscosity and should enable rapid cycling.

# Chapter 3

# Aluminum trifluoromethanesulfonate – Diglyme: A Multivalent Solvate Ionic Liquid

# 3.1 Introduction

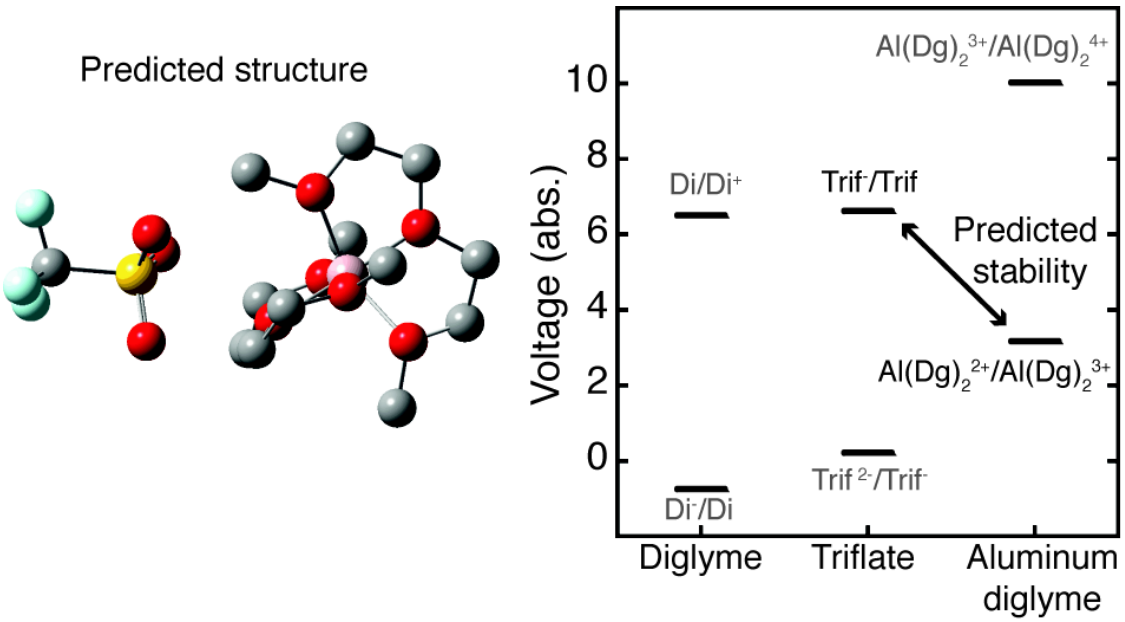


Figure 3.1. The Gaussian predicted solution phase structure of an aluminum / diglyme complex with a single coordinated triflate anion and the predicted absolute potentials of diglyme, an aluminum / diglyme complex and a triflate anion.

The physicochemical properties of aluminum trifluoromethanesulfonate in diglyme have been investigated as a function of concentration and temperature. The FTIR spectroscopic and electrochemical properties have been examined to determine speciation, conductivity and electrochemical stability. Gaussian calculations provide optimized molecular geometries and offer insight into the electrochemical behavior of the solutions. A binary mixture of approximately 1M concentration exhibits complex ion pairing with spectroscopic evidence of 4 distinct configurations coexisting in solution phase. Additionally, the ionic conductivity is maximized at this concentration, reaching 55 mS $cm^{-1}$ at 60 ˚C. The electrochemical window fluctuates as a

function of concentration, showing an increase of 700mV between the most dilute and most concentrated solutions.

The development of new electrolytes for energy applications is of great interest from both a scientific and practical standpoint. As new cathode materials and new chemistries are explored for advanced battery applications new electrolytes will be required to meet the demands of increased voltage and multivalent metals. Ionic liquids have been explored for many years as potential advanced electrolytes because of several well-known advantageous properties such as low volatility, high conductivity and wide electrochemical windows. However they have proven challenging to implement in commercial batteries due to various drawbacks, including high viscosity and increased cost.

Recent research has shown that at sufficiently high concentrations binary mixtures of conventional metal salts and organic solvents can exhibit behavior very similar to ionic liquids. These mixtures have been termed 'solvate ionic liquids' and have shown promise as both lithium ion and sodium ion electrolytes[102,103]. In general, early work done on highly concentrated electrolytes did not identify them by the term solvate ionic liquid; rather they were referred to and studied simply as concentrated electrolytes with a notable exception being an early work on equimolar mixes of lithium imide salts in glyme solvents[104]. The intent of the bulk of the early research was to expand the understanding of electrolytes that deviated from the theoretical behavior governed by empirical laws such as Debye-Huckel theory and its extension by Onsager. While some limited success was obtained with efforts to add to the theories of concentrated electrolytes, the research could be largely considered as relatively specialized and of limited interest to a general audience. Resurgence in the field, including investigation of possible device applications as well as the origination of the term 'solvate ionic liquid', seems to have been brought about primarily by Watanabe's detailed investigation of lithium electrolyte systems[103,105–107]. Further work by the same group expanded the range of the studies and was followed by papers investigating sodium trifluoromethanesulfonate in pentaglyme and ion size effects on solvate stability[102,108]. At some critical level of concentration, generally a 1:1 molar ratio of solvent:salt, all the systems studied exhibit a transition from attributes consistent with normal solvent/salt solutions to those more typically ascribed to ionic liquids.

To the best of our knowledge only combinations of solvents with monovalent metal ions have been investigated as solvate ionic liquids. Extending the work to multivalent ions presents unique challenges as the solubility of most multivalent metal salts limits the concentration of metal ions in solution to

levels below that needed for solvate ionic liquid character to appear. In this paper we report on the physicochemical properties of a solvate ionic liquid based on aluminum trifluoromethanesulfonate (AlTf or aluminum triflate) in 2-methoxy-ethyl ether (DG or diglyme), and compare these properties with properties calculated from DFT. The spectroscopic characteristics, investigated by FTIR, show evidence of multiple ion pairing configurations as a function of concentration. Assignments of the configurations are based on prior literature and DFT calculations examining the vibrational frequency of the $CF_3$ group of the triflate anion. The electrochemical window was measured as a function of concentration and the conductivity was measured as a function of concentration and temperature. The electrochemical window shows a maximum value at the highest concentration with complex behavior at intermediate concentrations. Results from DFT calculations of optimized geometries, normal modes and absolute redox potentials help explain both the spectroscopic and electrochemical properties.

## 3.2 Materials and methods.

### Materials

Aluminum triflate and diglyme were purchased from Sigma-Aldrich and were handled and stored in a VAC atmospheres glovebox with oxygen and water levels below 0.5ppm. The diglyme was purchased as ultra-dry and was further dried and stored over freshly activated molecular sieves. To activate the molecular sieves they are baked at >250C under vacuum in the vacuum oven. They are allowed to cool under vacuum and then transferred as quickly as possible into the antechamber of the glove box. If possible they should be allowed to sit under vacuum in the antechamber overnight before transferring into the glove box.

### Electrolyte preparation

All solutions were made in the glovebox by addition of appropriate amounts of aluminum triflate to diglyme to control the ratio of solvent molecules to aluminum ions. The solutions were stirred overnight to ensure complete dissolution of the aluminum triflate. Cyclic voltammetry of the solutions were measured with a Gamry potentiostat in a standard three-electrode configuration, with an aluminum wire counter electrode, an aluminum wire reference electrode, and either an aluminum wire or platinum wire working electrode. Electrochemical impedance spectroscopy was performed with a ParStat 2273 using a 10 mV AC signal and 0 V DC offset, over a frequency

range of 10 mHz to 100 kHz using an impedance cell prepared in the lab. The cell consisted of two platinum wires encased in flint glass tubing, with the exposed surface of the wires polished using 0.3um alumina, and was calibrated at 20 degrees C with a 0.1m KCl standard solution. FTIR data was collected on a Thermo Nicolet 380 with 1 $cm^{-1}$ resolution using 64 scans, KBr windows were used for the transmission cell. The more dilute solutions, 667 to 1 and 33 to 1, were gelled by addition of fumed silica at approximately 7wt% to increase the amount of material between the KBr windows. This technique has been previously utilized and has been shown to introduce no inference with the ion pairing of the electrolytes[109]. The spectra were curve fit using Galactic Grams to a Voigt profile with a linear baseline.

## Density functional calculations

All calculations were carried out with Gaussian 09[110]. Geometry optimization calculations for the molecules and complexes studied were carried out with the B3PW91 method using a 6-311G(d) basis set. Solvation free energies were evaluated by the self-consistent reaction field (SCRF) approach using the SMD model, implemented as the default SMD method in Gaussian[111]. As diglyme has not been parameterized for SMD, tetrahydrofuran was used as the solvent for all SMD calculations given its similar physical properties to diglyme.

# 3.3 Results and discussion

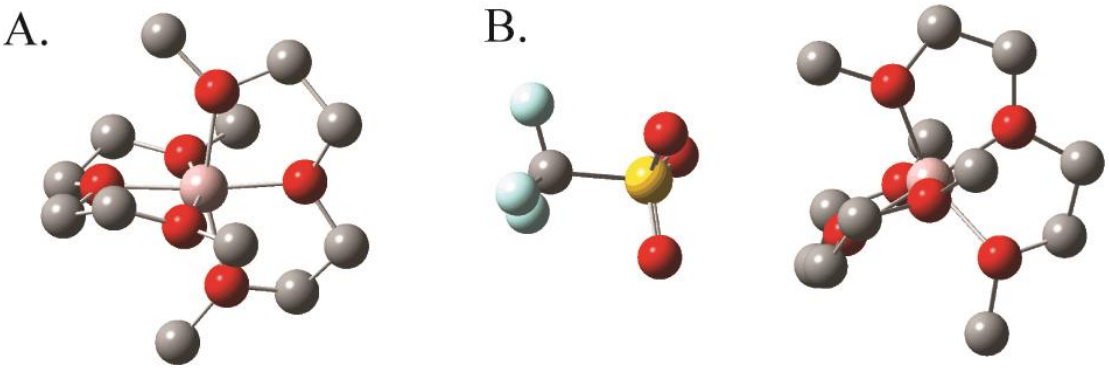


Figure 3.2- A) Optimized geometry of the aluminum-diglyme complex. B) Optimized geometry of the aluminum-diglyme complex with a bound triflate.

## Calculated geometries

Figure 3.2A shows the optimized solvent-phase structure for an $Al^{3+}$-diglyme complex, while figure 3.2B shows the optimized solvent-phase structure for the $Al^{3+}$-diglyme complex with a triflate anion. The calculated Gibbs energy for the reaction:

$Al^{3+} + 2$ diglyme -> $Al(dg)_2^{3+}$

is –1922 kJ $mol^{-1}$, corresponding to an equilibrium constant of $10^{335}$. While the complex in figure 3.2B is also very stable, given the additional coulombic attraction between the aluminum-diglyme complex and the triflate anion, there were no starting geometries that led to the triflate anion directly bound to the aluminum cation, suggesting that the diglyme molecule is a stronger Lewis base than the triflate anion. Based on these calculations we expect all of the aluminum ions to be chelated by two diglyme molecules, forming a stable $Al(diglyme)_2$ complex, which interacts with the triflate anions primarily via coulombic attraction.

## FTIR Analysis

*Preface to the analysis* – it must be made clear that the analysis included below is preliminary in nature. The comparisons of the spectroscopic response of aluminum triflate in diglyme with lithium triflate in diglyme can only be qualitative at this time. To definitively establish the nature of speciation and ion pairing in the $Al[DG]_2$ electrolyte considerably more spectroscopic and computational work is required.

Spectral characterization of the solutions reveals a concentration sensitive region between 750 and 775 $cm^{-1}$ corresponding to the $CF_3$ symmetric deformation mode, $\delta_s(CF_3)$, of the triflate anion[107,109,112]. It has been shown for numerous electrolytes that peak centers and relative areas can be examined as a function of concentration to provide insight into the nature of ion pairing in the solution phase electrolyte. For example, previous work has shown the vibrational frequency of the $\delta_s(CF_3)$ mode of triflate in monoglyme to be centered at 753 $cm^{-1}$, increasing to 758 $cm^{-1}$ upon forming contact ion pairs with solvated lithium ions, with a further increase to 769 $cm^{-1}$ for a single triflate anion triply coordinated by lithium ions[113]. The corresponding shifts of the $CF_3$ deformation in lithium triflate in diglyme are reported to be 752 $cm^{-1}$ for free triflate, shifting to 757 $cm^{-1}$ for contact ion pairs, 761 $cm^{-1}$ for dimers or triple cations and 762 $cm^{-1}$ for $Li_2Tf$ upon formation of the crystalline phase[109].

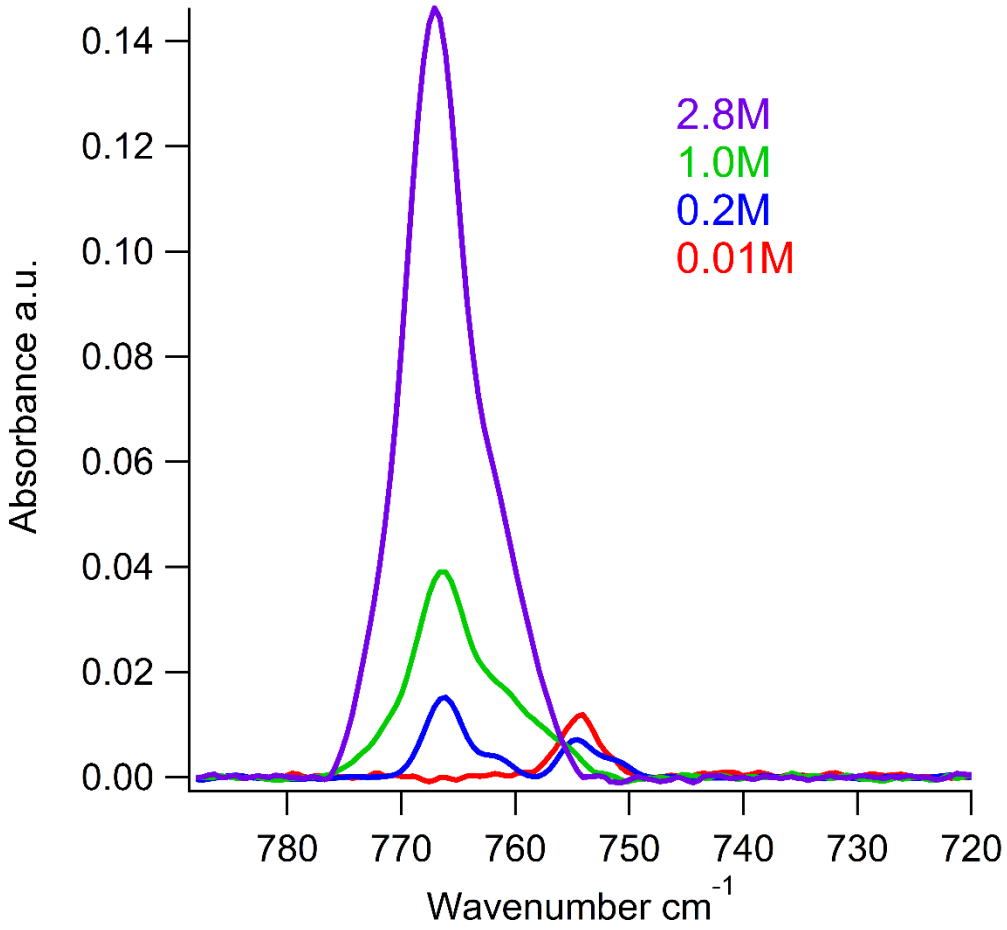


Figure 3.3 - FTIR spectra of 2.8M (purple), 1M (green), 0.2M (blue), and 0.01M (red) diglyme:aluminum triflate solutions, showing the shift in peak position of the $CF_3$ symmetric mode as a function of concentration.

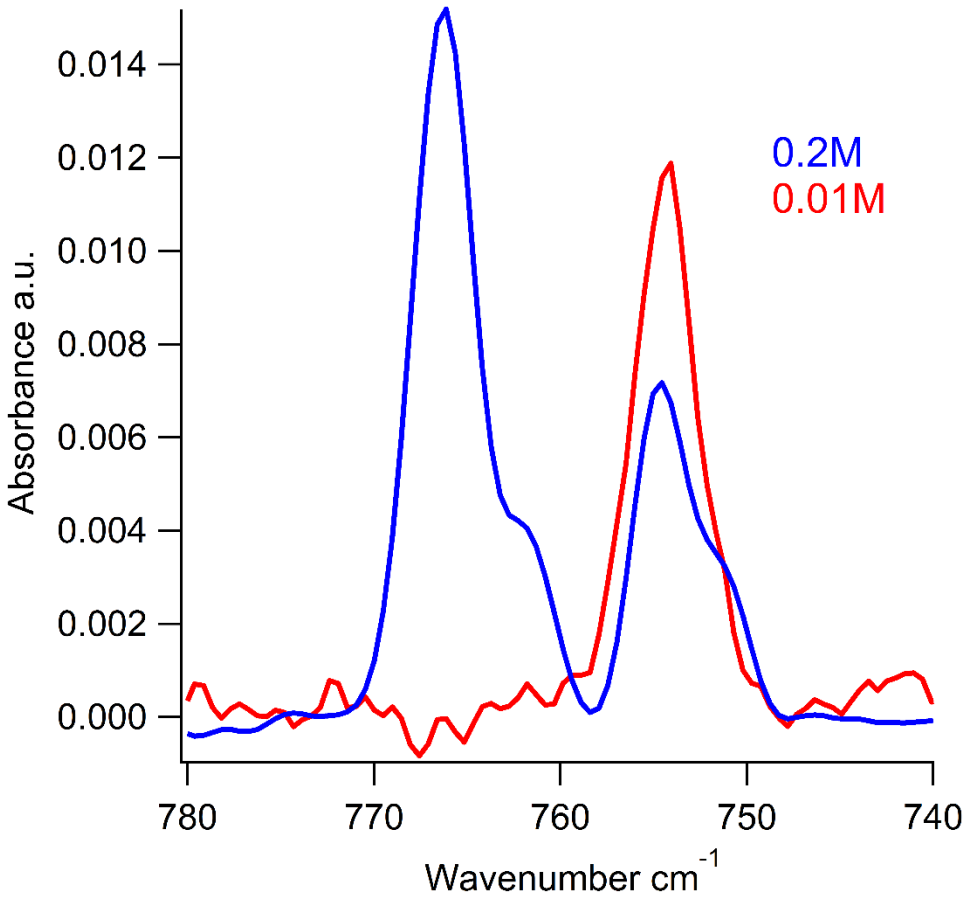


Figure 3.4. A close view of the 0.01M and 0.2M aluminum triflate in diglyme solutions. While primarily compose of free and coordinated triflate anions the shoulders of the 0.2M solution suggest complex ion pairing.

Figure 3.3 shows the $CF_3$ absorption region for four different concentrations of aluminum triflate in diglyme. The lowest frequency observed in the $CF_3$ region occurs at 752 $cm^{-1}$, similar to the peak position for free triflate in previous work, with a gradual progression in frequency to a maximum of 767 $cm^{-1}$ in the most concentrated solution. These frequencies are reasonably consistent with DFT calculations on free triflate in THF, which has a $CF_3$ vibrational frequency at 751 $cm^{-1}$, and an Al(diglyme)$_2$-triflate (figure 3.2B) complex in THF, which has a $CF_3$ vibrational frequency at 762 $cm^{-1}$. The shift observed in the $Al^{3+}$ based electrolyte extends over a slightly larger range of frequencies than that observed in monovalent ion solvate ionic liquids, e.g., $Li^+$ or $Na^+$ in glyme solvents[102,109]. Monovalent systems typically span regions of 10 $cm^{-1}$ for solution phase systems while the present $Al^{3+}$ system spans 15 $cm^{-1}$ from the most dilute to most concentrated solution. It has been shown that the shift in the $\delta_s(CF_3)$ frequency depends on the degree of electron withdrawal from the triflate anion by the coordinating cation[114]. It seems reasonable to postulate

that an aluminum ion would have a stronger electron withdrawing effect compared to a lithium ion. This in turn could cause the $\delta_s(CF_3)$ frequencies to shift to higher values than seen for monovalent systems. The FTIR spectra of the $Al(diglyme)_2$ electrolytes offer experimental evidence of this postulate. Further, it is interesting to note that monovalent systems generally show evidence of three spectroscopically measureable ion configurations at all concentrations[109,113] while the $Al(diglyme)_2$ electrolyte shows preliminary evidence of higher complexity. For example, three peaks appear at the extreme low and high concentrations, 10 mM and 2.8 M, while the mid-range concentrations show evidence of at least 4 peaks for the 1 M and possibly 5 peaks for the 0.2 M electrolytes. Preliminary curve fitting indicate 3 overlapping peaks to be present in the 10 mM electrolyte, centered at 752, 755 and 757 $cm^{-1}$. Increasing the concentration to a ratio of 0.2 M results in the appearance of 2 additional peaks, centered at 761 and 766 $cm^{-1}$ with no change in the center of the first 3 peaks. This trend continues for 1 M with 4 peaks, centered at 757, 761, 766 and 771 $cm^{-1}$. Finally, at 2.8 M only 3 peaks are observed, centered at 761, 766 and 771 $cm^{-1}$.

Again it should be pointed out that the exact nature of the speciation present in these solutions is being investigated. However, by making the assumption that the ion pairing of Al[DG]2 follows the trends seen in lithium triflate systems initial, tentative assignments are possible.

Based on the results of previous studies the lowest observable wavenumber, 752 $cm^{-1}$, can be assigned to "free" triflate anions. These "free" anions exist only in the dilute solutions (the 10 mM and 0.2 M $Al(diglyme)_2$ systems) with no evidence of their existence in the more concentrated electrolytes. The second band, at 755 $cm^{-1}$, has no clear analogue in previous studies but may be postulated to be a partially coordinated or solvent separated triflate anion. It is likely this configuration consists of an aluminum ion coordinated by two diglyme molecules with a partially coordinated triflate in the secondary solvent shell of the ion. This assignment is based upon the intermediate degree of shift, 3 $cm^{-1}$, versus the 5 $cm^{-1}$ shift observed between free anions and contact ion pairs in prior studies[113,114]. The 757 $cm^{-1}$ band is assigned to contact ion pairs (CIPs) followed by dimers at 761 $cm^{-1}$. The assignments of the 766 $cm^{-1}$ and 771 $cm^{-1}$ bands are more difficult and require extension of data taken from crystalline lithium – glyme systems as well as LiTf in a furan solvent to solution phase aluminum – diglyme data, thus making the assignments tentative. Based on solution phase data from LiTf in 2-methyltetrahydrofuran and corresponding ab initio modeling the 766 $cm^{-1}$ band may be reasonably assigned as a triply coordinated triflate in which each oxygen of the $SO_3$ group is coordinated to a cation[114]. This phase is termed 'psuedo crystalline' due to its existence in both crystalline phase LiTf – monoglyme and solution phase LiTf – 2-methyltetrahydrofuran[113,114]. The 771 $cm^{-1}$ band is very close in

frequency to the 770 $cm^{-1}$ band observed in room temperature crystalline LiTf – monoglyme and is therefore assigned as being due to micro-crystalline regions in the concentrated $Al(diglyme)_2$ electrolytes. In some of the more concentrated $Al(diglyme)_2$ solutions (concentration > 1M) a very fine precipitate was observed to form in sealed vials after considerable time (several months) which slowly settled. Unfortunately this precipitate was too fine to isolate for analysis, however it lends additional support, albeit qualitative, to the micro-crystalline assignment of the 771 $cm^{-1}$ band.

## Evidence of complex ion pairing

While the above assignments are speculative it is apparent from the shoulders in the FTIR spectra that some degree of complex ion pairing is occurring. This is also supported by $^{19}F$ NMR of the 10mM and 0.2M solutions. The NMR data, below, clearly shows a change from three distinct peaks in 10mM to 5 peaks in 0.2M.

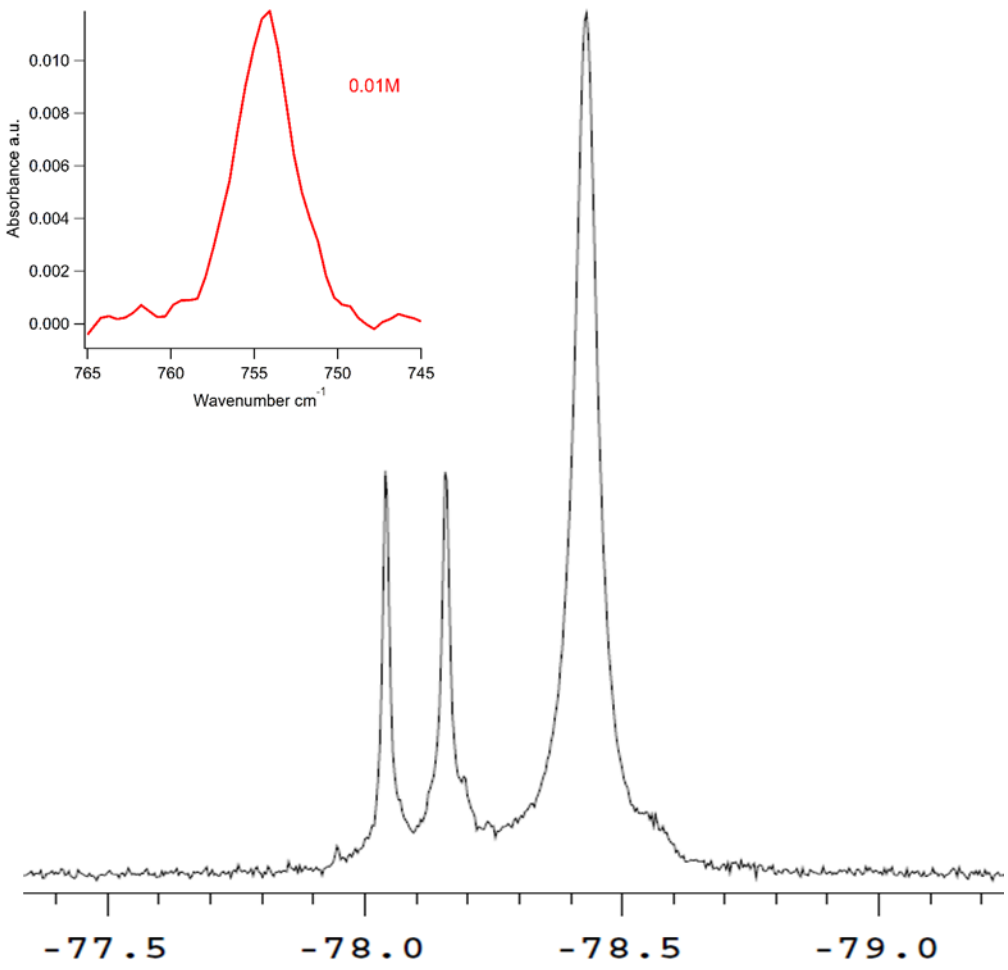


Figure 3.5. $^{19}F$ NMR of the 0.01M aluminum triflate in diglyme solution, inset showing the FTIR spectra. The three peaks in the NMR spectra suggest three distinct chemical environments of the $^{19}F$ nuclei, possibly indicating multiple types of ion pairs.

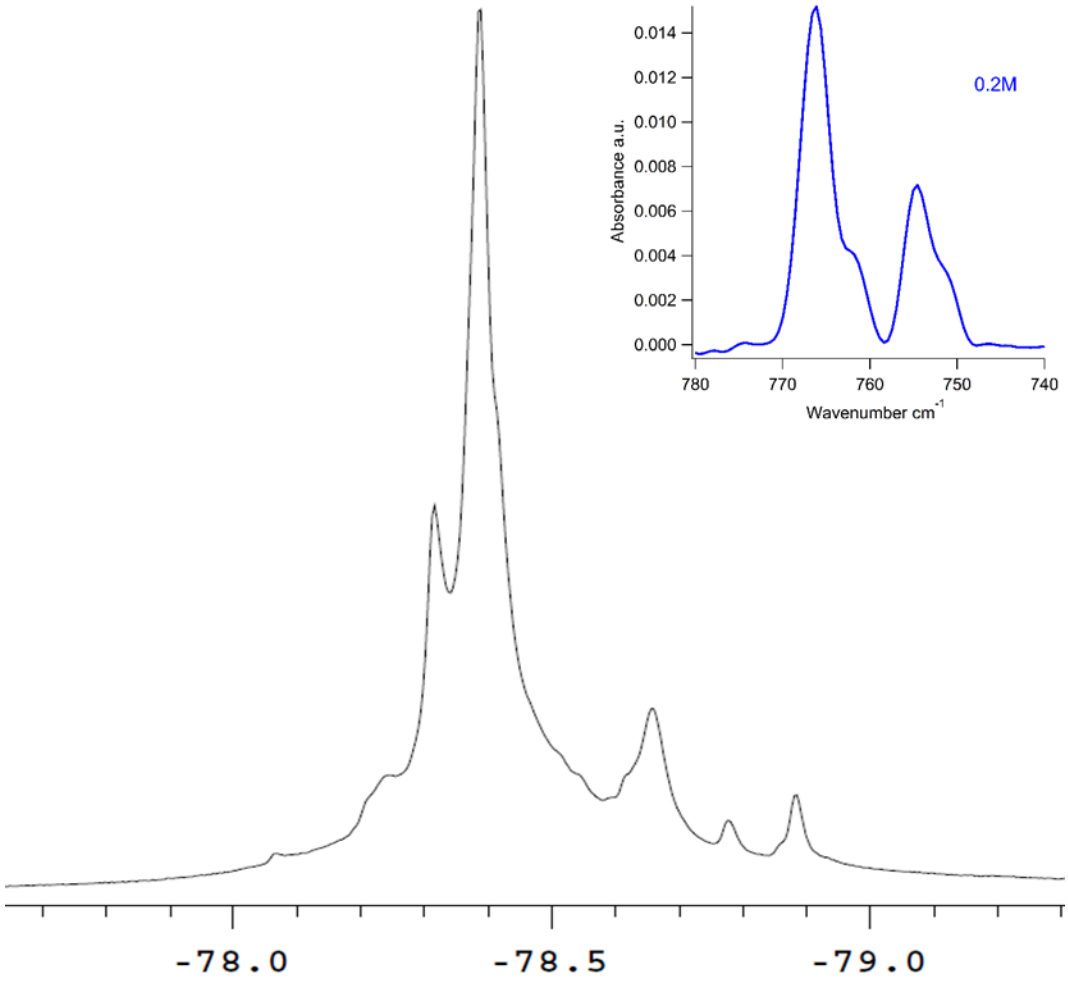


Figure 3.6. 19F NMR of the 0.2M aluminum triflate in diglyme solution, showing five distinct peaks, inset showing the FTIR spectra. The NMR spectra suggests a complex ion pairing environment.

Definitive assignments of ion pairing will require a careful set of experiments examining the trends in IR and NMR spectra as a function of concentration.

## Electrochemical characterization

Cursory analysis of the anodic region of the cyclic voltammograms of the electrolytes shows an increase of the oxidation edge as the concentration of aluminum triflate is increased, similar to previously published results on lithium and sodium triflate in diglyme[102,103]. However, because of the concentration dependent potential of the pseudo-reference electrode it is important to examine the entire electrochemical window as changes in

cathodic stability should also be expected. As seen in figures 3.7A and 3.7B the oxidation onset potential shifts by approximately 0.3 volts from 10 mM to 0.2 M, smaller shifts of about 0.2 volts and 0.3 volts are evident between 0.2 M and 1 M and between 1 M and 2.8 M, respectively. A larger shift of approximately 0.5 volts is observed in moving from 2.8 M to 3.5 M (not shown). This enhanced anodic stability has previously been attributed to the lowering of the HOMO level of the complex by the electron withdrawing effect of the solvated cations[102,103,108,115]. In the more dilute solutions the overall HOMO of the solution is dictated by the free diglyme, resulting in a lower relative anodic stability limit. As the concentration of the salt is increased the relative number of free diglyme molecules is reduced and an increase in anodic electrochemical stability is observed. As shown below the lowering of the HOMO continues to enhance the anodic edge of the electrochemical window until the HOMO of the triflate anion is higher in energy than the HOMO of the $Al(diglyme)_2$ complex.

Examining the entire electrochemical window reveals complex, concentration dependent behavior of the cathodic edge. Figure 3.7A shows the total potential window as a function of concentration. The lowest concentration shows the smallest potential window, approximately 6V, with an increase to 6.5V at 0.2 M, a decrease to 6.2V at 1 M and a maximum of 6.7V at 2.8 M. Further study is underway to understand how the complex interactions of concentration, activity, viscosity and solution structure dictate the total electrochemical window.

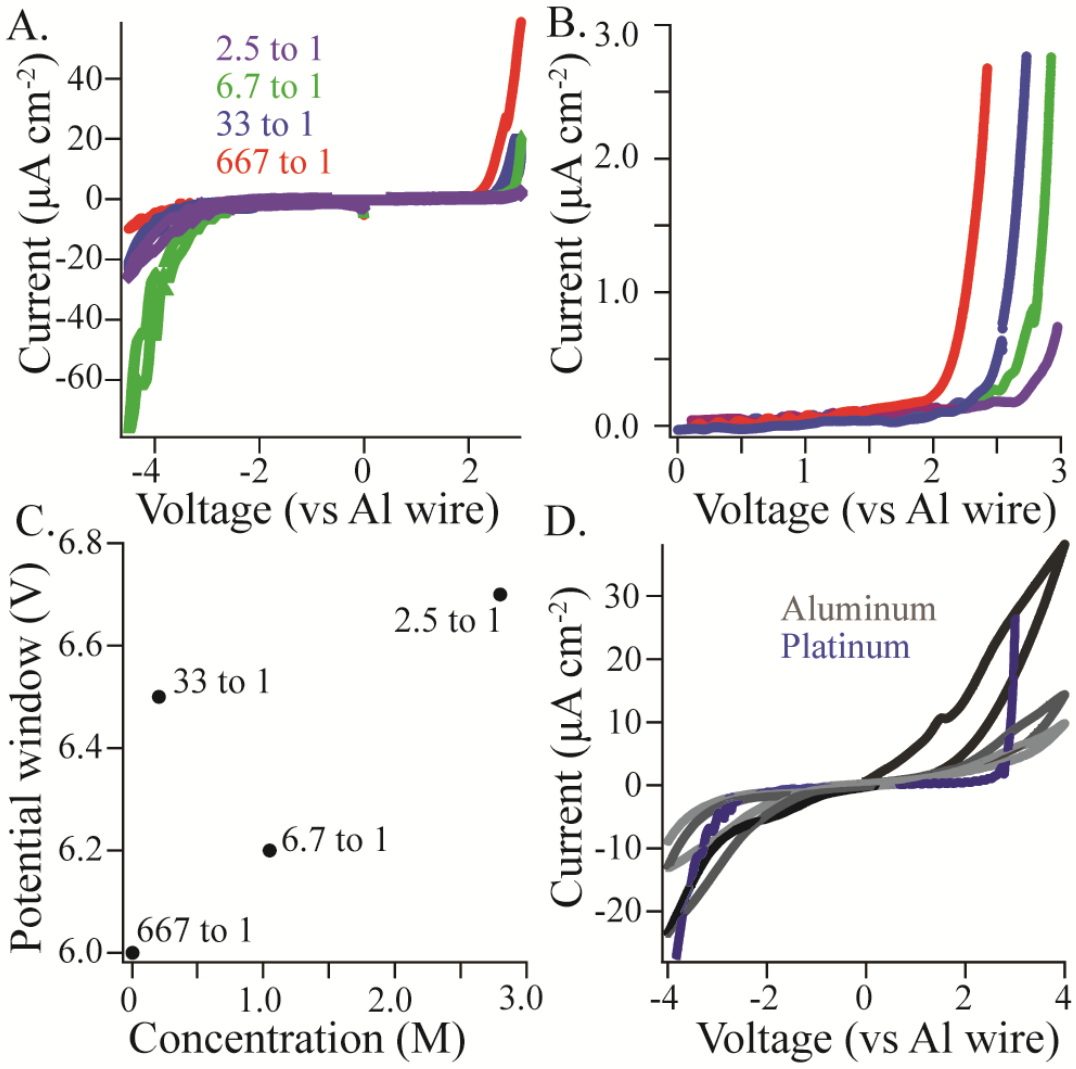


Figure 3.7. A) Cyclic voltammograms of 2.5:1 (purple), 6.7:1 (green), 33:1 (blue), and 667:1 (red) diglyme:aluminum triflate solutions on a platinum electrode. B) Expansion of the anodic potentials from A, showing a shift in oxidation potential as the aluminum triflate concentration increases. C) Electrochemical window of the electrolytes, showing a general increase in stability as the aluminum triflate concentration increases. D) Cyclic voltammograms of the 6.7:1 solution on a platinum working electrode (blue) compared with an aluminum working electrode, showing the electrochemical activity and passivation of the aluminum metal and the inactivity of the platinum.

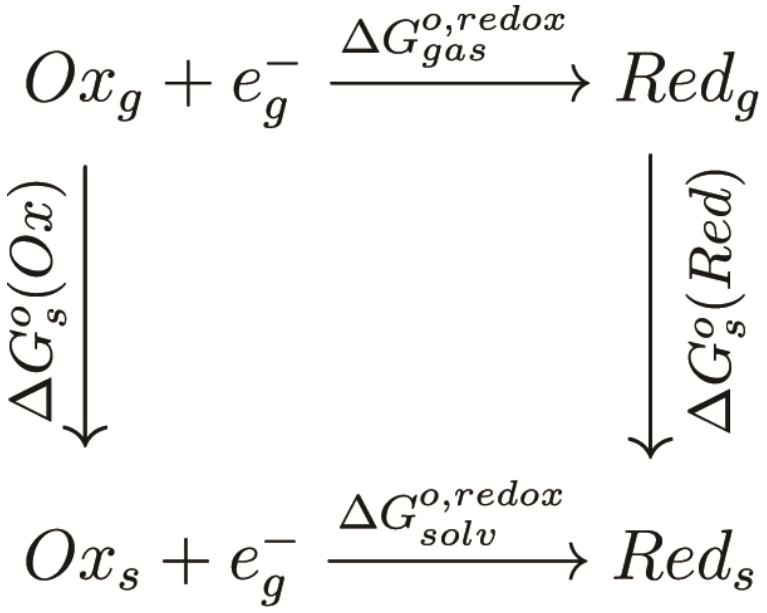


To better understand the change in electrochemical window, the Gibbs free energy change associated with the solution-phase reduction of six redox couples (diglyme oxidation and reduction, triflate oxidation and reduction, and the Al(diglyme)$_2$ complex oxidation and reduction) was calculated using the Born-Haber cycle shown above[116,117]. This Gibbs free energy is then converted to an absolute reduction potential using equation 1.

$$E_{calc}^{abs} = -\frac{\Delta G_{solv}^{o,redox}}{nF} \qquad (1)$$

where F is Faraday's constant, n is the number of electrons involved in the reduction, and the solution-phase Gibbs free energy is:

$$\Delta G_{solv}^{o,redox} = \Delta G_{gas}^{o,redox} + \Delta G_s^o(Red) - \Delta G_s^o(Ox) \qquad (2)$$

The results of these calculations are summarized in Table 3.1.

Table 3.1. Gibbs free energies and absolute reduction potentials of solvent, anion and complexes.

| Reaction | $\Delta G_{gas}^{o,redox}$ (hartree) | $\Delta G_s^o(Red)$ (hartree) | $\Delta G_s^o(Ox)$ (hartree) | $E_{calc}^{abs}$ (volts) |
|---|---|---|---|---|
| $Diglyme^+ + e^- \rightarrow Diglyme$ | -0.307566 | -0.007879 | -0.076279 | 6.508 |
| $Diglyme + e^- \rightarrow Diglyme^-$ | 0.083992 | -0.064593 | -0.007879 | -0.742 |
| $Triflate + e^- \rightarrow Triflate^-$ | -0.177474 | -0.071271 | -0.005188 | 6.627 |
| $Triflate^- + e^- \rightarrow Triflate^{2-}$ | 0.193534 | -0.272905 | -0.071271 | 0.220 |
| $Al(Dg)_2^{4+} + e^- \rightarrow Al(Dg)_2^{3+}$ | -0.735813 | -0.48723 | -0.854533 | 10.027 |
| $Al(Dg)_2^{3+} + e^- \rightarrow Al(Dg)_2^{2+}$ | -0.377725 | -0.226205 | -0.48723 | 3.176 |

From these calculations we predict that the electrochemical window for neat diglyme will be approximately 7.2 volts. As we increase the concentration of aluminum triflate, however, the oxidation edge will increase slightly as it becomes dominated by oxidation of the triflate anion, not the oxidation of the metal-diglyme complex as predicted by other work,[103] while the reduction edge will increase significantly as it becomes dominated by reduction of the aluminum-diglyme complex, resulting in an electrochemical window of approximately 3.5 volts at high aluminum triflate concentrations. While the measured electrochemical window for these electrolytes is wider than 3.5 volts, much of that can be attributed to kinetic factors as we expect electron transfer to the $Al(diglyme)_2$ complex to be slow, leading to a large overpotential, which is supported by the activity of the aluminum working electrode and inactivity of the platinum working electrode shown in figure 3.7D.

## Electrochemical activity of $Al^{3+}$

In contrast to the cyclic voltammograms measured on a platinum wire, the voltammograms on an aluminum working electrode, shown in figure 3.7D, show immediate electrochemical activity, which can be attributed to electrochemical accessibility of the $Al/Al^{3+}$ redox reaction. Although the aluminum is electrochemically active in the electrolyte it is apparent upon repeated cycling that passivation takes place during the course of cycling the anode. The observed passivation can be attributed to the formation of aluminum-fluoride surface species over time, as this behavior is well known from investigations of aluminum current collector corrosion in the presence of fluoride-based anions in lithium ion batteries[118–120].

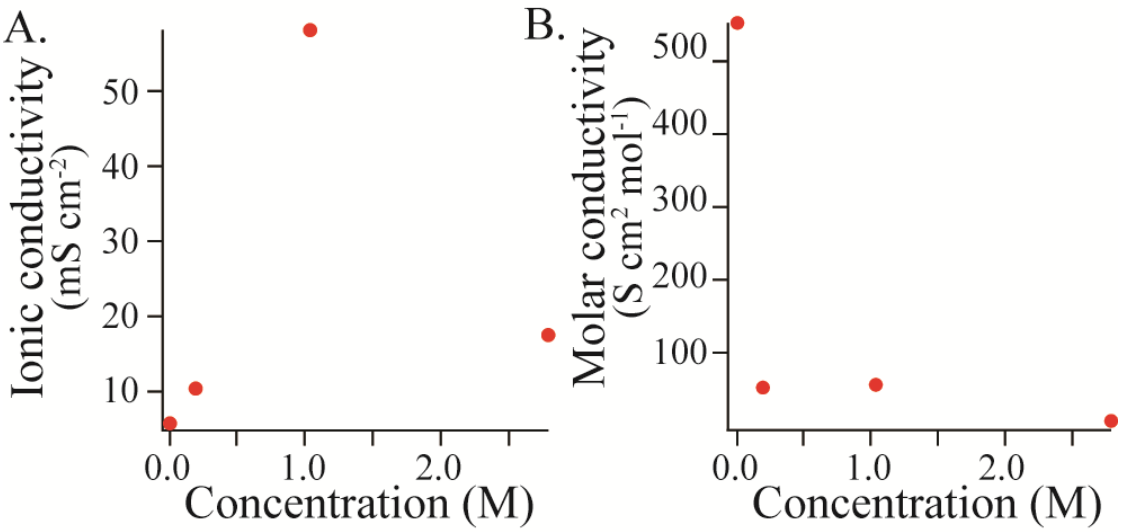


Figure 3.8. A) Ionic conductivity of the solution as a function of aluminum triflate concentration. B) Molar conductivity of the solution as a function of aluminum triflate concentration. The shape of the curve clearly indicates the weak electrolyte nature of the solvate ionic liquid.

### Solution conductivity

Electrolyte conductivities were measured using electrochemical impedance spectroscopy with a two electrode platinum cell. The conductivity at 60C shown in Figure 3.8A shows an initially low value at high concentration followed by a maximum of 55mS $cm^{-2}$ at a ratio of 6.7 to 1. While the measured conductivity is high it is not unprecedented and is elevated substantially by the increased temperature[121]. The fluctuating behavior of the molar conductivity, has been observed in other concentrated electrolyte systems and is due to the formation of ion pairs, aggregates and the change in viscosity with changing concentration[109,112].

## 3.4 Conclusions and future work

The spectroscopic, electrochemical and computational analysis of a multivalent solvate ionic liquid have been presented. The concentration dependent trends in the physicochemical properties of the electrolytes offer insight into the solvation and ion pairing character of the solutions. In contrast to the 3-4 peaks present in FTIR spectra of monovalent solvate ionic liquids, the FTIR spectra of the Al-diglyme electrolytes show 5-6 distinct peaks in the 752 to 771 $cm^{-1}$ region indicating more complex ion pairing due to the increased charge density of the $3^+$ cation. Initial assignments of ion configurations have been made based upon comparison with previous literature and computational results. Cyclic voltammetry shows an increase in electrochemical window of approximately 700mV between the most dilute and most concentrated electrolyte, with a local minimum observed at an intermediate concentration. DFT calculations show that the cathodic edge of the window is governed by the reductive stability of the $Al(diglyme)_2$ complexes and the anodic edge is governed by the oxidative stability of the triflate. The predicted electrochemical window ranges from 7.2V for neat diglyme to 3.5V for highly concentrated electrolyte. The discrepancy between the calculated, 3.5V, and measured, 6.7V, window for the most concentrated electrolyte can be explained by a large increase in viscosity as well as slow electron transfer kinetics, leading to a large overpotential. The ionic conductivity shows a maximum value of 55 mS $cm^{-1}$ for the 6.7:1 electrolyte at 60C while the molar conductivity of the solutions exhibits concentration dependent behavior characteristic of a weak electrolyte.

### Some additional electrochemical data.

In light of the somewhat unclear nature of the electrochemical response of the electrolytes some additional data on the electrochemical window, figure 3.9,

and conductivity, figure 3.10, is shown below. First, it is apparent that at low concentrations the predicted and measured value of the electrochemical window agree reasonably well. At high concentrations this agreement rapidly diverges as physical properties of the electrolyte (viscosity) begin to affect the measurements. The minimum in the electrochemical window at approximately 1 M can be explained by noting that the conductivity of the solution is maximized at 1 M. The kinetic hindrance to electrochemical activity of the electrolyte will be minimized at maximum conductivity and the measured window will most closely approach reality. At high concentrations (>3 M) the diffusion of electroactive species is extremely slow and the overpotential for oxidation / reduction becomes large.

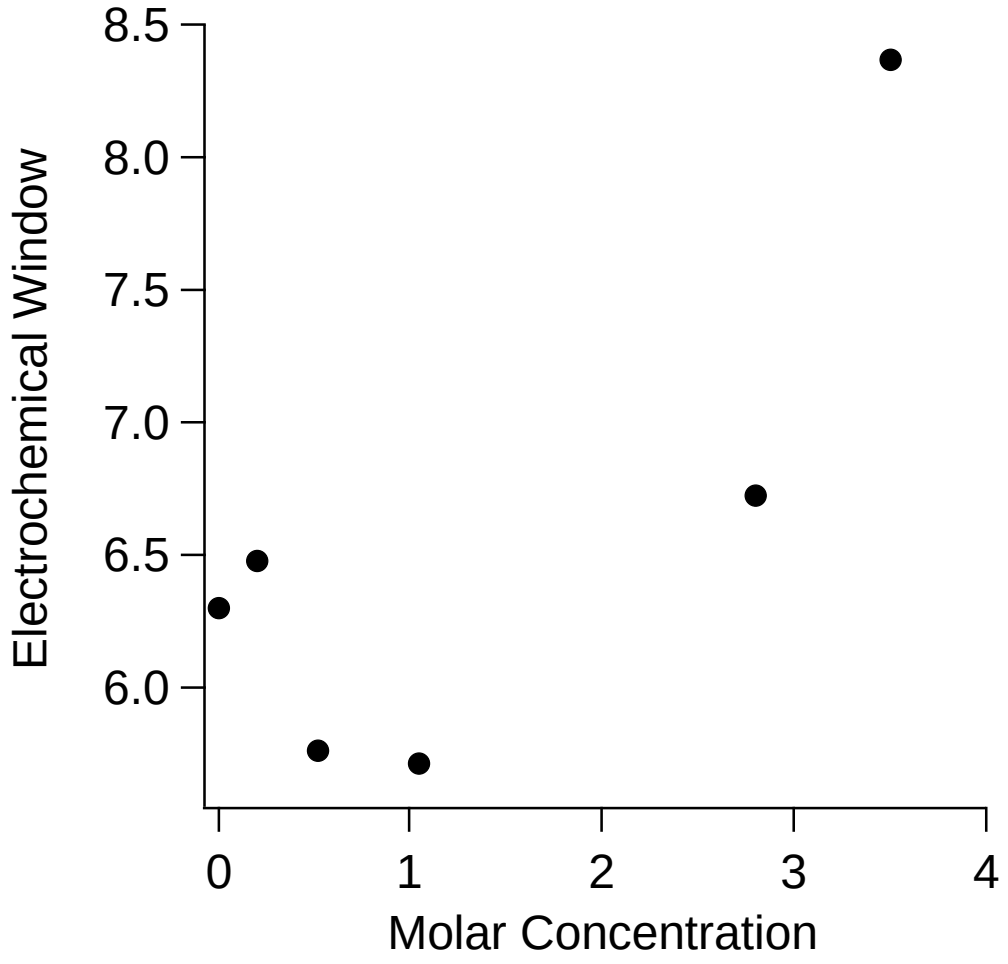


Figure 3.9. The electrochemical window of the electrolytes as a function of concentration. The details of the fluctuation are discussed in the text.

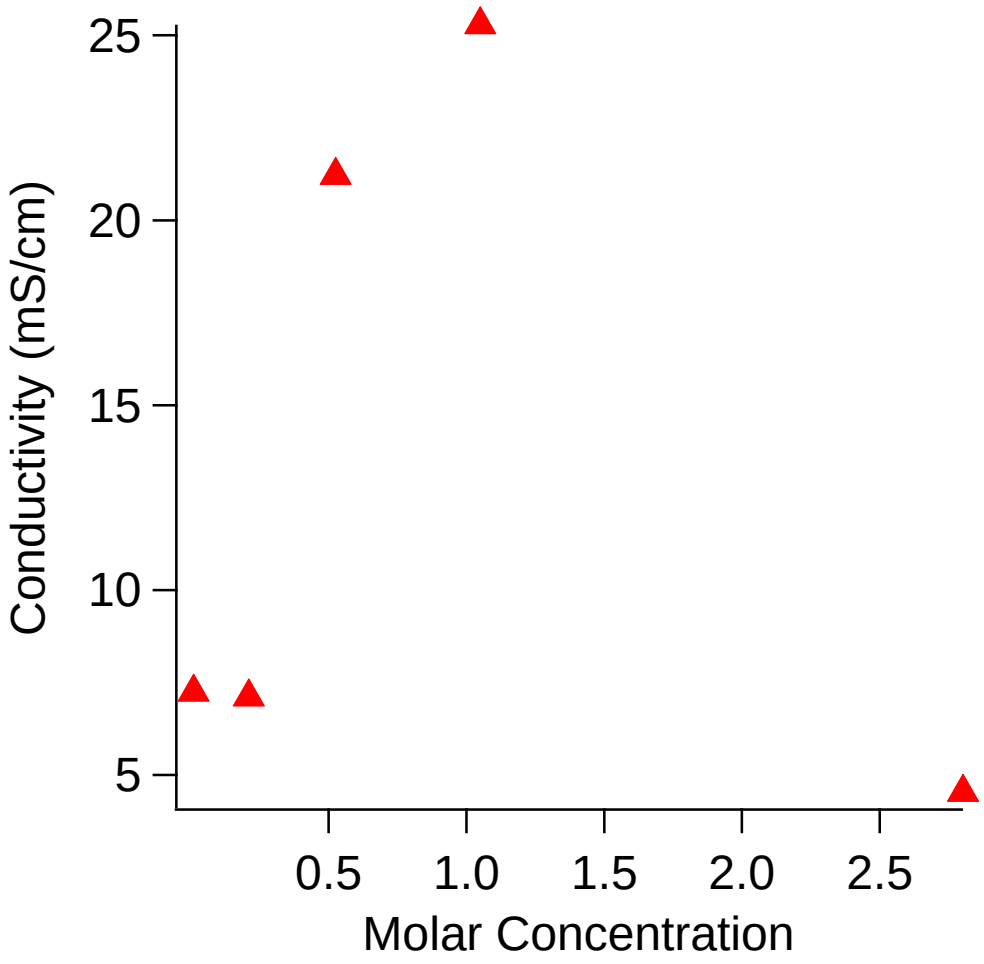


Figure 3.10. The ionic conductivity versus the molar concentration. The correlation of the maximum with the minimum seen in the electrochemical window is discussed in the text.

# Chapter 4

# A Rechargeable Aluminum-ion Battery Utilizing a Copper Hexacyanoferrate Cathode in an Organic Electrolyte

# 4.1 Introduction: Prussian blue and its analogues

Prussian blue, or ferric hexacyanoferrate, has been known for hundreds of years as a vivid blue dye. It is simply made by addition of a solution of an iron 2+ salt to a solution of potassium ferricyanide, resulting in the immediate precipitation of a nanoscale crystal in the $Fm\bar{3}m$ space group. The figure below shows the precipitation of Prussian blue.

Figure 4.1. Aqueous precipitation of Prussian blue. Used with permission under the creative commons license from: https://www.flickr.com/photos/jurvetson/6627153/

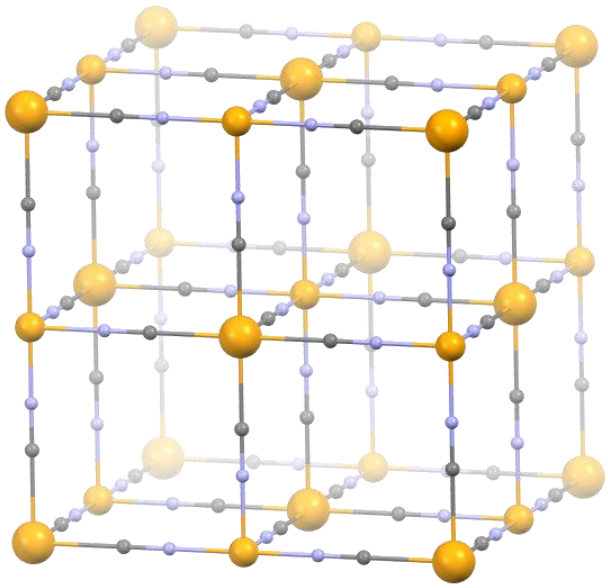

Figure 4.2. Crystal structure of ferric hexacyanoferrate; face centered cubic, Fm$\bar{3}$m space group. The 'A' sites, centered in the small sub-cubes, allow rapid, reversible intercalation/deintercalation of several ions in aqueous electrolytes.

Figure 4.2 shows the crystal structure of ferric hexacyanoferrate. The electrochemical properties of Prussian blue have been studied by detailed electrochemical analysis[122,123]. Because of the large interstitial sites and the rigid nature of the cyano-bridged framework the electrochemical cycling of Prussian blue in aqueous electrolytes shows remarkably small hysteresis. This results in high coulombic efficiencies, 99% at moderate currents, and extremely long cycle life, >40000 cycles, with small capacity loss[124]. Analogues of Prussian blue, in which the $Fe^{2+}$ centers are exchanged for alternative transition metal ions, can possess gravimetric capacities greater than ferric hexacyanoferrate. This is due to multiple redox centers being accessible during cycling. The copper analogue of Prussian blue, $CuFe(CN)_6$, shows theoretical capacities of approximately 70 mAh/g with experimental values of 55 to 60 mAh/g being common in the literature[124–127]. The unusual stability of Prussian blue and its analogues

as well as the simplicity of their synthesis make these materials appealing for use as battery cathodes.

This work presents the first known example of reversible aluminum intercalation / deintercalation from an organic electrolyte using a copper hexacyanoferrate cathode. Computations and experimental evidence suggest that an aluminum-solvent complex is the intercalating species. The system shows initial discharge capacities as high as 60mAh/g with characteristic reversible capacities of 14mAh/g based on total cathode mass.

To date, rechargeable batteries have primarily depended upon the well-explored electrochemistry of monovalent lithium ions. It is unquestionable that the monovalent systems have enabled technological revolutions over the last several decades and substantial improvements in power and energy density may still be possible[128,129]. In spite of this, the potential for increased power, safety, sustainability and reduced cost as well as the promise of new insight into the fundamental nature of multivalent electrochemistry provide excellent motivation for investigation of multivalent systems. However, despite several decades of research into multivalent battery chemistries few examples of metal anode, secondary divalent systems exist and none have been shown for trivalent ions[96,130,131].

Research into multivalent chemistries for battery applications has been hindered by the difficulties in identifying suitable electrolytes and cathode materials. Most electrolytes identified to date have been highly flammable, corrosive or exhibit limited anodic stability[132,133]. Additionally, the insertion kinetics of multivalent ions are greatly hindered by strong columbic interaction with the host lattice[133,134]. This kinetic limitation places restrictions upon the possible cathode materials; requiring a combination of a highly open lattice to allow facile intercalation/deintercalation, sufficient redox centers near host sites to maintain charge neutrality in the presence of multivalent ions and stability against phase transitions under cycling[96]. These limitations drastically reduce the number of potential cathode materials, with Chevrel phase $M_6S_8$ (M = Mo, Te, Se) and analogues of Prussian blue ($Fe_4[Fe(CN)_6]_3$) being the most prominent systems showing clear evidence of electrochemical reversibility in the presence of multivalent ions[96,134–136]. In this communication we show that an ether based electrolyte and a copper-substituted Prussian blue analogue cathode facilitate reversible trivalent electrochemistry, thus demonstrating the first trivalent, secondary, non-aqueous cell in the literature.

# 4.2 Materials and methods

The CuHCF was synthesized following a standard precipitation method. Briefly, a 0.05M solution of $K_3Fe(CN)_6$ was slowly added, drop wise with strong stirring, to a 0.1M solution of $CuSO_4$. The resulting solution was stirred for 30 minutes, sonicated for two hours and allowed to stand overnight to facilitate the aggregation of crystallites, thereby simplifying the filtration process. The solution was then filtered, washed extensively with ultrapure water, 18MΩ-cm, and dried under vacuum at 70˚C overnight. The electrodes were prepared by grinding CuHCF and carbon black together in a mortar and pestle followed by addition of PVDF in NMP to achieve a weight ratio of 80:10:10, active material to carbon black to binder. The resulting slurry was applied to platinum strip current collectors which were dried under vacuum at 70˚C overnight with a resultant active mass loading of approximately 2 mg/cm$^2$. The aluminum triflate electrolytes were prepared in an argon-filled glove box (VAC Atmospheres, residual water and oxygen <0.5ppm) by addition of diglyme to the salt followed by stirring overnight. The electrochemical testing was carried out in a three-electrode cell using aluminum wire as the counter and reference electrodes. The data were collected on a Gamry Series G potentiostat.

## Materials Characterization

The crystal structure of the as synthesized CuHCF was analyzed by powder X-ray diffraction on Panalytical diffractometer from 10 to 70 degrees two theta. The reflections match the expected cubic $Cu[Fe(CN)_6]_2$ with space group $Fm\bar{3}m$ and correlate with JCPDS 53-0084. No evidence of impurities or secondary phases appear in the XRD spectrum.

## Computations

DFT calculations on the aluminum/diglyme complex were carried out in Gaussian 09 using the B3PW90 functional with a 6-311G (d) basis set[110].

## 4.3 Results and discussion

Prussian blue, a cyano-bridged coordination polymer, has been known for hundreds of years as a pigment. Its electrochemical properties were first investigated by Neff with further work by Itaya[122,123]. Little work was done on its application as a battery material until a resurgence in interest was spurred by work from the Cui group, where they describe its use as a fast, highly reversible and stable cathode material for aqueous rechargeable systems[124,137]. These initial reports, which investigated monovalent aqueous electrochemistry, were followed by reports on divalent ion insertion, most notably the work by Wang et al. which describes the electrochemistry of Prussian blue analogues in the presence various divalent ions, all of which showed reversible electrochemical behavior[38]. More recently Mizuno et al. described in detail the electrochemistry of the copper-analogue of Prussian blue (copper hexacyanoferrate, CuHCF) during cycling with aqueous $Mg^{2+}$. This work showed that in addition to the redox of the iron centers there is an additional redox peak attributable to the $Cu^{2+}$ to $Cu^{+}$ reduction[135,138].

Very few reports exist on the electrochemical behavior of aluminum ions in intercalation systems. Two recent papers have reported reversible electrochemistry of aluminum with an ionic liquid electrolyte in conjunction with $V_2O_5$ and $VO_2$[37,38]. Further work, however, subsequently demonstrated that these results are attributable to side reactions of the ionic liquid with the stainless steel current collectors rather than aluminum intercalation into vanadium oxides[40]. More recent reports make use of aqueous phase electrolytes with $TiO_2$ nanotubes and nanoleaves, 2D $Ti_3C_2$ and copper substituted Prussian blue[39,88,126,139,140]. While these reports show promising results the electrochemical data suggest primarily capacitive, rather than faradaic, charge storage is occurring.

Based on the natural extension of this recent work we have investigated CuHCF as a cathode material for aluminum ions in an electrolyte of aluminum trifluoromethanesulfonate (triflate) dissolved in diethylene glycol dimethyl ether (diglyme). Cyclic voltammograms (CVs) of 5:1 molar ratio diglyme:aluminum triflate on a CuHCF working electrode, shown in blue in Figure 4.3A, reveals little-to-no hysteresis and three sets of redox peaks, while CVs of 500:1 molar ratio diglyme:aluminum triflate on a CuHCF working electrode, shown in orange in Figure 4.3A, show only capacitive effects, indicating the CuHCF is active as a cathode material only in highly concentrated electrolytes.

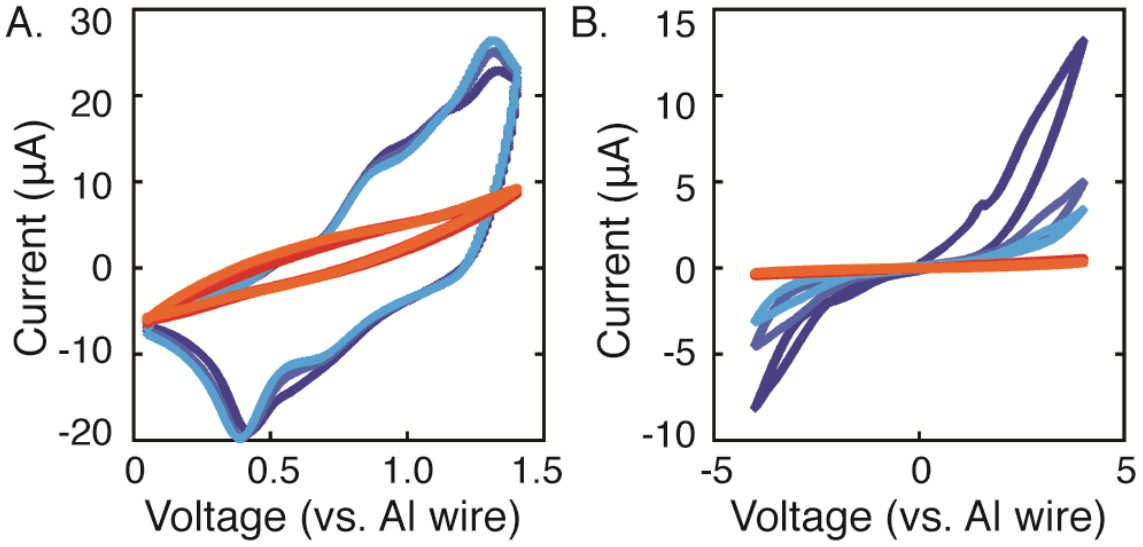


Figure 4.3. A) Cyclic voltammetry of a CuHCF electrode in 5:1 molar ratio diglyme:aluminum electrolyte (cycles 1-3, dark blue to light blue) and 500:1 molar ratio diglyme:aluminum electrolyte (cycles 1-3, dark red to light orange). Clear evidence of reversible redox chemistry is seen in the 5:1, while none is observed in the 500:1. B) Cyclic voltammetry of an aluminum electrode in 5:1 molar ratio diglyme:aluminum electrolyte (cycles 1-3, dark blue to light blue) and 500:1 molar ratio diglyme:aluminum electrolyte (cycles 1-3, dark red to light orange). Clear evidence of redox chemistry is seen in the 5:1 electrolyte, albeit with evidence of passivation effects, while none is observed in the 500:1.

While monovalent aqueous systems can access only the $Fe^{2+}/Fe^{3+}$ couple,[124,137] multivalent aqueous systems are able to access the redox chemistry of both Fe and Cu, as shown in recent work by Mizuno et al., due to the increased Lewis acidity and higher columbic charge density of the higher-valence ion[135]. Based on this, we hypothesize that the peaks in the CV at 0.45 volts and 0.85 volts versus $Al/Al^{3+}$ are due the $Cu^{+}/Cu^{2+}$ and $Fe^{2+}/Fe^{3+}$ redox couples, respectively[135]. Furthermore, we postulate that the third peak in the cyclic voltammogram, at 1.3 volts versus $Al/Al^{3+}$, results from the $Fe^{3+}/Fe^{4+}$ redox couple, as this has been shown to be accessible in other systems[141,142]. In addition to cyclic voltammograms on the CuHCF electrode, CVs on an aluminum wire in the 5:1 and 500:1 electrolyte exhibit very different behavior. The CVs, seen in Figure 4.3B, clearly show that the aluminum electrode is active in the 5:1 electrolyte, although evidence of passivation is apparent, while the aluminum electrode is inactive in the 500:1 electrolyte.

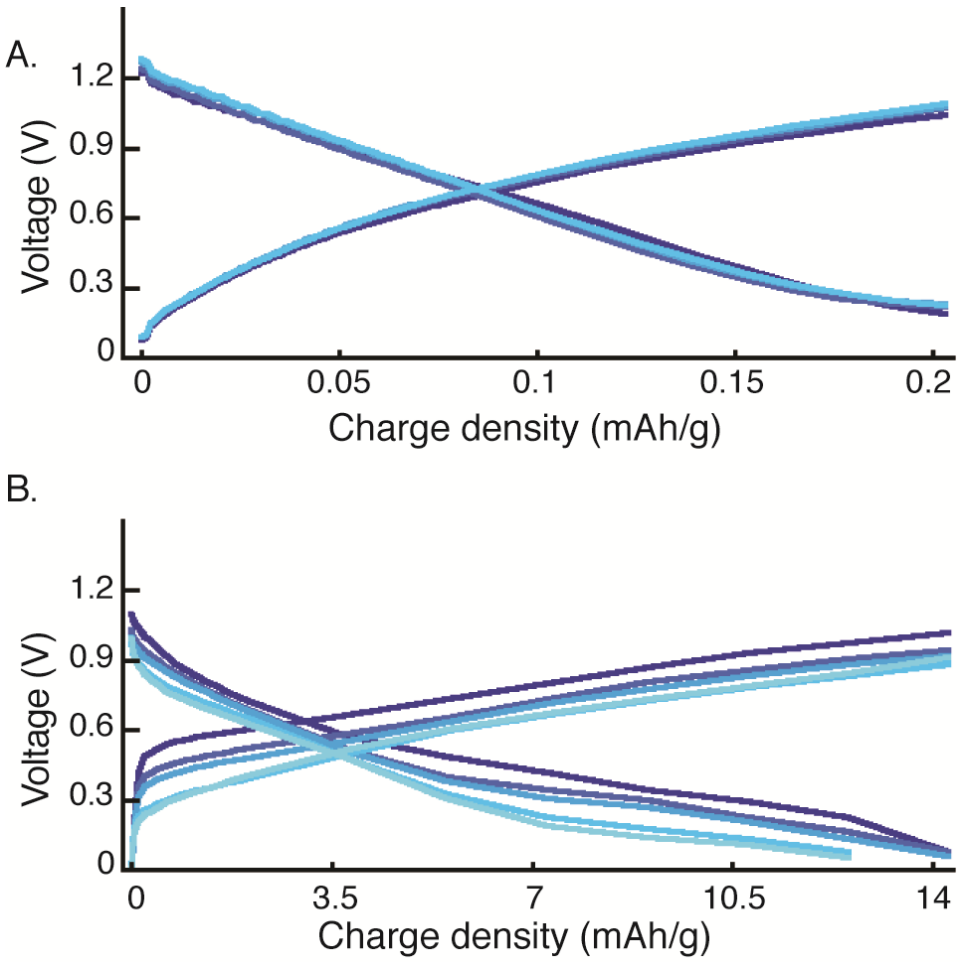


Figure 4.4. (A) 2nd, 5th, 10th and 15th charge/discharge cycles (dark blue to light blue) of a carbon black electrode exhibiting capacitive behavior with low charge density. (B) 2nd, 5th, 10th and 15th charge/discharge cycles (dark blue to light blue) of a CuHCF electrode showing a sloping discharge curve characteristic of a single-phase discharge reaction.

Charge/discharge curves for the aluminum triflate in diglyme on a carbon black electrode, shown in Figure 4.4A, exhibits purely capacitive behavior and very low charge-storage densities, while charge/discharge curves for the aluminum triflate in diglyme on a CuHCF electrode, shown in Figure 4.4B, exhibit a sloping discharge potential and large hysteresis, as well as much larger charge-storage densities. The sloping discharge potential and hysteresis is characteristic of a kinetically hindered insertion reaction,[143] which has also been observed in lithium ion systems, and has been attributed to the effects of nanoscale crystallites[144,145].

For the CuHCF cathodes, the specific capacity of the first discharge varied widely amongst tested electrodes, ranging from 24 to 60 mAh/g. In addition,

the cathodes showed varying levels of capacity fade, with some cathodes failing after 10 cycles and other cathodes lasting more than 50. The capacity fade of bi-metallic Prussian blue analogues is known to occur in lithium ion systems via phase separation and it is possible the same phenomenon occurs in the present study,[144,146–148] although the passivation of the aluminum anode, which was seen in the CV data in Figure 4.3B, probably also contributes to the capacity fade. The data shown in Figure 4.4B portrays a reversible capacity of 14 mAh/g, based on total cathode mass, with a columbic efficiency of 89 percent for the cycles shown, which is fairly typical across cathodes. Based on a calculated theoretical capacity of 73 mAh/g for one $Al^{3+}$ ion inserted per CuHCF unit cell versus the obtained reversible capacities of approximately 14 mAh/g, it is likely that only a partial intercalation is possible when good reversible behavior is seen.

Figure 4.5A shows the computationally optimized geometry of a diglyme-chelated aluminum ion ($Al(Di)_2^{3+}$), showing hexadentate coordination with the diglyme oxygens, similar to lithium-diglyme and sodium-diglyme complexes observed in solvate ionic liquids[103,115]. Figures 4.5B and C show the cubic unit cell of CuHCF, with zeolitic water and vacancy sites omitted for clarity, and the powder XRD pattern obtained from the as synthesized material respectively. The reflections match the expected cubic $Cu[Fe(CN)_6]_2$ with space group $Fm\bar{3}m$ and correlate with JCPDS 53-0084, in good agreement with prior results[146], no evidence of impurities or secondary phases were evident.

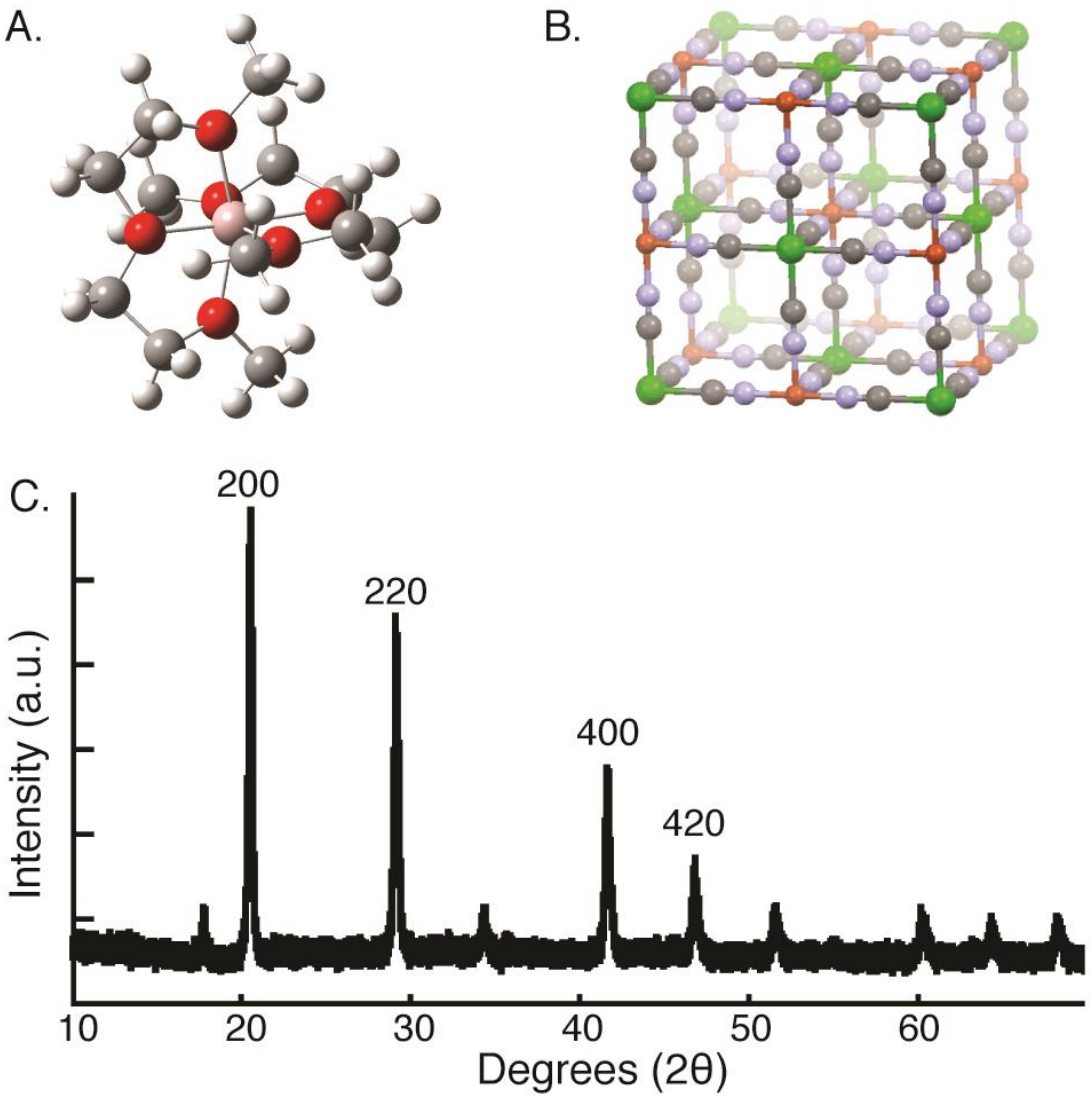


Figure 4.5. (A) The Gaussian optimized structure of the aluminum-diglyme complex with a diameter of approximately 7Å. (B) A representation of the cubic CuHCF unit cell, with an edge length of approximately 10Å. (C) Powder XRD of the synthesized CuHCF obtained with CoK(α) radiation of wavelength 1.79801Å.

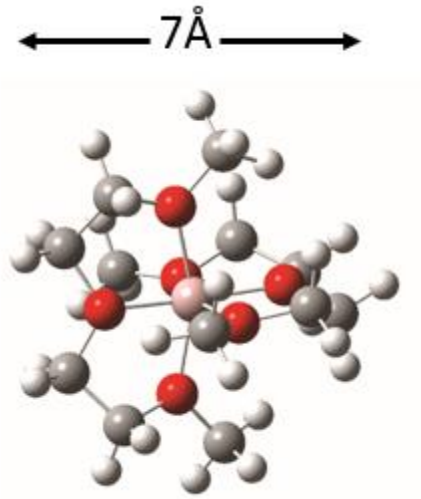


Figure 4.6. The Guassian predicted size of the aluminum/diglyme complex is approximately 7A. Because of the high stability of the complex it is unlikely that any significant desolvation of the $Al^{3+}$ occurs during intercalation. Thus, it is likely that the entire complex intercalates/de-intercalates during cycling.

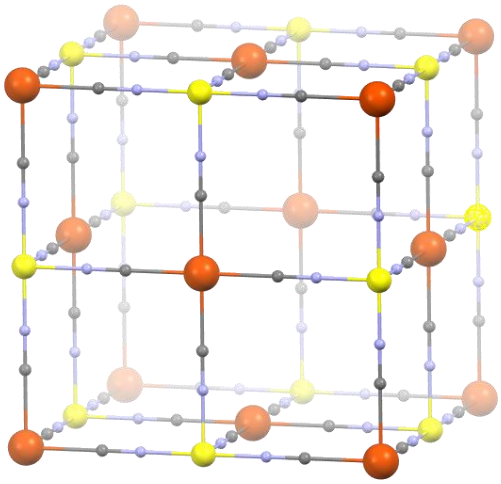

Figure 4.7. The crystal structure of copper hexacyanoferrate showing a metal-$(CN)_6$ vacancy. The size of the vacancy sites is approximately 5A and we hypothesize these are the sites of intercalation/de-intercalation for the aluminum/diglyme complexes.

The literature reports $Fe(CN)_6$ vacancies of approximately 25% in Prussian blue and its analogues[149,150]. These vacancies present a larger pore diameter of approximately 5Å compared to the interstitial sites with a diameter of 3.2Å[38]. Given the calculated diameter of approximately 7Å for an $Al(Di)_2^{3+}$ complex

and the high energetic barrier to desolvation of the aluminum ions it is unlikely that reversible intercalation/deintercalation would occur via routes other than the vacancy sites. Based on these calculations and measurements we hypothesize that the behavior of the CuHCF cathode in the aluminum triflate/diglyme electrolyte is governed by the aluminum/diglyme complex, rather than aluminum ions, intercalating into the copper-analogue Prussian blue cathode. Additionally, intercalation of the complex would minimize electrostatic interactions between the metal ion and the cathode and allow for reversible intercalation/deintercalation, similar to an intercalation mode previously observed for magnesium intercalation into $V_2O_5$[134].

## Capacity fade

The capacity fade of hexacyanoferrate materials in aqueous electrolytes is remarkably small. It is therefore somewhat surprising to observe rapid capacity loss in the aluminium/diglyme electrolyte. To gain some insight into the possible mechanism of capacity loss x-ray diffraction studies were performed. The electrochemical response of an electrode over several cycles, below, shows the capacity fade as a function of cycle number. The x-ray diffraction patterns of several electrodes as made and after treatment are also shown.

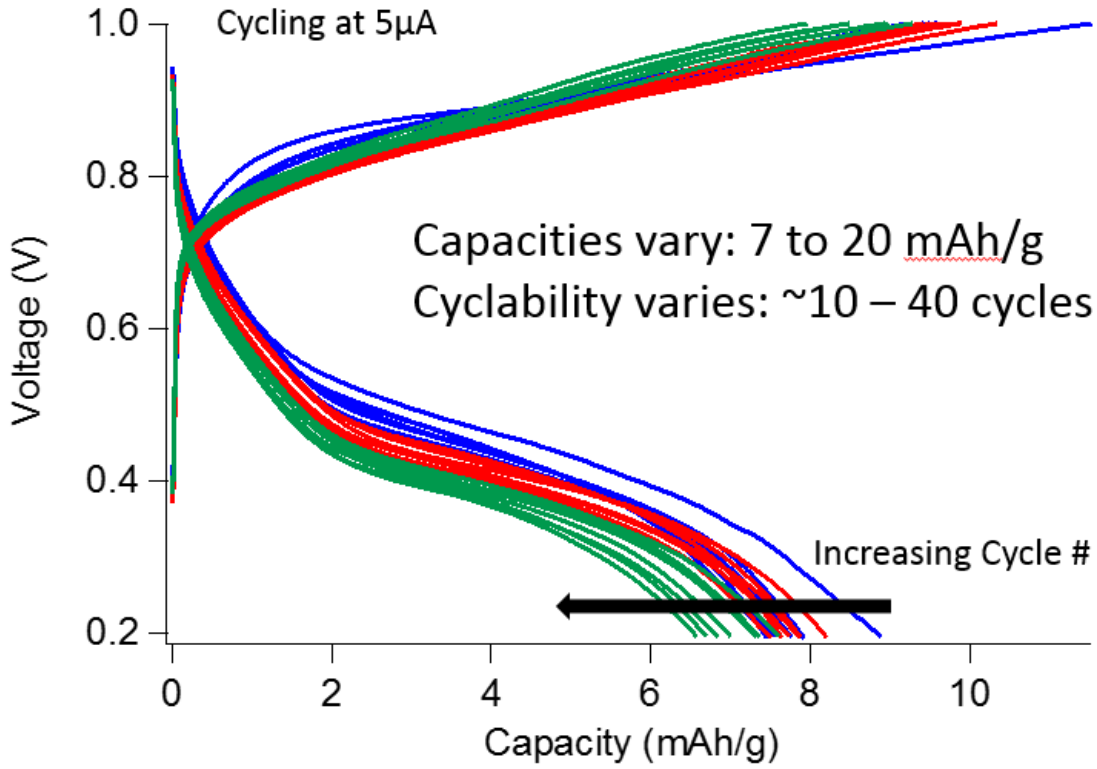


Figure 4.8. Cycling data of a CuHCF electrode showing the capacity fade as cycling occurs.

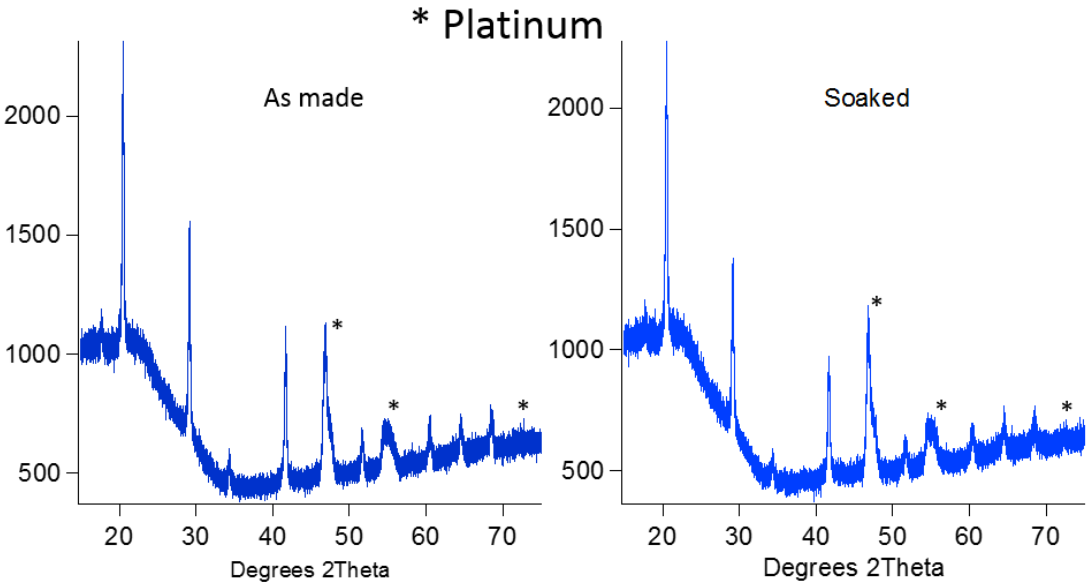


Figure 4.9. The x-ray diffraction patterns of an electrode, as made, and after soaking in the 1M aluminum/diglyme electrolyte for 5 days. The patterns show minimal changes, indicating good chemical stability of the CuHCF in the electrolyte.

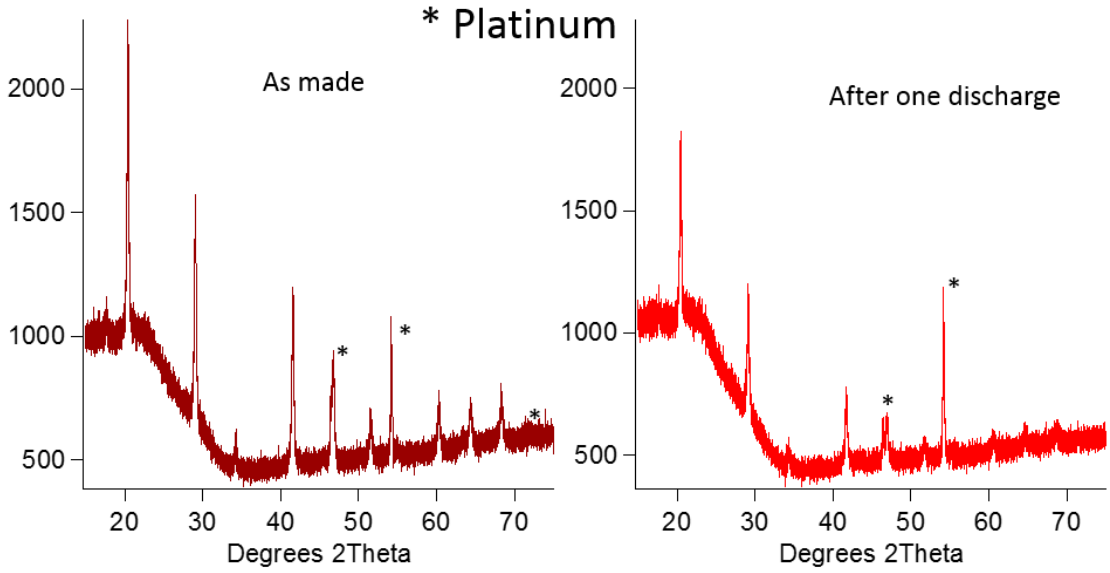


Figure 4.10. The x-ray diffraction patterns of a CuHCF electrode, as made, and after first discharge. Loss of peak intensity is evident, indicating some loss of crystallinity and possibly increasing amorphous character.

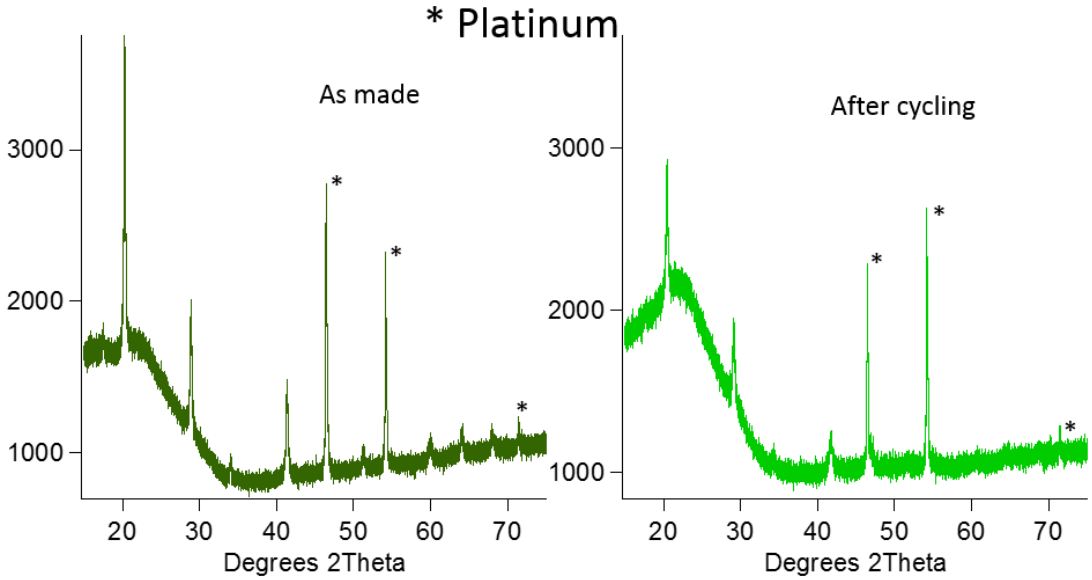


Figure 4.11. X-ray diffraction patterns of a CuCHF electrode after being cycled ~20 times in 1M aluminum/diglyme electrolyte. There is clear loss of peak intensity as well as an amorphous bump at low 2Theta. The data indicate dramatic loss of crystallinity of the CuHCF crystal structure after repeated electrochemical cycling.

## 4.4 Conclusions and future work

In summary we have shown initial results for a CuHCF electrode in the presence of aluminum triflate in diglyme. This system shows the first known results for a non-aqueous trivalent electrochemical system demonstrating any degree of reversibility. Initial discharge capacities as high as 60mAh/g were obtained with reversible capacities of 14mAh/g. The cyclic voltammograms indicate redox activity of $Fe^{2+}/Fe^{3+}$ and $Cu^{+}/Cu^{2+}$ and also a third redox peak that may be due to the $Fe^{3+}/Fe^{4+}$ redox couple. Capacity analysis and Gaussian calculations suggest that an aluminum/diglyme complex, rather than an aluminum ion, is the intercalating species. From the known values of defect density in hexacyanoferrate materials we believe that the intercalation sites for the aluminum/diglyme complex are the $Fe(CN)_6$ vacancies. This hypothesis is supported by the electrochemical data, which show capacities ranging from approximately 10 to 25% of the theoretical value. These capacities (7 to 20 mAh/g) correspond well with the range of defect densities for these materials. Future studies of these materials could include analysis of thin films of hexacyanoferrate materials electrodeposited on high surface area current collectors. In this way it may be possible to stabilize the crystal structures and

obtain longer cycle life. Since a thin film would eliminate the complexity of multiple interfaces which are present in a composite cathode this approach could also analysis of charge transfer using electrochemical impedance spectroscopy. Another possible approach to stabilizing the crystal structure would be synthesis of a core shell morphology. By using the CuHCF as a core and coating it with a stabilizing shell, perhaps NiHCF, it may be possible to slow the degradation of the materials. Finally, it would be interesting to attempt synthesis which would expand the crystal lattice of the hexacyanoferrate. Replacing the cyano-bridging unit with a thiocyanate may increase the metal-metal distance and enable higher capacity cycling with the aluminum/diglyme complex. Another interesting and enlightening method of analysis would be ICP-MS to quantify the elements present in the electrodes…good luck to whomever dares attempt use of the UCM ICP-MS system…

# Appendix A. A Guide to DOSY NMR

## A practical guide for beginners using Agilents vNMRj

*A note to the reader*

By the time you read this guide the exact system to which it primarily refers will no longer be in operation. You will never understand how fortunate you are to have avoided this particular beast of a machine and all its unique idiosyncrasies. Because the new system will have many improvements and new components you be able to happily ignore some of the details of what will be included below. Attempts to highlight these areas will be made so that you will be aware of their outdated information. However, in the event that a technological Armageddon should take place and a regression to manual operation of the system become necessary the outdated information will again be useful and will therefore be included. Additionally, it may also give some small degree of amusement to read about how prior graduate students operated the system and provides the author an opportunity to take the grandfatherly position of relating how, in my day, we hiked, drove and sweated uphill both ways in the sweltering California sun just to have the opportunity of getting some data if the system was in a good mood and felt like bestowing a small sense of triumph upon us. More typically it was in a sour mood from recording nothing but proton and carbon data and being stuck in Professor Meyer's lab; a completely understandable yet infuriating state to find it in.

In summary, the guide will be of use regardless of the system on which you are working but some of the details will have changed and some information may be missing as the author will not have worked extensively on the new system. Perhaps an ongoing effort to keep it updated may be kept by future students.

# Table of Contents

## Scope and purpose of the guide

*What this guide is intended to be*. This is meant to be a practical, step-by-step, guide to running an NMR (an abbreviation of Nuclear Magnetic Resonance used as a catch all to refer to the instrument itself as well as the technique) to obtain Diffusion Ordered SpectroscopY, or DOSY, spectra. Enough background information will be included to give a rudimentary understanding of what NMR is, how it works and what the data are good for. Some information regarding the hardware that is used in NMR will be given although this will be far from exhaustive and is only intended to familiarize a new user with the systems components. Some background of the theory of NMR will be given as well. This is intended to be theory from a practical view point and much of the detailed mathematics behind the theory will not be included. Hopefully this will be enough information to give an intuitive sense of what happens when you put a sample into an NMR and collect a spectrum rather than a solid mathematical foundation upon which numerous headaches may be obtained.

The instructions will be given in as much detail as possible and will be as practical as the author can make them; essentially every effort will be taken to make this guide as dissimilar as possible to the average manual or help file typically included with instrumentation such as an NMR spectrometer. The knowledge recorded here was gained over the course of a rather mentally painful year in which the author progressed from having never seen an NMR to being a reasonably competent user. This knowledge was gleaned from hours of reading, many more hours of sitting at the NMR tinkering, other students, professors and one remarkably knowledgeable British expert in the field of DOSY NMR who is named, recognized and thanked heartily on the dedication page. I hope this document can save you from many painful hours duplicating the course by which it was created.

*What this guide is not*. This guide is not meant to be a lesson in quantum mechanics and as such it will not provide a great deal of information regarding the quantum mechanics of nuclei and electrons although certainly much relevant information can be gleaned from that field of study and the reader is certainly encouraged to move beyond the theoretical framework of this guide. Nor will this be a guide for 1D NMR, its uses and interpretation. Only enough information to obtain a clean, properly corrected, 1D spectrum will be included. Additionally, no instructions on programming pulse sequences or macros are included as the author never delved into that particular aspect of NMR operation. Finally, although this is a guide for DOSY NMR it will not cover that subject in its totality as a large book would be needed to do so.

## Fundamentals of NMR

To fully understand NMR and all theory connected to the processes which occur during its use would require years of dedicated study. Fortunately, the fundamentals of operating the system, collecting high quality, publication worthy data and of understanding, in a simplified manner, the science behind the machine may be grasped in a relatively short period of time. This section and those which follow should be a good place to begin for someone not familiar with an NMR and will be aimed towards individuals with no prior experience regarding NMR.

## The hardware – introduction to physical objects

Before delving into the theory of NMR or the practical aspects of operating the instrument it will be of use to familiarize the reader with the equipment itself and some of the basic makeup of the hardware and accessories used for the NMR experiment. This is intended to provide a sense of familiarity and to instill a clear 'mental image' of the components in order to aid in the understanding of the instructions which will follow as well as to provide a framework in which the theoretical aspects of NMR may be couched, i.e., to provide a connection between the physical objects used during the course of operating an NMR and the theory which governs the behavior of the samples and the processes occurring in the instrumentation.

### *The magnet*

The magnet is the heart of the NMR; its core is a coil of superconducting wire cooled by liquid helium to about 4.2K. This core is surrounded by a variety of insulation and shielding; all of which is inside a large Dewar filled with liquid nitrogen. The liquid nitrogen Dewar is insulated and shielded as well in an effort to reduce the rate of cryogen loss as well as to shield the surroundings from the powerful magnetic fields generated by the coil. Even with the shielding in place the magnetic fields near the external wall of the magnet can be sufficiently strong to cause a variety of safety concerns and therefore individuals with implanted devices such as pacemakers should not approach an NMR. It is also advisable to remove objects such as phones, keys, wallets, etc., from ones pockets and leave them some distance from the NMR to eliminate the risk of having them interact with the magnetic fields. Although in practice the shielding of modern NMR systems is advanced enough to almost eliminate appreciable levels of external magnetic fields it is still good practice to behave as though the magnet is out to get you at the first opportunity. The purpose of the magnet is to generate a multi-tesla magnetic field which will cause alignment of nuclear dipoles when a sample is placed in the NMR.

*The probe*

Only a portion of the probe is visible when an NMR is fully assembled. The probe extends into the center of the superconducting coil and is the component responsible for manipulating and measuring the properties of the sample being studied. These manipulations and measurements are performed by means of magnetic fields which are generated via coils of wire in the probe. Below are some images of a Varian ASWPFG 4-nucleus broadband probe (ASWPFG = AutoSwitchable Pulsed Field Gradient), this is the type of probe which was used by the author. The images were kindly supplied by Dr. Shoemaker at the University of Colorado Boulder.

Figure A.1. A Varian ASWPFG broadband NMR probe. Two channels with two nuclei per channel are available on this probe, making it a 4-nucleus probe. This image shows the probe as it would appear when removed from the NMR.

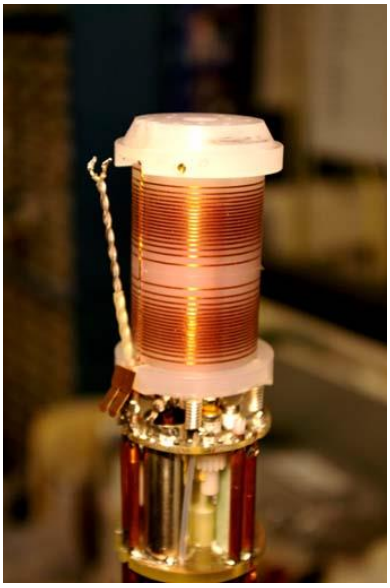

Figure A.2. These are the outer coils of the PFG coil assembly. The coils which are visible are active shielding coils which protect the main magnet coil from the gradient pulses applied during an experiment. The actual pulse coils are beneath the plastic on which the shielding coils are wrapped. The leads (wires on the left hand side) have been desoldered to allow the assembly to be removed for the next image.

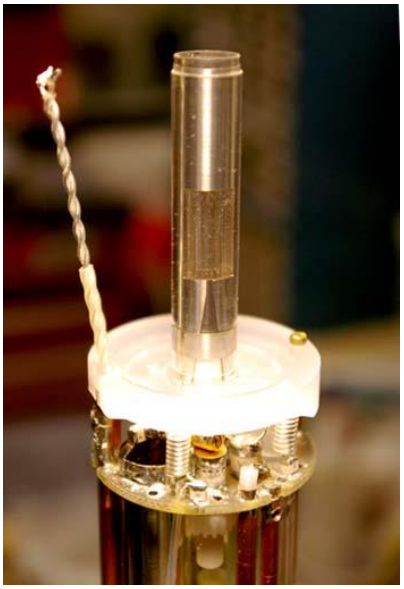

Figure A.3. The outer RF coil. The structure of this coil is known as a 'saddle coil' due to its shape somewhat resembling that of a saddle. In this configuration the current flows up one side and down the other. Because it is physically further from the sample this coil is used as the proton/fluorine channel.

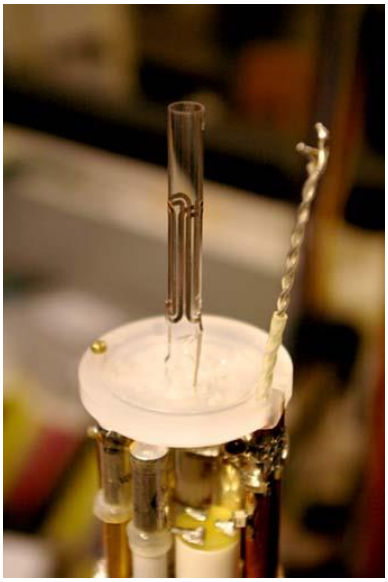

Figure A.4. The inner RF coil. This coil is known as a 'Helmholtz coil' and is more suitable for the detection of less sensitive nuclei such as carbon and phosphorus given its closer proximity to the sample.

### *The spectrometer*

The spectrometer generates the pulses which travel through the coils in the probe. These pulses are generated in the radio frequency range which corresponds to the frequency at which nuclei move in the magnetic field of the superconducting coil. Little interaction is needed with the spectrometer at the user level.

### *The NMR tube*

The NMR tube is a precision made tube of borosilicate glass (other varieties are made but are more costly) which requires careful handling. The tube will hold the chemical which you are investigating and when placed in the NMR, floats, by means of airflow, with the sample containing portion residing in the top of the probe. It is important to handle the tubes carefully and to keep them clean in order to avoid contamination of your sample as well as contamination of the probe. A variety of tube capping systems are available, the most standard is a simple cap which fits snuggly over the open end. If your sample must be kept air and moisture free there are tubes available which have more secure capping systems, ranging from Teflon lined screw top to valved tubes which provide a complete seal, capable of operating under vacuum or pressure.

### *The spinner*

The spinner, at first glance, appears to be a rather cheaply made piece of plastic which only serves to hold the NMR tube. In fact it is another precision made component which must be manufactured to exacting specifications to ensure proper positioning of the NMR tube in the probe. It also acts as a part of the floatation system, riding on a cushion of air which ensures no physical contact between the probe and the tube. The reason for the name "spinner" is quite literal; it used to be customary (and still is in places) to spin the sample to increase the apparent homogeneity of the magnetic field. This was more necessary on older NMR spectrometers which were not able to generate the extremely uniform magnetic fields of more modern systems.

### *The depth gauge*

This device ensures proper vertical position of your NMR tube in the spinner. If the tube sits too high in the spinner it will not extend into the probe and will be outside the homogenous region of the magnetic field; this will result in attenuation of signal and difficult to impossible shimming. On the other hand, if the tube is too low it will crash into the probe head and break, resulting in glass shards and chemicals being introduced into the probe. This will almost certainly cause damage to more modern probes although older probes such as the Varian ASWPFG can survive such an incident if immediately and carefully cleaned.

## Basic NMR theory

Now that the reader is introduced to the hardware it seems reasonable to introduce a basic level of NMR theory. To fully understand the theory of NMR would require extensive study and dedication on the part of the reader and would require far more time and space than the author currently has. Therefore, the reader would be well advised to consult other texts and sources of information to fill in the gaps which must be left in this document. A particularly useful text is Understanding NMR Spectroscopy by Dr. James Keeler. This text is written specifically for a student of NMR who is familiar with its use and operation but who needs to gain a deeper understanding of the theory governing NMR. Although the order of NMR theory can be arranged in many ways the following sections will begin with a simplified version of how to visualize the nuclei of the samples and how they behave when placed in a multi-Tesla magnetic field. This will be followed by an explanation of radio frequency pulses and how they are utilized in an NMR to control the nuclei in order to obtain a useful signal. Finally, a few brief sections will introduce what happens to the nuclei after the RF pulse is applied.

### *Magnetic dipoles – how to visualize a nuclei*

The nucleus of an atom is generally difficult to visualize; being a collection of charged and neutral particles whose properties are governed by quantum mechanics. Fortunately, for the purposes of basic NMR theory a nucleus can be thought of simply as a magnetic dipole. Although this is most certainly a tremendous simplification it serves as a useful method of thinking about the samples you will examine and will be helpful later when studying the pulse sequences and their effects on the nucleus.

### *Interaction of the dipoles with the magnet – what happens when you put a sample in the magnet*

Before a sample is placed in an NMR the nuclear dipoles of the molecules are arranged in a completely random way; unable to reach any type of stable organization due in large part to the effects of constantly fluctuating thermal energy. This thermal energy causes continual motion and collision of the molecules which results in exchange of energy and disruption of any alignment of the nuclear dipoles. Upon being placed into an NMR the sample is exposed to the multi-tesla magnetic field along the Z axis which is generated by the superconducting coils. For reference, the magnetic field of the earth ranges from 3 to $6x10^{-5}$ Tesla depending on location versus the 9.4 Tesla of the 400MHz NMR referred to in this document. The field of the NMR is strong enough to overcome to a small degree the tendency of the dipoles to be randomly aligned and results in a reorientation of the dipoles, causing them to have an overall alignment with the magnetic field as shown below.

### *Radio frequency pulses – Manipulating the dipoles*

Because the magnetic field of the NMR is constant there is continuous force acting on the nuclear dipoles to keep them aligned in a minimum energy arrangement. However, to obtain data from a sample it is necessary to perturb this bulk alignment in a carefully controlled way and then monitor the nuclei as they return to the equilibrium state. The perturbation comes in the form of a radio frequency pulse which lasts several microseconds. The duration of the pulse governs how far the dipoles are moved away from their equilibrium positions (termed the tip angle) and is typically timed to give a 90 degree rotation for a 1D NMR spectrum as this provides maximum signal. It is possible to time the pulse for any desired rotation and many experiments make use of tip angles other than 90 degrees. The radio frequency pulses are generated by the spectrometer and pass through either the inner or outer RF coils shown in the figures above. This results in a magnetic field oscillating in the XY plane at the frequency of the RF pulse. The interaction of the RF pulse with the dipoles causes them to move from alignment along the Z axis to alignment in the XY plane.

In summary, the sample is placed in the NMR which causes the dipoles to align with the magnetic field rather than being randomly distributed. The dipoles are then moved in a controlled manner by the RF pulse from the Z axis to the XY plane.

### *Precessing dipoles – the source of the signal*

As was mentioned above the magnetic field of the NMR is constant and continuously acts to align the nuclear dipoles with the Z axis. After the RF pulse has tipped the dipoles away from their Z alignment it is shut off and the magnetic field begins to realign them with the Z axis. In contrast to the simple rotation from one axis to another caused by the RF pulse the realignment which occurs due to the magnetic field takes place by means of precession, or spinning (this is not an accurate term but it serves for visualization), around the Z axis. As the nuclear dipole precession occurs the bulk magnetization gradually returns to its preferred Z alignment. The precession takes place at a characteristic frequency for each nuclei and is known as the Larmor frequency:

$$\omega = -\gamma B_0 \text{ in rad/s} \quad \text{Equation 1}$$

$$\omega = \frac{-\gamma B_0}{2\pi} \text{ in Hz} \quad \text{Equation 2}$$

Where γ is the gyromagnetic ratio of the nuclei and $B_0$ is the magnetic field strength.

The motion of the nuclear dipoles at the Larmor frequency causes a current to be induced in the coils of the probe, similar to a magnet moving through a coil of wire. This current is amplified and recorded, resulting in a free induction decay or FID. As a side note, the precession frequency of a proton in an NMR is typically the frequency by which the system is labeled, i.e., a 400 has a 1H Larmor frequency of 400MHz, a 600 has a frequency of 600MHz etc. After acquisition of the FID it is transformed by a Fourier transform, which moves it from time domain data to chemical shift data. This transformed FID is the data one typically pictures when thinking of NMR spectra and is, in general, more useful to the standard operator.

## Relaxation

The process of the bulk magnetization of the sample returning to its equilibrium state with the magnetic field is known as relaxation. If the relaxation time is relatively long, on the order of hundreds of milliseconds to seconds, a well-defined peak will be seen in the spectrum. On the other hand, if the relaxation occurs in a few milliseconds or less the spectrum will show broad, ill defined, peaks. DOSY NMR requires time delays for diffusion which range from tens of milliseconds to more than one second and therefore can only

be successfully performed on a nucleus with a relaxation time greater than the diffusion delay.

The time required for complete relaxation of a nucleus depends on several factors including the quadrupolar moment of the nucleus and its chemical environment in the sample.

The relaxation process can be split into two components; the first is the realignment of the bulk magnetization vector with the magnetic field, called T1. The second is the dephasing of the nuclear spins during precession, called T2. These two components and their influence on DOSY are discussed below.

### T1

The first type of relaxation typically discussed is known as T1 relaxation, also referred to as spin lattice relaxation. This form of relaxation can thought of as the bulk magnetization vector re-aligning, over time, with the external field applied by the magnet of the NMR. It can be visualized simply as a vector rotating from the XY-plane into a parallel orientation with the Z-axis. The time over which this relaxation occurs is the time during which the FID is collected. Each nucleus will have a characteristic time of relaxation (known simply as the T1 time or just T1) which is dependent upon the nuclear traits as well as the details of the chemical environment of the sample.

### T2

Another form of relaxation is known as T2, spin-spin or dipole-dipole relaxation. This relaxation mechanism is more complex than T1 and takes a little more visualization to grasp. After the initial RF pulse the magnetization vector is reoriented from Z-axis alignment to XY-plane alignment. The dipoles then begin precessing, at the Larmor frequency, around the Z-axis. Initially all the dipoles which have undergone rotation precess in a synchronous manner, that is, they are in phase. The synchronous alignment of the precessing dipoles begins to be disrupted as they interact with each other. Thus, T2 may be thought of as a dephasing of the nuclear dipoles brought about by interaction of one molecular dipole with another. These interactions cause variations of the local magnetic field at the molecular level and serve as a means via which energy can be transferred. The net effect of this energy transfer and molecular inhomogeneity's in the magnetic field is to reorient, in a random manner, the orientation of the dipoles, i.e. dephasing. In somewhat simpler terms: all the dipoles initially point in the same direction but they don't precess at the same rate so over time they end up spreading out.

## Commands you'll need to know and what they do

This is a list of commands used during a standard session of DOSY NMR data collection and an explanation of what they do. There are literally hundreds of

commands not listed; those left out can be found in the documentation in the Vnmrj software under the "Help" menu. Time and effort will be required to understand what they do and it is highly recommended that the curious student ask someone more experienced rather than attempt to read the help file documentation.

- d1? Shows the recycle delay, this is a time delay at the beginning of a pulse sequence which allows the nuclei to undergo full relaxation before another pulse sequence is run. If the nuclei have not fully relaxed the signal measured during the following pulse sequence will not be maximized. A d1 value of 5xT1 is typically recommended for full relaxation although in practice it will be rare to find a situation in which it is necessary to measure T1 and adjust d1 accordingly.

- nt? Displays the number of times a pulse sequence will be repeated. By repeating the sequence several times the signal to noise ratio is improved. This number is always entered in powers of 2, typically ranging from 2 to 64 for nuclei of reasonable sensitivity and up to 256 or 512 for a nucleus like 27Al.

- time No question mark is input at the end of this command. This simply displays the time the experiment will take with the current parameter set.

- at? Acquisition time, the length of time for which the FID is acquired. If the acquisition time is too short the resulting spectra will have 'ringing' in the baseline around the peaks. If it is too long time is wasted and noise is collected. Usually the default values are serviceable.

- ga or go Begins the data acquisition.

- wft Weighted Fourier Transform, this transforms the data from the time domain to the frequency domain so we can view it in a way that our minds can understand.

- aph Auto phase, this phases the spectra so the bases of the peaks are properly aligned. For some samples it may be necessary to phase by hand.

- dc Occasionally the spectra will have a 'drift', this results in a vertical shift of the baseline and you will not be able to see your spectrum. If you acquire and process your data like normal but can't see your spectra it may be worth trying the 'dc' command.

- ds This stands for 'display spectra' and will return the view to the spectra you've collected if, for some reason, the view has changed.

- df Displays the FID, this can be useful to look at for certain nuclei. Looking at the decay of the FID can give you an estimate of what the acquisition time should be. If you see a long flat section at the end of FID you can safely reduce the acquisition time.

- dssh This command is 'Display Spectra Stacked Horizontally', it is used to look at a series of 1D spectra side by side. This will be used in every DOSY experiment.

- dssl Should label the spectra 1 through however many there are, typically 15 for DOSY. There seems to be a bug with this command which causes it to do nothing now and then.

## Making your samples

A typical NMR sample is made by dissolving the compound of interest directly in a deuterated solvent. This doesn't work for DOSY unless you happen to want the diffusion coefficient of your molecule in the deuterated solvent. Sample preparation of electrolytes for DOSY studies requires some method of holding the neat electrolyte. There are two approaches available for this. The first is to put the electrolyte into a capillary tube and flame seal the open end to preserve the electrolyte. The top of the capillary tube is wrapped with Teflon tape to make sure it stays vertical in the NMR tube. Then, the deuterated solvent is put into an NMR tube and the capillary tube is loaded. This is shown in the pictures below.


Figure A.5. An NMR tube, a capillary tube containing electrolyte, and a quarter for scale. The Teflon tape is used to ensure vertical alignment in the NMR tube.


Figure A.6. Showing the capillary tube in the NMR tube. Enough deuterated solvent should be added to fill the NMR tube to about the same level as the level of the electrolyte in the capillary.

The second approach is to put the electrolyte directly in an NMR tube and seal the tube as well as possible. The author generally used the capillary tube and had reasonable success. This method becomes difficult or impossible when attempting to measure dilute samples as the volume of electrolyte is quite small in a capillary tube. The direct use of an NMR tube allows more sample to be examined but makes the process of collecting spectra more challenging. It will require some assistance from the NMR director.

Whatever method you use it is important to use the same approach for all samples. Changing the physical parameters of your sample can have unpredictable results on the measurement.

## Collecting your first 1D spectra

Collecting good DOSY data requires that you first have parameters to obtain a well shimmed, properly phased 1D spectra. This should not be challenging as 1D spectra are routine and the NMR will essentially do all the work for you. The figure below shows a 1D spectra of a neat diglyme sample. This sample was made with the capillary method as described above. Collecting the spectra required no adjustment of parameters by the author, locking, shimming and processing were all done using the defaults of the NMR. One note is that the NMR will automatically remove your sample after an automated spectrum has been collected. To put your sample back in by hand: Tools -> Sample in Magnet, select the appropriate options and click OK. This will keep the sample in the NMR until you manually remove it or someone begins an automated run after you've walked away and forgotten you left your sample in the magnet.

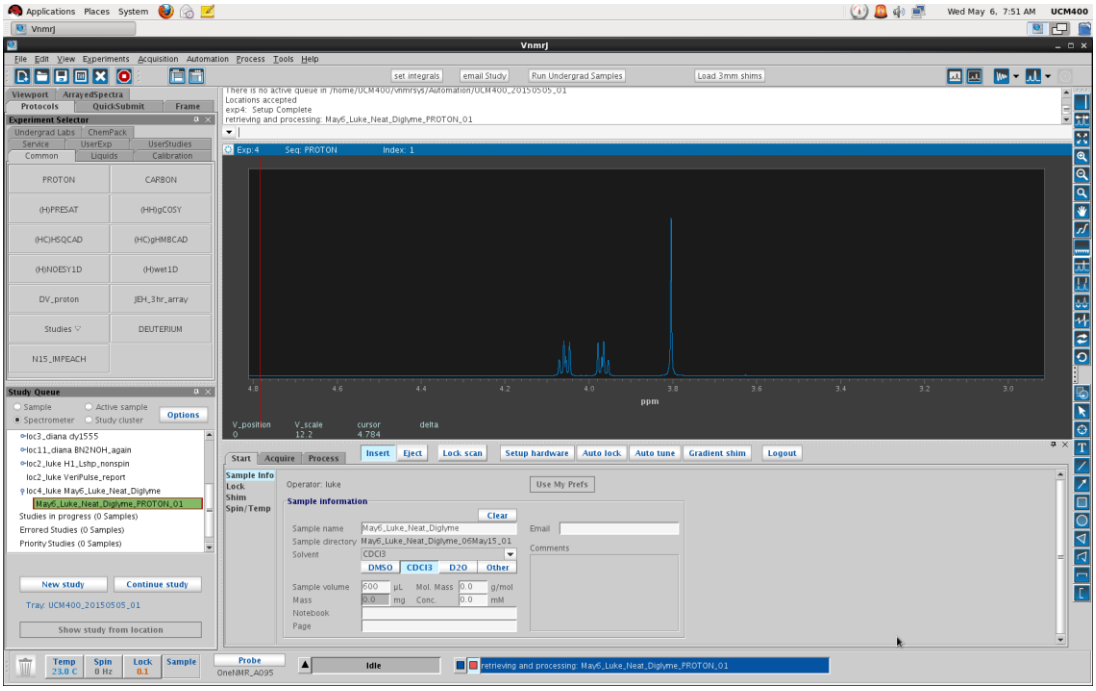


Figure A.7. Proton spectrum of neat diglyme contained in a capillary tube. This spectrum becomes the starting point for collecting DOSY data.

## Converting to DOSY

After a good 1D spectrum has been collected you can start working one collecting DOSY data. To do this we need to convert the experiment to a DOSY setup. This is done by going to 'Experiments' -> 'Convert current parameters' -> DOSY -> select a pulse sequence. This process imports the settings and

parameters from the 1D sequence to the DOSY sequence, usually providing a good starting point for DOSY experiments. The figure below shows the initial screen for running DOSY NMR, you can copy this image into PowerPoint or some other program and expand it to see the various options.

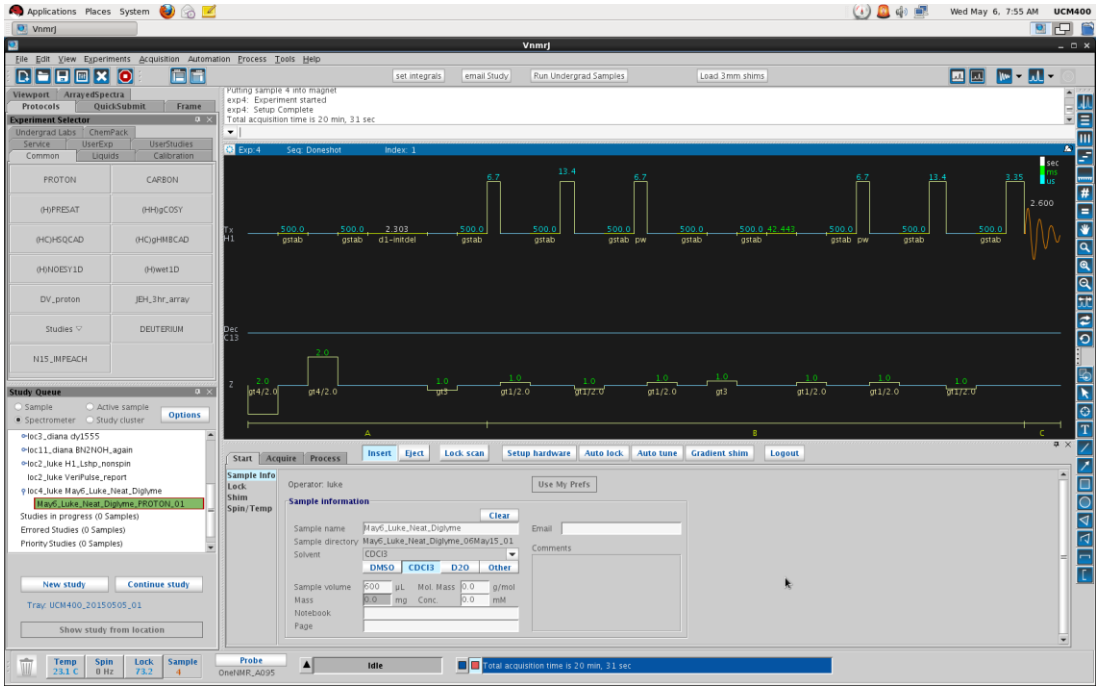

Figure A.8. The initial screen after converting from a 1D experiment to a DOSY experiment. In this case the DOSY-ONESHOT pulse sequence was selected.

## Choosing a pulse sequence

There are several options for pulse sequences under the DOSY menu. The most recently developed and generally best option to start with is the DOSY-ONESHOT sequence. There are two possible reasons to select a different pulse sequence. The first is that for some samples the ONESHOT sequence simply can't collect good data. There are no rules as to what sample will have problems, the only way to know is to run the experiment. If, in spite of all efforts, good data is not forthcoming from the ONESHOT sequence you should try a simpler sequence such as the Diffusion Gradient Compensated Stimulated Echo or Dgcste sequence. This is an older pulse sequence which contains fewer conditioning pulses. For difficult samples fewer pulses can sometimes allow successful data collection. The second reason you may need a different pulse sequence is if there is a risk of convection taking place in your sample. In such a case one of the convection compensated pulse sequences will be needed. Be aware that they will result in a loss of signal and collecting data will take longer.

## Setting the initial parameters

After converting the 1D parameters to a DOSY pulse sequence there are a few options and parameters that should be changed. Figure A.5 shows the first two.

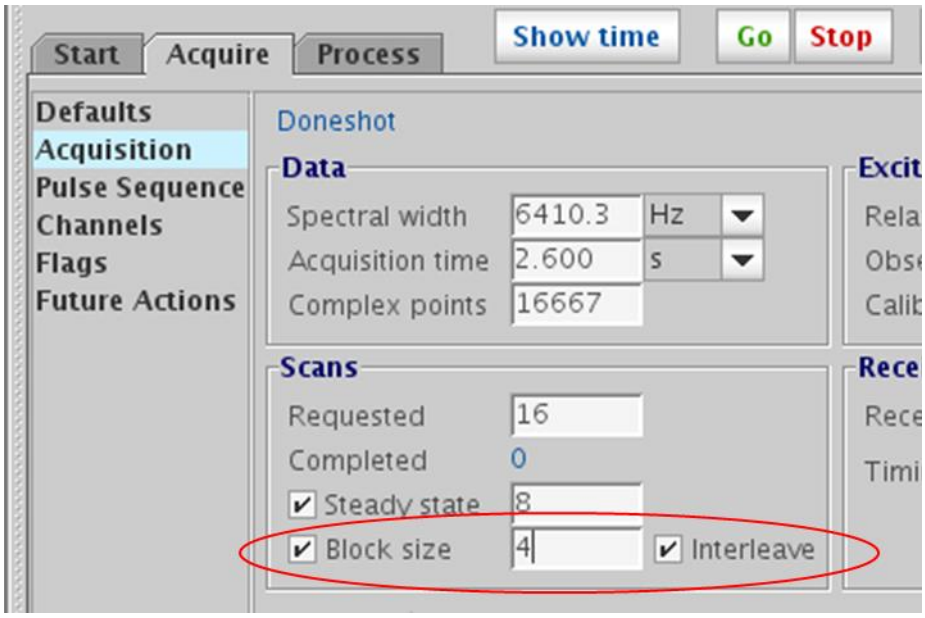


Figure A.9. Options under the Acquire tab that should be adjusted include the Block size and Interleave.

Adjust the block size to 4 and check the interleave option. This allows you to observe the spectra as they are collected rather than waiting for the experiment to run to completion.

Next, go to the Pulse Sequence section, just below Acquisition, as shown in the figure below. Under this section you should increase the diffusion delay to 100 to 150 ms, the default value is too low for electrolytes.

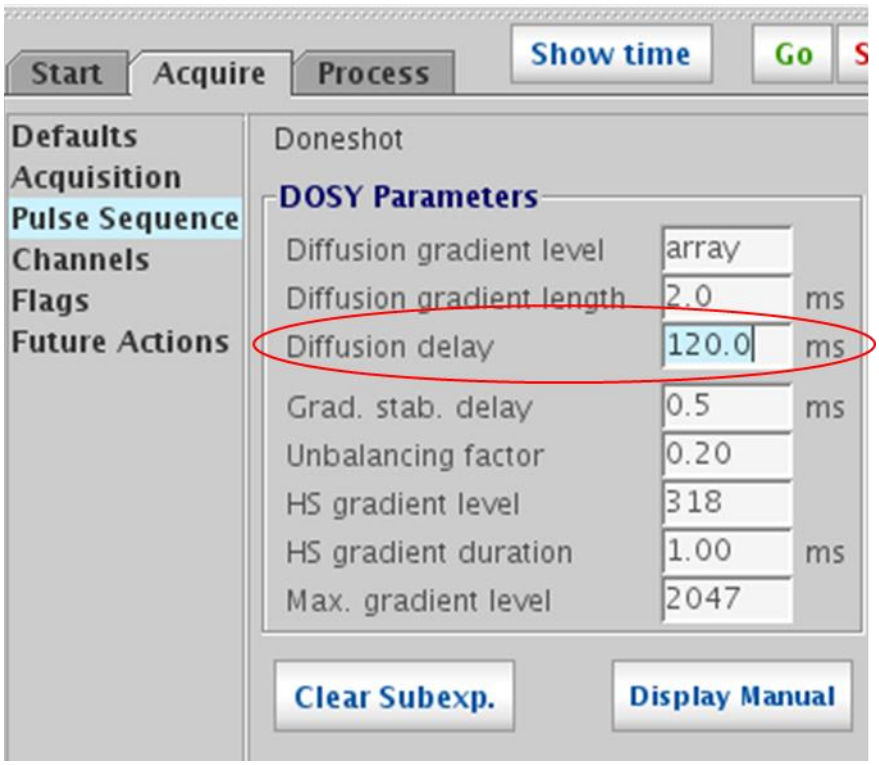


Figure A.10. Adjust the diffusion delay to something around 120 ms as a starting point.

You should also make sure the 'Alternate gradient sign' option is checked, see figure below. If this is turned off it is very likely you see something called phase roll when you collect the full range of DOSY data. Phase roll makes it impossible to extract meaningful diffusion coefficients.

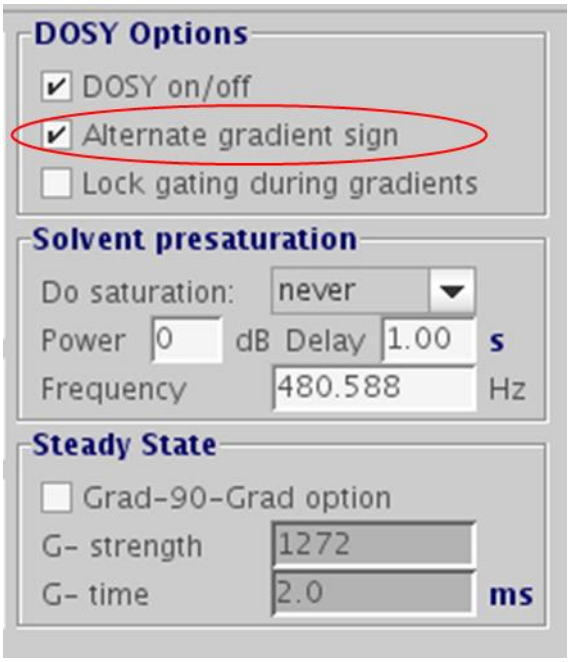


Figure A.11. Turning the 'Alternate gradient sign' option on is almost always necessary.

## Starting DOSY

At this point you could simply type 'go' or 'ga' or click the Go button and the data collection would begin. However, by default, the software is set to collect 15 spectra, see the figure below.

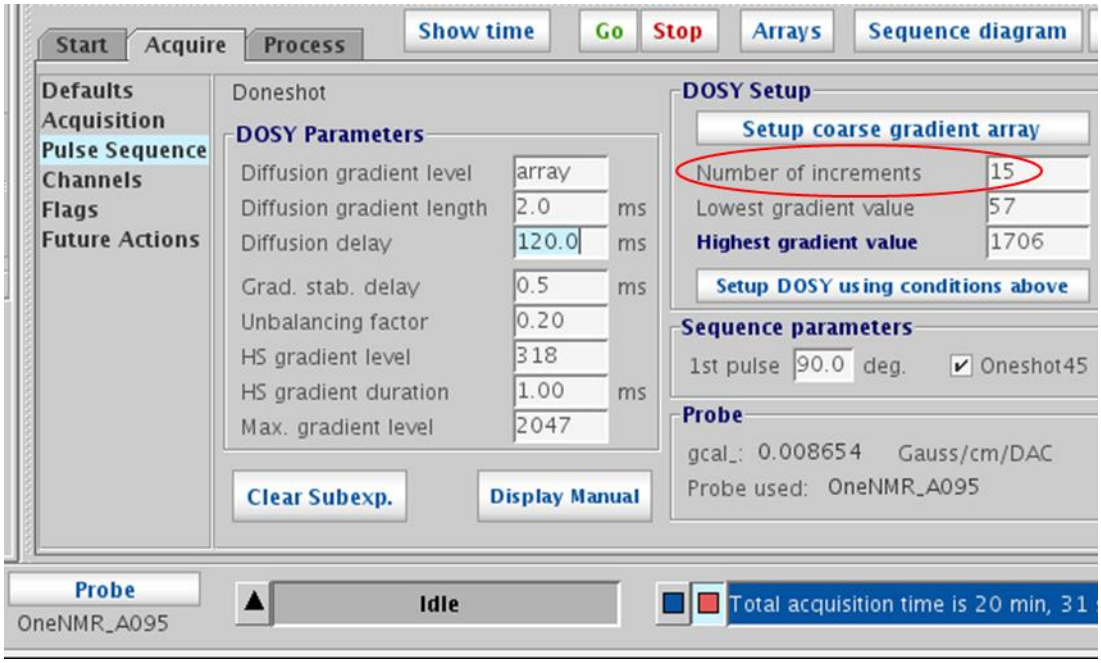

Figure A.12. The default number of gradient levels is too fine for the first run.

This will take approximately twenty minutes for 1H DOSY and much longer for other nuclei. Therefore, the best way to proceed is to reduce the number of increments to 2. This is done with the following command:

gzlvl1 = 60, 1700

This command tells the spectrometer to apply two different strength magnetic pulses to the sample. The first is a weak pulse which will return a stronger signal, the second is a stronger pulse which will return the most attenuated signal. The numbers are meaningless in and of themselves. To convert them to a number with units of Gauss/cm you can multiply by the gradient calibration, gcal_, value.

The result of using this command is that your initial DOSY spectra will take less time to collect (~3 minutes) since you have removed 12 gradient levels. The figure below shows a "first try" 2 gradient DOSY spectra.

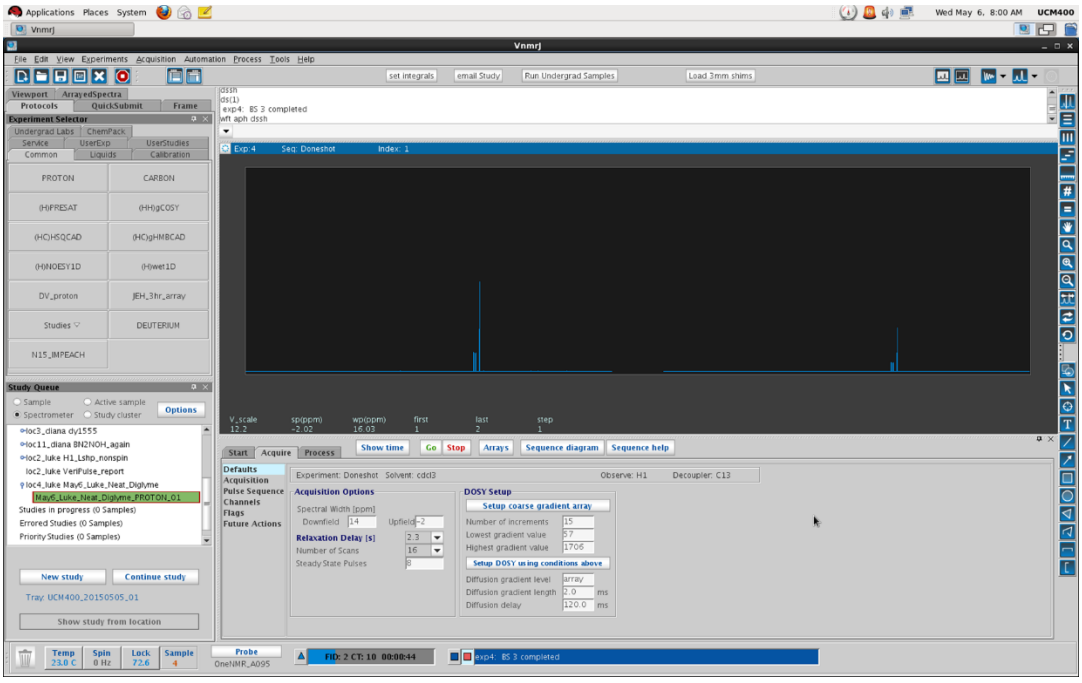


Figure A.13. The first try, 2 increment, DOSY spectra.

The first set of parameters is unlikely to be optimal. In the figure above it is apparent that either the diffusion delay time or the length of the gradient pulse needs to be increased. What makes this clear is the intensity difference of the two spectra. The second spectrum should be about 10% of the intensity of the first. Although it won't be possible to achieve this for every sample it's reasonable to aim for with dilute samples when collecting 1H DOSY.

Of the two options, the delay time or the gradient pulse length, it is preferable to begin with the delay time. Increasing the gradient pulse length has a stronger effect on the measurement but can result in nonlinear gradients or in burning out the gradient coils. If you have increased the delay time until it is on the order of 2-4 seconds and still can't get good DOSY data, find the NMR director and ask about increasing the gradient pulse length.

By increasing the diffusion delay, either with the control panel or by typing del = x, where 'x' is the time in s (typically 0.080 to 0.500, although sometimes much longer, up to 2-4 seconds in cases) the molecules diffuse further before the FID is collected. This longer diffusion results in a reduced signal intensity as shown below.

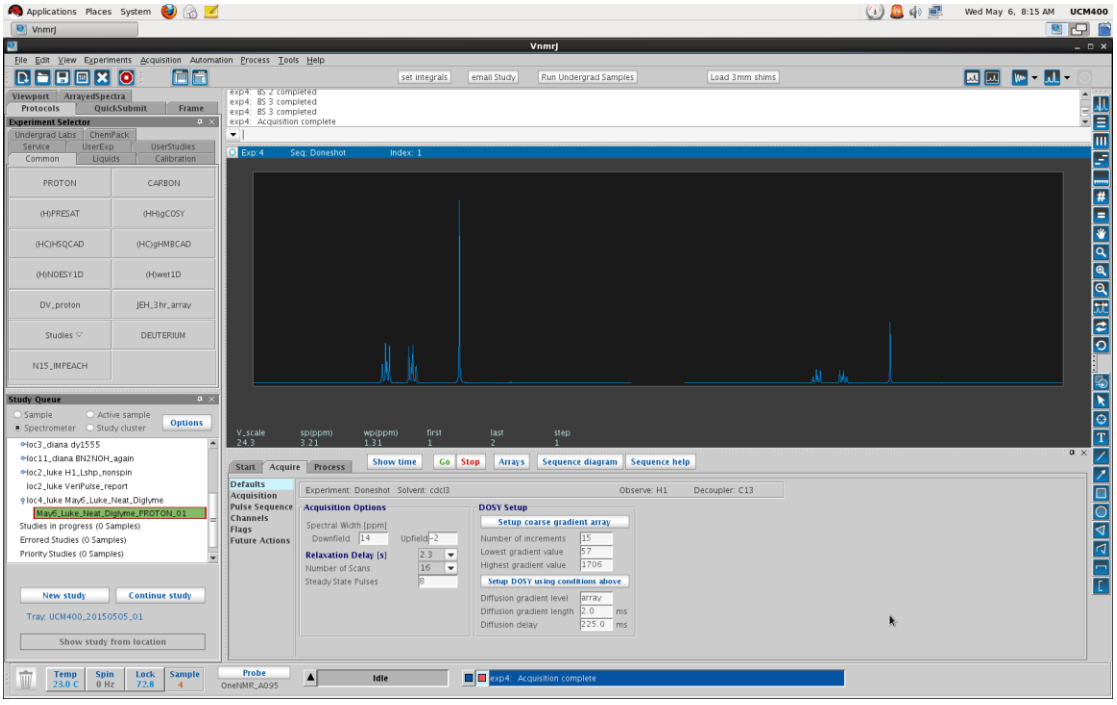

Figure A.14. After increasing the diffusion delay the relative intensity of the second spectrum is reduced.

Although not immediately obvious the relative intensity of the second spectrum has been considerably reduced. It is above the optimal level of ~10% of the first but is good enough to collect meaningful data.

After the diffusion delay has been adjusted you can setup the full 15 index experiment by clicking on 'Setup DOSY using conditions above' as shown below.

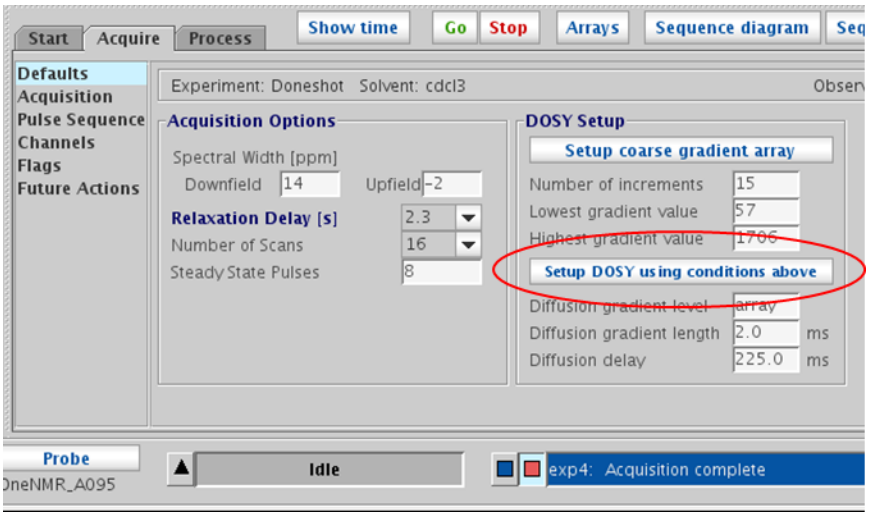


Figure A.15. Button to setup 15 index DOSY array.

This button generates an array of experiments, each one will collect a 1D spectrum with a unique gradient pulse applied. After the experiment has run for several minutes you can check its progress by typing:

wft aph dssh

These three commands tell the system to Fourier transform the FID, auto-phase the spectra and display them lined up horizontally. If all goes well you should see something similar to the figure below.

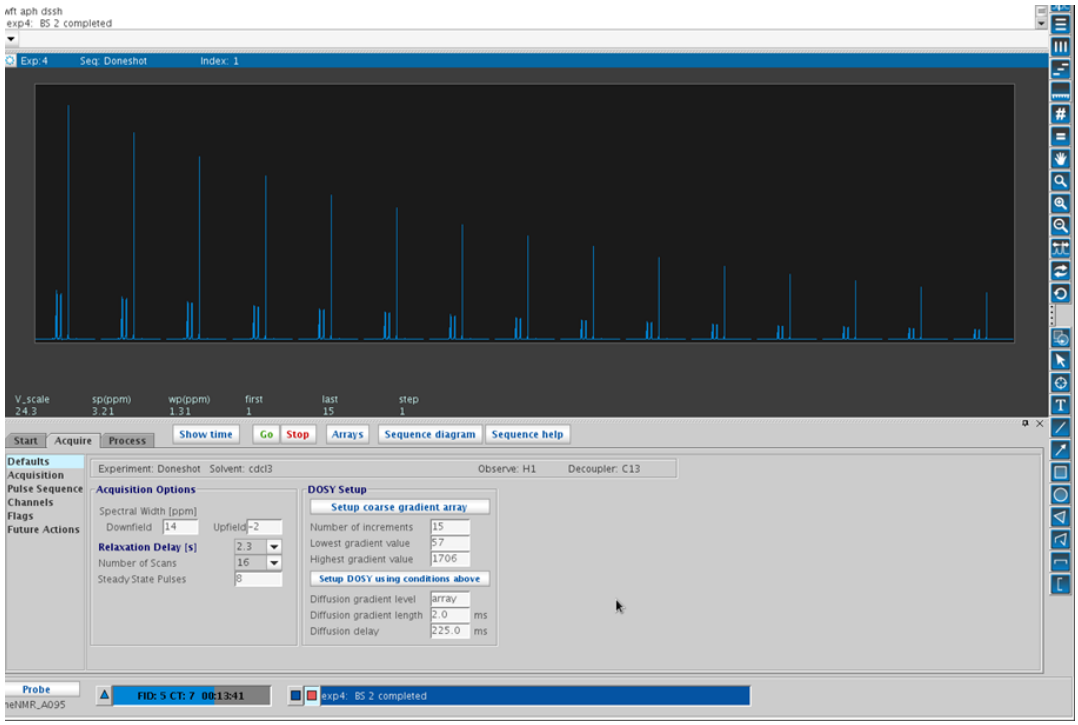


Figure A.16. The DOSY spectra during data collection.

The figure above shows what a DOSY experiment in progress should look like. The intensities of the signals reduce in an exponential fashion with no shift along the ppm axis and no variation in the baseline. To check the shift and baseline you will need to look at the spectra one by one. This is done by typing:

ds(1)

This will display the first spectrum in the sequence, you can then scroll through the remaining spectra and watch for shifts along the ppm axis or changes in the shape of the baseline.

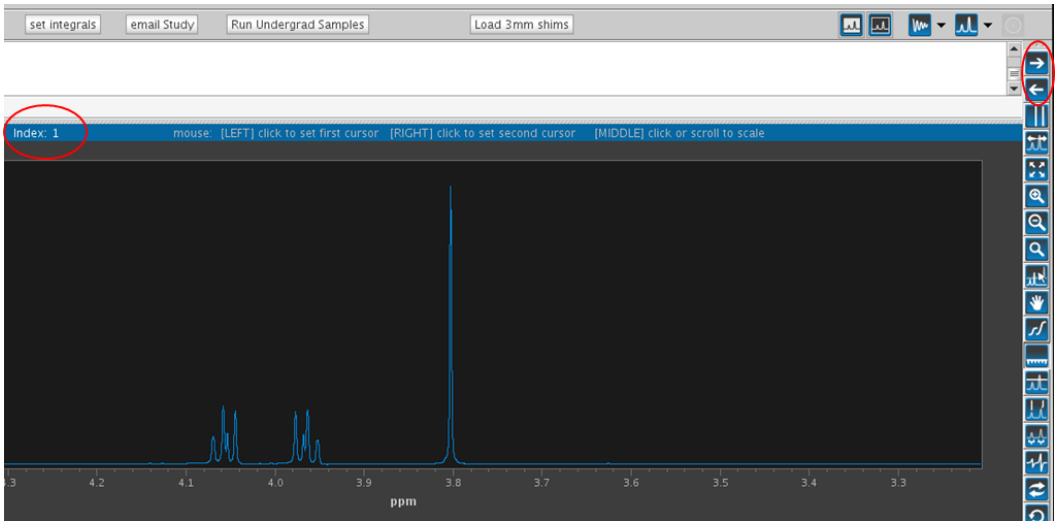


Figure A.17. Showing the first spectra, indicated by the index number, and the arrows that are used to scroll through the spectra.

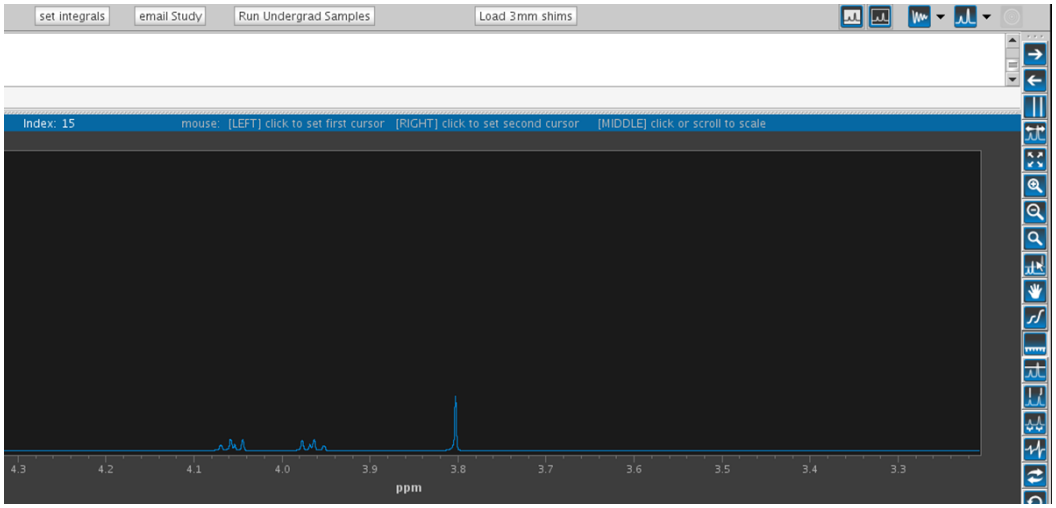


Figure A.18. The last spectrum, index 15, showing very little change in peak position along the ppm axis and almost no change in the baseline or peak shape.

If you see dramatic shifts along the ppm axis or large changes in the shape of the baseline you will need to rerun the experiment. Double check that the 'Alternate gradient sign' option is checked. If it was you may need to change to one of the other pulse sequences. If you continue to have problems you will most likely need to talk with the NMR director to find a solution.

After you have successfully collected the DOSY spectra you need to process the data to extract diffusion coefficients. This first step is to display the first spectrum in the series. Type

ds(1) ff

This will show the first spectrum and set it to fill the screen. Then, as shown below, use the threshold button on the right side of the screen to set the threshold for peak detection. Typically it is set to the top of the smallest peak you wish to include.

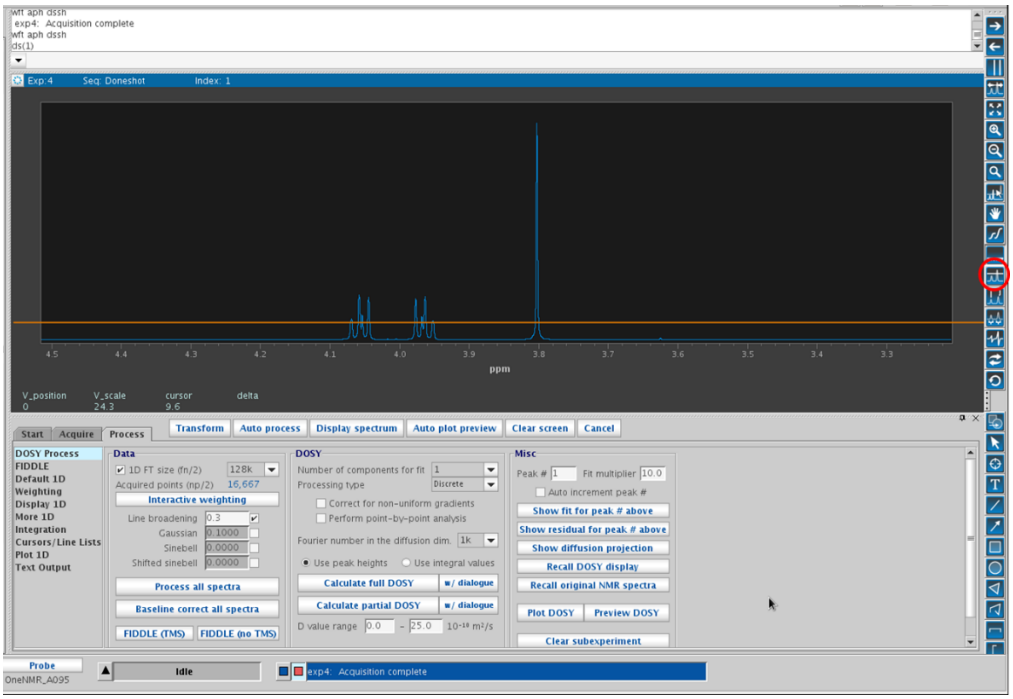


Figure A.19. Setting the threshold for peak detection.

After the threshold is set click on the integration option and then click 'Auto find integrals', as shown below.

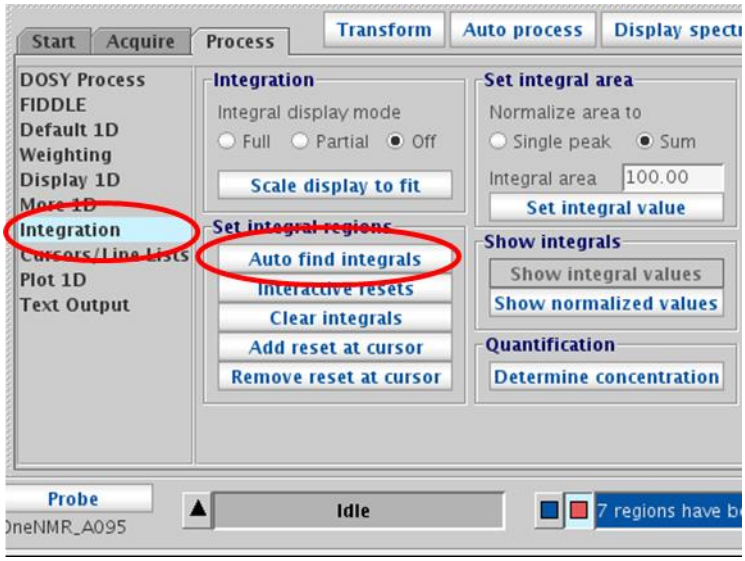


Figure A.20. Setting the integral regions.

This step tells the software which peaks to use for the DOSY processing. Return to the DOSY Process option and click 'Process all spectra' followed by 'Baseline correct all spectra', shown below. Doing this cleans up the data if small baseline errors exist.

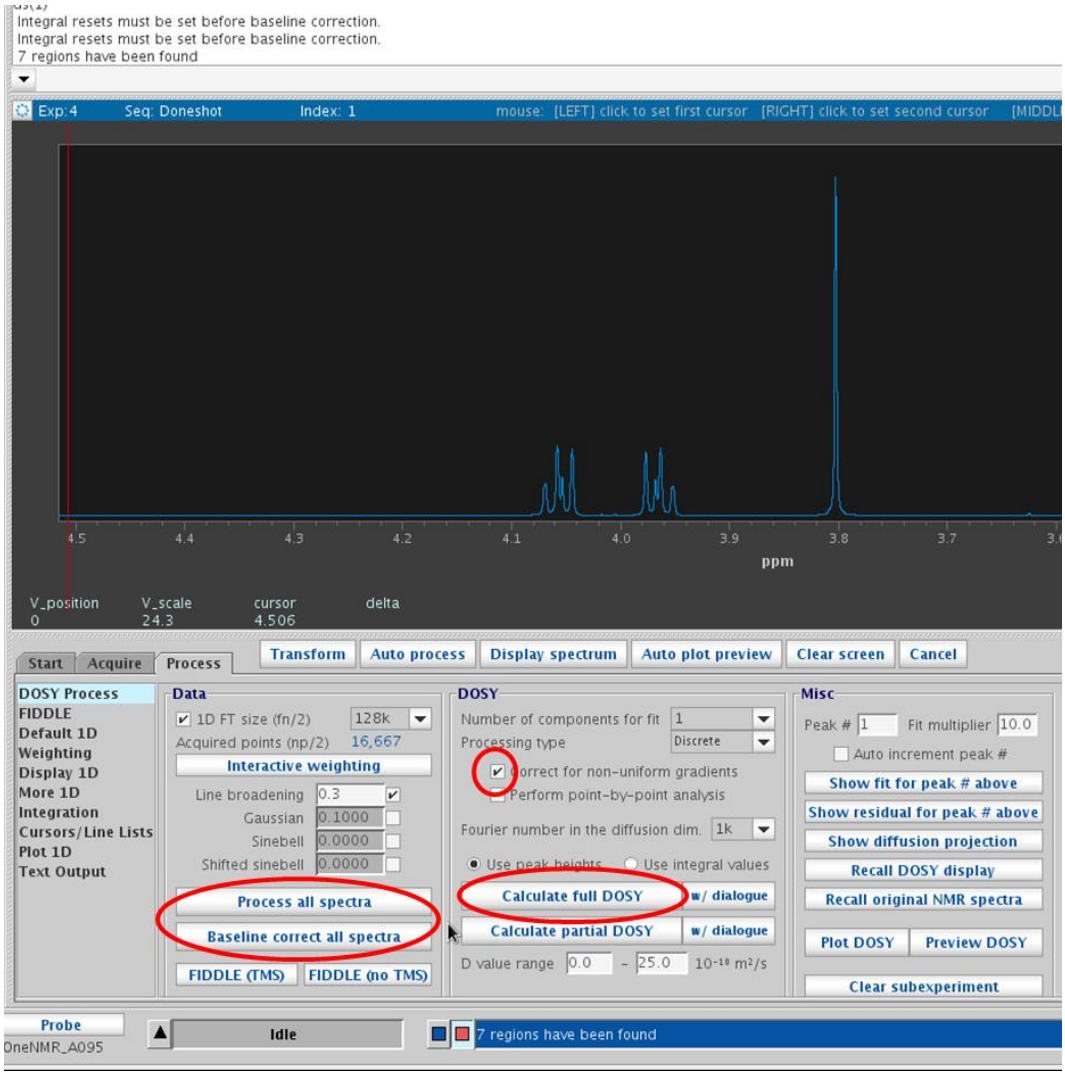


Figure A.21. The final buttons for DOSY processing.

The NMR has been calibrated for non-uniformities in the field gradient pulses so check the 'Correct for non-uniform gradients' box and then click 'Calculate full DOSY'. After the data has been processed you will see something similar to the figure below.

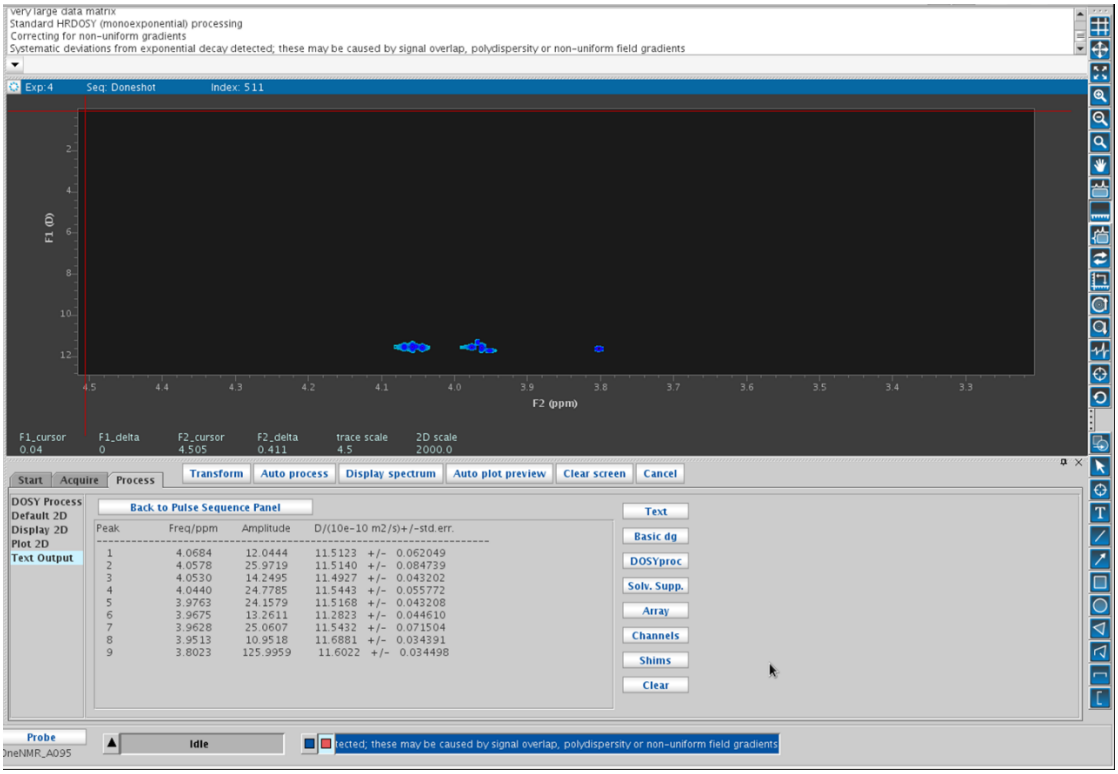


Figure A.22. DOSY display and text output.

You can see there is a small spread along the diffusion axis which is not expected as all the peaks being observed come from the same molecule and each group of protons on that molecule should diffuse at the same rate. Looking closely you will see a warning in the text at the top of the screen that warns about this problem. It states: "Systematic deviations from exponential decay detected: these may be caused by signal overlap, polydispersity or non-uniform field gradients". This rather opaque statement is telling you that the data does not exactly follow the exponential decay predicted by the Stejskal-Tanner equation (the fundamental equation of NMR diffusion measurements). Rarely will this warning not appear as it is difficult to properly adjust all the experimental parameters to obtain an exact exponential decay. It is not impossible and with a good amount of practice it becomes relatively straight forward but the time required can be excessive. Additionally, looking more closely at the diffusion coefficients, below, there is very little difference from one peak to another.

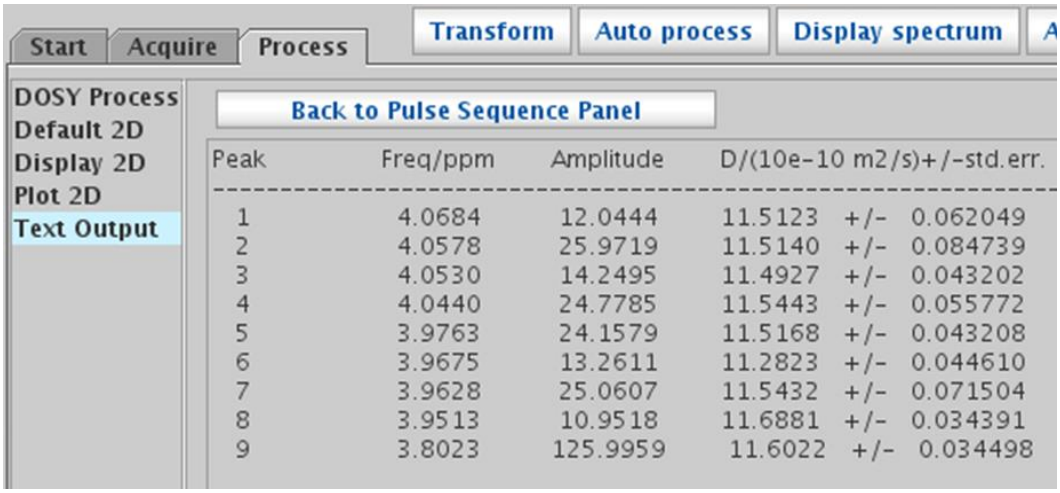


Figure A.23. The spread in diffusion coefficients for neat diglyme.

The diffusion coefficients range from a low of 11.28 +/- 0.045 to a high of 11.68 +/- 0.034. Considering the error in the measurement and the intended purpose of the data a 3.5% difference should not be of concern.

Congratulations! You can now collect DOSY NMR!

## DOSY related problems

### *My signal shows up in 1D but disappears during DOSY!*

Three possible problems come to mind. 1) Make sure the system is actually tuned to the nuclei you want, ask the NMR director for help if you don't know how to do this. 2) The signal to noise ratio in DOSY is worse than for 1D NMR. You may need to run more scans, increase nt. 3) You may be trying to observe a nucleus with a very short T1 such as 27Al. The T1 places a fundamental limitation on diffusion measurements. If T1 is less than the time it takes to run a DOSY sequence you're out of luck for that nuclei.

### *Some of my spectra look bad and mess up my analysis!*

You can leave the bad spectra out by using the 'w/ Dialogue' button next to the 'Calculate full DOSY' button. This option will ask you how many spectra are bad and what the index numbers of the offending data are. After entering the values the processing will take place as normal, simply ignoring the bad spectra.

### *The exponential decay isn't there.*

Try a different pulse sequence, a longer diffusion delay, longer gradient pulse or all three. For some samples the diffusion is slow enough to make the measurement very challenging. Keep in mind that even if the decay is not visible to your eye it may be present mathematically and it can be worthwhile to try the processing even if you can't see a decay.

# Bibliography


(1) Muldoon, J.; Bucur, C. B.; Gregory, T. Quest for Nonaqueous Multivalent Secondary Batteries: Magnesium and Beyond. *Chem. Rev.* **2014**.

(2) Development of New Alloys of Commercial Aluminium (2S) with Zinc, Indium, Tin, and Bismuth as Anodes for Alkaline Batteries. *J. Power Sources*.

(3) Macdonald, D. D. Evaluation of Alloy Anodes for Aluminum-Air Batteries. *J. Electrochem. Soc.* **1988**, *135*, 2397.

(4) Macdonald, D. D. Evaluation of Alloy Anodes for Aluminum-Air Batteries. *J. Electrochem. Soc.* **1988**, *135*, 2410.

(5) Real, S. Evaluation of Alloy Anodes for Aluminum-Air Batteries. *J. Electrochem. Soc.* **1988**, *135*, 1633.

(6) Real, S. Evaluation of Alloy Anodes for Aluminum-Air Batteries. *J. Electrochem. Soc.* **1988**, *135*, 1633.

(7) Tuck, C. D. S. The Electrochemical Behavior of Al-Ga Alloys in Alkaline and Neutral Electrolytes. *J. Electrochem. Soc.* **1987**, *134*, 2970.

(8) MACDONALD, D.; REAL, S.; URQUIDIMACDONALD, M. DEVELOPMENT AND EVALUATION OF ANODE ALLOYS FOR ALUMINUM AIR BATTERIES. *J. Electrochem. Soc.* **1987**, *134*, C411–C411.

(9) Pino, M.; Cuadrado, C.; Chacón, J.; Rodríguez, P.; Fatás, E.; Ocón, P. The Electrochemical Characteristics of Commercial Aluminium Alloy Electrodes for Al/air Batteries. *J. Appl. Electrochem.* **2014**, *44*, 1371–1380.

(10) Tang, Y.; Lu, L.; Roesky, H. W.; Wang, L.; Huang, B. The Effect of Zinc on the Aluminum Anode of the Aluminum–air Battery. *J. Power Sources* **2004**, *138*, 313–318.

(11) Licht, S. The Organic Phase for Aluminum Batteries. *Electrochem. Solid-State Lett.* **1999**, *2*, 262.

(12) Rudd, E. J.; Gibbons, D. W. High Energy Density Aluminum-Oxygen Cell. **1993**.

(13) Licht, S.; Tel-Vered, R.; Levitin, G.; Yarnitzky, C. Solution Activators of Aluminum Electrochemistry in Organic Media. *J. Electrochem. Soc.* **2000**, *147*, 496.

(14) Glicksman, R. The Performance of Zinc, Magnesium and Aluminum Primary Cell Anodes. A Review. *J. Electrochem. Soc.* **1959**, *106*, 457.

(15) Mears, R. B.; Brown, R. H. A Unified Mechanism of Passivity and Inhibition. Part II. *J. Electrochem. Soc.* **1950**, *97*, 75.

(16) Macdonald, D. D.; English, C. Development of Anodes for Aluminium/air Batteries ? Solution Phase Inhibition of Corrosion. *J. Appl. Electrochem.* **1990**, *20*, 405–417.

(17) Macdonald, D. D.; Lee, K. H.; Moccari, A.; Harrington, D. Evaluation of Alloy Anodes for Aluminum-Air Batteries: Corrosion Studies. *Corrosion* **1988**, *44*, 652–657.

(18) Peled, E. The Electrodeposition of Aluminum from Aromatic Hydrocarbon. *J. Electrochem. Soc.* **1976**, *123*, 15.

(19) Couch, D. E.; Brenner, A. A Hydride Bath for the Electrodeposition of Aluminum. *J. Electrochem. Soc.* **1952**, *99*, 234.

(20) Yoshio, M.; Ishibashi, N. High-Rate Plating of Aluminium from the Bath Containing Aluminium Chloride and Lithium Aluminium Hydride in Tetrahydrofuran. *J. Appl. Electrochem.* **1973**, *3*, 321–325.

(21) Zhao, Y.; VanderNoot, T. J. Electrodeposition of Aluminium from Nonaqueous Organic Electrolytic Systems and Room Temperature Molten Salts. *Electrochim. Acta* **1997**, *42*, 3–13.

(22) Del Duca, B. S. Electrochemical Behavior of the Aluminum Electrode in Molten Salt Electrolytes. *J. Electrochem. Soc.* **1971**, *118*, 405.

(23) Holleck, G. L.; Giner, J. The Aluminum Electrode in AlCl[sub 3]-Alkali-Halide Melts. *J. Electrochem. Soc.* **1972**, *119*, 1161.

(24) Gale, R. J.; Osteryoung, R. A. Investigation of Subvalent Ion Effects During Aluminum Anodization in Molten NaCl-AlCl[sub 3] Solvents. *J. Electrochem. Soc.* **1974**, *121*, 983.

(25) Hulot, M. Compt. Rend. *Compt. Rend.* **1855**, *40*, 148.

(26) Tommasi, D. Traite Des Piles Electriques. *Georg. Carre, Paries* **1889**, 131.

(27) Brown, C. H. US Patent 503,567. **1893**.

(28) Barnes, H. T.; Shearer, G. W. A Hydrogen Peroxide Cell. *J. Phys. Chem.* **1907**, *12*, 155–162.

(29) Heise, G. W.; Schumacher, E. A.; Cahoon, N. C. A Heavy Duty Chlorine-Depolarized Cell. *J. Electrochem. Soc.* **1948**, *94*, 99.

(30) Sargent, D. E. US Patent. **1951**, *2,554,447*.

(31) Ruben, S. US Patent. **1953**, *2,638,489*.

(32) Ruben, S. US Patent. **1957**, *2,796,456*.

(33) Cahoon, N. C.; Korver, M. P. A New Separator for the Aluminum Dry Cell. *J. Electrochem. Soc.* **1959**, *106*, 469.

(34) Zaromb, S. The Use and Behavior of Aluminum Anodes in Alkaline Primary Batteries. *J. Electrochem. Soc.* **1962**, *109*, 1125.

(35) Bockstie, L.; Trevethan, D.; Zaromb, S. Control of Al Corrosion in Caustic Solutions. *J. Electrochem. Soc.* **1963**, *110*, 267.

(36) Holleck, G. L. The Reduction of Chlorine on Carbon in AlCl[sub 3]-KCl-NaCl Melts. *J. Electrochem. Soc.* **1972**, *119*, 1158.

(37) Jayaprakash, N.; Das, S. K.; Archer, L. A. The Rechargeable Aluminum-Ion Battery. *Chem. Commun. (Camb).* **2011**, *47*, 12610–12612.

(38) Wang, W.; Jiang, B.; Xiong, W.; Sun, H.; Lin, Z.; Hu, L.; Tu, J.; Hou, J.; Zhu, H.; Jiao, S. A New Cathode Material for Super-Valent Battery Based on Aluminium Ion Intercalation and Deintercalation. *Sci. Rep.* **2013**, *3*, 3383.

(39) Liu, S.; Hu, J. J.; Yan, N. F.; Pan, G. L.; Li, G. R.; Gao, X. P. Aluminum Storage Behavior of Anatase TiO2 Nanotube Arrays in Aqueous Solution for Aluminum Ion Batteries. *Energy Environ. Sci.* **2012**, *5*, 9743.

(40) Reed, L. D.; Menke, E. The Roles of V2O5 and Stainless Steel in Rechargeable Al-Ion Batteries. *J. Electrochem. Soc.* **2013**, *160*, A915–A917.

(41) Ritschel, M.; Vielstich, W. Sea Water Activated Aluminium-Air Cell. *Electrochim. Acta* **1979**, *24*, 885–886.

(42) COOPER, J. PERFORMANCE-CHARACTERISTICS OF ALUMINUM AIR CELLS. *Abstr. Pap. Am. Chem. Soc.* **1979**, 75–75.

(43) HOMSY, R. ALUMINUM-AIR POWER-CELL SYSTEM-DESIGN - MASS AND ENTHALPY BALANCE. *J. Electrochem. Soc.* **1980**, *127*, C352–C352.

(44) Zečević, S.; Gajić, L.; Despić, A. R.; Drazić, D. M. Effect of Pulsating Current on Anode Polarisation in an Aluminium Anode Battery with a Neutral Aqueous Electrolyte. *Electrochim. Acta* **1981**, *26*, 1625–1631.

(45) LEVY, D.; HOLLANDSWORTH, R.; GONZALES, E.; LITTAUER, E. PROTOTYPE ALUMINUM-AIR CELL. *J. Electrochem. Soc.* **1983**, *130*, C73–C73.

(46) Tajima, S. Aluminium and Manganese as Anodes for Dry and Reserve Batteries. *J. Power Sources* **1984**, *11*, 155–161.

(47) Sarangapani, K. B.; Balaramachandran, V.; Kapali, V.; Iyer, S. V.; Potdar, M. G.; Rajagopalan, K. S. Aluminium as Anode in Primary Alkaline Batteries. Influence of Additives on the Corrosion and Anodic Behaviour of 2S Aluminium in Alkaline Citrate Solution. *J. Appl. Electrochem.* **1984**, *14*, 475–480.

(48) OCALLAGHAN, W.; KNOWLES, S. DEVELOPMENT OF AN ELECTROLYTE MANAGEMENT-SYSTEM FOR ALUMINUM-AIR BATTERIES. *J. Electrochem. Soc.* **1985**, *132*, C336–C336.

(49) MAIMONI, A.; MUELDER, S. ALUMINUM-AIR POWER CELL - OVERVIEW AND SUMMARY OF RECENT EXPERIMENTS AT LLNL. *J. Electrochem. Soc.* **1985**, *132*, C336–C336.

(50) KNERR, L.; SCHUE, T.; KRAUSE, C.; WHEELER, D. THE EFFECTS OF DISSOLVED SPECIES ON ALUMINUM-AIR BATTERY ANODE PERFORMANCE. *J. Electrochem. Soc.* **1985**, *132*, C336–C336.

(51) CHASE, G.; SAVINELL, R. CURRENT DISTRIBUTION IN A WEDGE-TYPE ALUMINUM-AIR SINGLE CELL. *J. Electrochem. Soc.* **1985**, *132*, C336–C336.

(52) Despić, A. R. Design Characteristics of an Aluminium-Air Battery with Consumable Wedge Anodes. *J. Appl. Electrochem.* **1985**, *15*, 191–200.

(53) Sarangapani, K. B.; Balaramachandran, V.; Kapali, V.; Venkatakrishna Iyer, S.; Potdar, M. G. Aluminium as the Anode in Primary Alkaline Batteries. *Surf. Technol.* **1985**, *26*, 67–76.

(54) ILIEV, I.; GAMBURZEV, S.; KAISHEVA, A. AIR ELECTRODES FOR ALUMINUM-AIR SALINE BATTERIES. *J. Electrochem. Soc.* **1985**, *132*, C336–C336.

(55) SCAMANS, G. DEVELOPMENT OF THE ALUMINUM/AIR BATTERY. *Chem. Ind.* **1986**, 192–196.

(56) HAMLEN, R.; FITZPATRICK, N. ALUMINUM-AIR SALINE BATTERY PRODUCT OPPORTUNITIES. *J. Electrochem. Soc.* **1987**, *134*, C129–C129.

(57) RAO, B.; KOBASZ, W.; HOGE, W.; HAMLEN, R.; HALLIOP, W.; FITZPATRICK, N. ADVANCES IN ALUMINUM - AIR SALT-WATER BATTERIES. *Abstr. Pap. Am. Chem. Soc.* **1988**, *195*, 282 – COLL.

(58) HASVOLD, O. DEVELOPMENT OF AN ALKALINE ALUMINUM AIR BATTERY SYSTEM AT THE NORWEGIAN-DEFENCE-RESEARCH-ESTABLISHMENT. *Chem. Ind.* **1988**, 85–88.

(59) Budevski, E.; Iliev, I.; Kaisheva, A.; Despić, A.; Krsmanović, K. Investigations of a Large-Capacity Medium-Power Saline Aluminium-Air Battery. *J. Appl. Electrochem.* **1989**, *19*, 323–330.

(60) Hjuler, H. A. A Novel Inorganic Low Melting Electrolyte for Secondary Aluminum-Nickel Sulfide Batteries. *J. Electrochem. Soc.* **1989**, *136*, 901.

(61) Albert, I. J.; Kulandainathan, M. A.; Ganesan, M.; Kapali, V. Characterisation of Different Grades of Commercially Pure Aluminium as Prospective Galvanic Anodes in Saline and Alkaline Battery Electrolyte. *J. Appl. Electrochem.* **1989**, *19*, 547–551.

(62) Development of Aluminum-Air Batteries for EV's. *Electr. Veh. Dev.*

(63) Licht, S. A Novel Aqueous Aluminum/Ferricyanide Battery. *J. Electrochem. Soc.* **1992**, *139*, L109.

(64) Licht, S.; Levitin, G.; Tel-Vered, R.; Yarnitzky, C. The Effect of Water on the Anodic Dissolution of Aluminum in Non-Aqueous Electrolytes. *Electrochem. commun.* **2000**, *2*, 329–333.

(65) Licht, S. A Novel Aqueous Aluminum | permanganate Fuel Cell. *Electrochem. commun.* **1999**, *1*, 33–36.

(66) Licht, S. Aluminum/Sulfur Battery Discharge in the High Current Domain. *J. Electrochem. Soc.* **1997**, *144*, L133.

(67) Licht, S. A High Energy and Power Novel Aluminum/Nickel Battery. *J. Electrochem. Soc.* **1995**, *142*, L179.

(68) Licht, S. Novel Aqueous Aluminum/Sulfur Batteries. *J. Electrochem. Soc.* **1993**, *140*, L4.

(69) Zu, C.-X.; Li, H. Thermodynamic Analysis on Energy Densities of Batteries. *Energy Environ. Sci.* **2011**, *4*, 2614.

(70) Licht, S.; Jeitler, J. R.; Hwang, J. H. Aluminum Anodic Behavior in Aqueous Sulfur Electrolytes. *J. Phys. Chem. B* **1997**, *101*, 4959–4965.

(71) Medeiros, M. G.; Zoski, C. G. Investigation of a Sodium Hypochlorite Catholyte for an Aluminum Aqueous Battery System. *J. Phys. Chem. B* **1998**, *102*, 9908–9914.

(72) Levitin, G.; Yarnitzky, C.; Licht, S. Fluorinated Graphites as Energetic Cathodes for Nonaqueous Al Batteries. *Electrochem. Solid-State Lett.* **2002**, *5*, A160.

(73) Xue, B.; Fu, Z.; Li, H.; Liu, X.; Cheng, S.; Yao, J.; Li, D.; Chen, L.; Meng, Q. Cheap and Environmentally Benign Electrochemical Energy Storage and Conversion Devices Based on AlI3 Electrolytes. *J. Am. Chem. Soc.* **2006**, *128*, 8720–8721.

(74) Li, C.; Ji, W.; Chen, J.; Tao, Z. Metallic Aluminum Nanorods: Synthesis via Vapor-Deposition and Applications in Al/air Batteries. *Chem. Mater.* **2007**, *19*, 5812–5814.

(75) Nestoridi, M.; Pletcher, D.; Wood, R. J. K.; Wang, S.; Jones, R. L.; Stokes, K. R.; Wilcock, I. The Study of Aluminium Anodes for High Power Density Al/air Batteries with Brine Electrolytes. *J. Power Sources* **2008**, *178*, 445–455.

(76) Mohamad, A. A. Electrochemical Properties of Aluminum Anodes in Gel Electrolyte-Based Aluminum-Air Batteries. *Corros. Sci.* **2008**, *50*, 3475–3479.

(77) Mori, R. A New Structured Aluminium–air Secondary Battery with a Ceramic Aluminium Ion Conductor. *RSC Adv.* **2013**, *3*, 11547.

(78) Mori, R. A Novel aluminium–Air Rechargeable Battery with Al 2 O 3 as the Buffer to Suppress Byproduct Accumulation Directly onto an Aluminium Anode and Air Cathode. *RSC Adv.* **2014**, *4*, 30346.

(79) Hibino, T.; Kobayashi, K.; Nagao, M. An All-Solid-State Rechargeable Aluminum–air Battery with a Hydroxide Ion-Conducting Sb(v)-Doped SnP2O7 Electrolyte. *J. Mater. Chem. A* **2013**, *1*, 14844.

(80) Pino, M.; Cuadrado, C.; Chacon, J.; Rodriguez, P.; Fatas, E.; Ocon, P. The Electrochemical Characteristics of Commercial Aluminium Alloy Electrodes for Al/air Batteries. *J. Appl. Electrochem.* **2014**, *44*, 1371–1380.

(81) Cho, Y.-J.; Park, I.-J.; Lee, H.-J.; Kim, J.-G. Aluminum Anode for Aluminum–air Battery – Part I: Influence of Aluminum Purity. *J. Power Sources* **2015**, *277*, 370–378.

(82) Zhang, Z.; Zuo, C.; Liu, Z.; Yu, Y.; Zuo, Y.; Song, Y. All-Solid-State Al–air Batteries with Polymer Alkaline Gel Electrolyte. *J. Power Sources* **2014**, *251*, 470–475.

(83) Revel, R.; Audichon, T.; Gonzalez, S. Non-Aqueous Aluminium-Air Battery Based on Ionic Liquid Electrolyte. *J. Power Sources* **2014**, *272*, 415–421.

(84) Gelman, D.; Shvartsev, B.; Ein-Eli, Y. Aluminum–air Battery Based on an Ionic Liquid Electrolyte. *J. Mater. Chem. A* **2014**, *2*, 20237–20242.

(85) Wang, L.; Liu, F.; Wang, W.; Yang, G.; Zheng, D.; Wu, Z.; Leung, M. K. H. A High-Capacity Dual-Electrolyte Aluminum/air Electrochemical Cell. *RSC Adv.* **2014**, *4*, 30857.

(86) Sivashanmugam, A.; Prasad, S. R.; Thirunakaran, R.; Gopukumar, S. Electrochemical Performance of Al/MnO[sub 2] Dry Cells: An Alternative to Lechlanche Dry Cells. *J. Electrochem. Soc.* **2008**, *155*, A725.

(87) Chen, L. D.; Norskov, J. K.; Luntz, A. C. Al-Air Batteries: Fundamental Thermodynamic Limitations from First Principles Theory. *J. Phys. Chem. Lett.* **2014**, *6*, 141217100007001.

(88) He, Y. J.; Peng, J. F.; Chu, W.; Li, Y. Z.; Tong, D. G. Black Mesoporous Anatase TiO2 Nanoleaves: A High Capacity and High Rate Anode for Aqueous Al-Ion Batteries. *J. Mater. Chem. A* **2014**, *2*, 1721.

(89) Liu, Y.; Sang, S.; Wu, Q.; Lu, Z.; Liu, K.; Liu, H. The Electrochemical Behavior of Cl− Assisted Al3+ Insertion into Titanium Dioxide Nanotube Arrays in Aqueous Solution for Aluminum Ion Batteries. *Electrochim. Acta* **2014**, *143*, 340–346.

(90) Kobayashi, Y.; Egawa, T.; Tamura, S.; Imanaka, N.; Adachi, G. Trivalent Al 3+ Ion Conduction in Aluminum Tungstate Solid. *Chem. Mater.* **1997**, *9*, 1649–1654.

(91) Imanaka, N.; Hasegawa, Y.; Yamaguchi, M.; Itaya, M.; Tamura, S.; Adachi, G. Extraordinary High Trivalent Al 3+ Ion Conduction in Solids. *Chem. Mater.* **2002**, *14*, 4481–4483.

(92) Zhou, Y.; Adams, S.; Rao, R. P.; Edwards, D. D.; Neiman, A.; Pestereva, N. Charge Transport by Polyatomic Anion Diffusion in Sc 2 (WO 4 ) 3. *Chem. Mater.* **2008**, *20*, 6335–6345.

(93) Wang, H.; Bai, Y.; Chen, S.; Luo, X.; Wu, C.; Wu, F.; Lu, J.; Amine, K. Binder-Free V2O5 Cathode for Greener Rechargeable Aluminum Battery. *ACS Appl. Mater. Interfaces* **2015**, *7*, 80–84.

(94) Lin, M.-C.; Gong, M.; Lu, B.; Wu, Y.; Wang, D.-Y.; Guan, M.; Angell, M.; Chen, C.; Yang, J.; Hwang, B.-J.; et al. An Ultrafast Rechargeable Aluminium-Ion Battery. *Nature* **2015**, *520*, 324–328.

(95) Kim, H. S.; Arthur, T. S.; Allred, G. D.; Zajicek, J.; Newman, J. G.; Rodnyansky, A. E.; Oliver, A. G.; Boggess, W. C.; Muldoon, J. Structure and Compatibility of a Magnesium Electrolyte with a Sulphur Cathode. *Nat. Commun.* **2011**, *2*, 427.

(96) Aurbach, D.; Lu, Z.; Schechter, A.; Gofer, Y.; Gizbar, H.; Turgeman, R.; Cohen, Y.; Moshkovich, M.; Levi, E. Prototype Systems for Rechargeable Magnesium Batteries. *Nature* **2000**, *407*, 724–727.

(97) Li, Q.; Bjerrum, N. J. Aluminum as Anode for Energy Storage and Conversion: A Review. *J. Power Sources* **2002**, *110*, 1–10.

(98) Donahue, F. M.; Mancini, S. E.; Simonsen, L. Secondary Aluminium-Iron (III) Chloride Batteries with a Low Temperature Molten Salt Electrolyte. *J. Appl. Electrochem.* **1992**, *22*, 230–234.

(99) Gifford, P. R. An Aluminum/Chlorine Rechargeable Cell Employing a Room Temperature Molten Salt Electrolyte. *J. Electrochem. Soc.* **1988**, *135*, 650.

(100) Peramunage, D.; Licht, S. A Solid Sulfur Cathode for Aqueous Batteries. *Science* **1993**, *261*, 1029–1032.

(101) Chaput, F.; Dunn, B.; Fuqua, P.; Salloux, K. Synthesis and Characterization of Vanadium Oxide Aerogels. *J. Non. Cryst. Solids* **1995**, *188*, 11–18.

(102) Terada, S.; Mandai, T.; Nozawa, R.; Yoshida, K.; Ueno, K.; Tsuzuki, S.; Dokko, K.; Watanabe, M. Physicochemical Properties of Pentaglyme-Sodium Bis(trifluoromethanesulfonyl)amide Solvate Ionic Liquid. *Phys. Chem. Chem. Phys.* **2014**, *16*, 11737–11746.

(103) Yoshida, K.; Nakamura, M.; Kazue, Y.; Tachikawa, N.; Tsuzuki, S.; Seki, S.; Dokko, K.; Watanabe, M. Oxidative-Stability Enhancement and Charge Transport Mechanism in Glyme-Lithium Salt Equimolar Complexes. *J. Am. Chem. Soc.* **2011**, *133*, 13121–13129.

(104) Pappenfus, T. M.; Henderson, W. A.; Owens, B. B.; Mann, K. R.; Smyrl, W. H. Complexes of Lithium Imide Salts with Tetraglyme and Their Polyelectrolyte Composite Materials. *J. Electrochem. Soc.* **2004**, *151*, A209.

(105) Kitazawa, Y.; Iwata, K.; Imaizumi, S.; Ahn, H.; Kim, S. Y.; Ueno, K.; Park, M. J.; Watanabe, M. Gelation of Solvate Ionic Liquid by Self-Assembly of Block Copolymer and Characterization as Polymer Electrolyte. *Macromolecules* **2014**, *47*, 6009–6016.

(106) Moon, H.; Tatara, R.; Mandai, T.; Ueno, K.; Yoshida, K.; Tachikawa, N.; Yasuda, T.; Dokko, K.; Watanabe, M. Mechanism of Li Ion Desolvation at the Interface of Graphite Electrode and Glyme–Li Salt Solvate Ionic Liquids. *J. Phys. Chem. C* **2014**, *118*, 20246–20256.

(107) Zhang, C.; Ueno, K.; Yamazaki, A.; Yoshida, K.; Moon, H.; Mandai, T.; Umebayashi, Y.; Dokko, K.; Watanabe, M. Chelate Effects in Glyme/lithium Bis(trifluoromethanesulfonyl)amide Solvate Ionic Liquids. I. Stability of Solvate Cations and Correlation with Electrolyte Properties. *J. Phys. Chem. B* **2014**, *118*, 5144–5153.

(108) Mandai, T.; Yoshida, K.; Tsuzuki, S.; Nozawa, R.; Masu, H.; Ueno, K.; Dokko, K.; Watanabe, M. Effect of Ionic Size on Solvate Stability of Glyme-Based Solvate Ionic Liquids. *J. Phys. Chem. B* **2015**, *119*, 1523–1534.

(109) Petrowsky, M.; Frech, R.; Suarez, S. N.; Jayakody, J. R. P.; Greenbaum, S. Investigation of Fundamental Transport Properties and Thermodynamics in Diglyme-Salt Solutions. *J. Phys. Chem. B* **2006**, *110*, 23012–23021.

(110) Www.gaussian.com/g_tech/g_ur/m_citation.htm. Gaussian 09.

(111) Marenich, A. V; Cramer, C. J.; Truhlar, D. G. Universal Solvation Model Based on Solute Electron Density and on a Continuum Model of the Solvent Defined by the Bulk Dielectric Constant and Atomic Surface Tensions. *J. Phys. Chem. B* **2009**, *113*, 6378–6396.

(112) Petrowsky, M.; Frech, R. A Spectroscopic Investigation of the Mechanism of Gel Formation in Tetraglyme/fumed Silica Composites. *Electrochim. Acta* **2003**, *48*, 2093–2097.

(113) Rhodes, C. P.; Frech, R. Local Structures in Crystalline and Amorphous Phases of Diglyme−LiCF 3 SO 3 and Poly(ethylene oxide)−LiCF 3 SO 3 Systems: Implications for the Mechanism of Ionic Transport. *Macromolecules* **2001**, *34*, 2660–2666.

(114) Huang, W.; Frech, R.; Wheeler, R. A. Molecular Structures and Normal Vibrations of Trifluoromethane Sulfonate (CF3SO3-) and Its Lithium Ion Pairs and Aggregates. *J. Phys. Chem.* **1994**, *98*, 100–110.

(115) Zhang, C.; Yamazaki, A.; Murai, J.; Park, J.-W.; Mandai, T.; Ueno, K.; Dokko, K.; Watanabe, M. Chelate Effects in Glyme/Lithium

Bis(trifluoromethanesulfonyl)amide Solvate Ionic Liquids, Part 2: Importance of Solvate-Structure Stability for Electrolytes of Lithium Batteries. *J. Phys. Chem. C* **2014**, *118*, 17362–17373.

(116) Konezny, S. J.; Doherty, M. D.; Luca, O. R.; Crabtree, R. H.; Soloveichik, G. L.; Batista, V. S. Reduction of Systematic Uncertainty in DFT Redox Potentials of Transition-Metal Complexes. *J. Phys. Chem. C* **2012**, *116*, 6349–6356.

(117) Roy, L. E.; Jakubikova, E.; Guthrie, M. G.; Batista, E. R. Calculation of One-Electron Redox Potentials Revisited. Is It Possible to Calculate Accurate Potentials with Density Functional Methods? *J. Phys. Chem. A* **2009**, *113*, 6745–6750.

(118) Brito, P. S. D.; Sequeira, C. A. C. Organic Inhibitors of the Anode Self-Corrosion in Aluminum-Air Batteries. *J. Fuel Cell Sci. Technol.* **2013**, *11*, 011008.

(119) Hyams, T. C.; Go, J.; Devine, T. M. Corrosion of Aluminum Current Collectors in High-Power Lithium-Ion Batteries for Use in Hybrid Electric Vehicles. *J. Electrochem. Soc.* **2007**, *154*, C390.

(120) Zhang, X.; Devine, T. M. Identity of Passive Film Formed on Aluminum in Li-Ion Battery Electrolytes with LiPF[sub 6]. *J. Electrochem. Soc.* **2006**, *153*, B344.

(121) McEwen, A. B. Electrochemical Properties of Imidazolium Salt Electrolytes for Electrochemical Capacitor Applications. *J. Electrochem. Soc.* **1999**, *146*, 1687.

(122) Neff, V. D. Electrochemical Oxidation and Reduction of Thin Films of Prussian Blue. *J. Electrochem. Soc.* **1978**, *125*, 886.

(123) Itaya, K.; Uchida, I.; Neff, V. D. Electrochemistry of Polynuclear Transition Metal Cyanides: Prussian Blue and Its Analogues. *Acc. Chem. Res.* **1986**, *19*, 162–168.

(124) Wessells, C. D.; Huggins, R. A.; Cui, Y. Copper Hexacyanoferrate Battery Electrodes with Long Cycle Life and High Power. *Nat. Commun.* **2011**, *2*, 550.

(125) Trócoli, R.; La Mantia, F. An Aqueous Zinc-Ion Battery Based on Copper Hexacyanoferrate. *ChemSusChem* **2015**, *8*, 481–485.

(126) Liu, S.; Pan, G. L.; Li, G. R.; Gao, X. P. Copper Hexacyanoferrate Nanoparticles as Cathode Material for Aqueous Al-Ion Batteries. *J. Mater. Chem. A* **2014**, *3*, 959–962.

(127) Jia, Z.; Wang, B.; Wang, Y. Copper Hexacyanoferrate with a Well-Defined Open Framework as a Positive Electrode for Aqueous Zinc Ion Batteries. *Mater. Chem. Phys.* **2015**, *149-150*, 601–606.

(128) Chan, C. K.; Peng, H.; Liu, G.; McIlwrath, K.; Zhang, X. F.; Huggins, R. A.; Cui, Y. High-Performance Lithium Battery Anodes Using Silicon Nanowires. *Nat. Nanotechnol.* **2008**, *3*, 31–35.

(129) Suo, L.; Hu, Y.-S.; Li, H.; Armand, M.; Chen, L. A New Class of Solvent-in-Salt Electrolyte for High-Energy Rechargeable Metallic Lithium Batteries. *Nat. Commun.* **2013**, *4*, 1481.

(130) Shao, Y.; Gu, M.; Li, X.; Nie, Z.; Zuo, P.; Li, G.; Liu, T.; Xiao, J.; Cheng, Y.; Wang, C.; et al. Highly Reversible Mg Insertion in Nanostructured Bi for Mg Ion Batteries. *Nano Lett.* **2014**, *14*, 255–260.

(131) Zhang, R.; Mizuno, F.; Ling, C. Fullerenes: Non-Transition Metal Cluster For Rechargeable Magnesium Battery Cathode. *Chem. Commun.* **2014**.

(132) Muldoon, J.; Bucur, C. B.; Oliver, A. G.; Sugimoto, T.; Matsui, M.; Kim, H. S.; Allred, G. D.; Zajicek, J.; Kotani, Y. Electrolyte Roadblocks to a Magnesium Rechargeable Battery. *Energy Environ. Sci.* **2012**, *5*, 5941.

(133) Yoo, H. D.; Shterenberg, I.; Gofer, Y.; Gershinsky, G.; Pour, N.; Aurbach, D. Mg Rechargeable Batteries: An on-Going Challenge. *Energy Environ. Sci.* **2013**, *6*, 2265.

(134) Levi, E.; Gofer, Y.; Aurbach, D. On the Way to Rechargeable Mg Batteries: The Challenge of New Cathode Materials †. *Chem. Mater.* **2010**, *22*, 860–868.

(135) Mizuno, Y.; Okubo, M.; Hosono, E.; Kudo, T.; Oh-ishi, K.; Okazawa, A.; Kojima, N.; Kurono, R.; Nishimura, S.; Yamada, A. Electrochemical Mg2+ Intercalation into a Bimetallic CuFe Prussian Blue Analog in Aqueous Electrolytes. *J. Mater. Chem. A* **2013**, *1*, 13055.

(136) Wang, R. Y.; Wessells, C. D.; Huggins, R. A.; Cui, Y. Highly Reversible Open Framework Nanoscale Electrodes for Divalent Ion Batteries. *Nano Lett.* **2013**, *13*, 5748–5752.

(137) Wessells, C. D.; Peddada, S. V; Huggins, R. A.; Cui, Y. Nickel Hexacyanoferrate Nanoparticle Electrodes for Aqueous Sodium and Potassium Ion Batteries. *Nano Lett.* **2011**, *11*, 5421–5425.

(138) Mizuno, Y.; Okubo, M.; Hosono, E.; Kudo, T.; Zhou, H.; Oh-ishi, K. Suppressed Activation Energy for Interfacial Charge Transfer of a Prussian Blue Analog Thin Film Electrode with Hydrated Ions (Li + , Na + , and Mg 2+ ). *J. Phys. Chem. C* **2013**, *117*, 10877–10882.

(139) Li, Z.; Xiang, K.; Xing, W.; Carter, W. C.; Chiang, Y.-M. Reversible Aluminum-Ion Intercalation in Prussian Blue Analogs and Demonstration of a High-Power Aluminum-Ion Asymmetric Capacitor. *Adv. Energy Mater.* **2014**, n/a – n/a.

(140) Lukatskaya, M. R.; Mashtalir, O.; Ren, C. E.; Dall'Agnese, Y.; Rozier, P.; Taberna, P. L.; Naguib, M.; Simon, P.; Barsoum, M. W.; Gogotsi, Y. Cation Intercalation and High Volumetric Capacitance of Two-Dimensional Titanium Carbide. *Science* **2013**, *341*, 1502–1505.

(141) Yabuuchi, N.; Kajiyama, M.; Iwatate, J.; Nishikawa, H.; Hitomi, S.; Okuyama, R.; Usui, R.; Yamada, Y.; Komaba, S. P2-Type Na(x)[Fe(1/2)Mn(1/2)]O2 Made from Earth-Abundant Elements for Rechargeable Na Batteries. *Nat. Mater.* **2012**, *11*, 512–517.

(142) Zhou, H.; Upreti, S.; Chernova, N. A.; Hautier, G.; Ceder, G.; Whittingham, M. S. Iron and Manganese Pyrophosphates as Cathodes for Lithium-Ion Batteries. *Chem. Mater.* **2011**, *23*, 293–300.

(143) Huggins, R. A. Advanced Batteries. *Springer* **2009**, 474.

(144) Okubo, M.; Asakura, D.; Mizuno, Y.; Kudo, T.; Zhou, H.; Okazawa, A.; Kojima, N.; Ikedo, K.; Mizokawa, T.; Honma, I. Ion-Induced Transformation of Magnetism in a Bimetallic CuFe Prussian Blue Analogue. *Angew. Chem. Int. Ed. Engl.* **2011**, *50*, 6269–6273.

(145) Okubo, M.; Mizuno, Y.; Yamada, H.; Kim, J.; Hosono, E.; Zhou, H.; Kudo, T.; Honma, I. Fast Li-Ion Insertion into Nanosized LiMn(2)O(4) without Domain Boundaries. *ACS Nano* **2010**, *4*, 741–752.

(146) Asakura, D.; Li, C. H.; Mizuno, Y.; Okubo, M.; Zhou, H.; Talham, D. R. Bimetallic Cyanide-Bridged Coordination Polymers as Lithium Ion Cathode Materials: Core@shell Nanoparticles with Enhanced Cyclability. *J. Am. Chem. Soc.* **2013**, *135*, 2793–2799.

(147) Kajiyama, S.; Mizuno, Y.; Okubo, M.; Kurono, R.; Nishimura, S.; Yamada, A. Phase Separation of a Hexacyanoferrate-Bridged Coordination Framework under Electrochemical Na-Ion Insertion. *Inorg. Chem.* **2014**, *53*, 3141–3147.

(148) Okubo, M.; Honma, I. Ternary Metal Prussian Blue Analogue Nanoparticles as Cathode Materials for Li-Ion Batteries. *Dalton Trans.* **2013**, *42*, 15881–15884.

(149) Bennett, M. V.; Beauvais, L. G.; Shores, M. P.; Long, J. R. Expanded Prussian Blue Analogues Incorporating [Re 6 Se 8 (CN) 6 ] 3-/4- Clusters: Adjusting Porosity via Charge Balance. *J. Am. Chem. Soc.* **2001**, *123*, 8022–8032.

(150) Buser, H. J.; Schwarzenbach, D.; Petter, W.; Ludi, A. The Crystal Structure of Prussian Blue: Fe4[Fe(CN)6]3.xH2O. *Inorg. Chem.* **1977**, *16*, 2704–2710.